INVESTIGATION OF MIXING IN A MULTISTAGE AXIAL COMPRESSOR

by

Sasi K. Digavalli
B.Tech., Indian Institute of Technology, (1986)

SUMMITED IN PARTIAL FULFILLMENT

OF THE REQUIREMENTS FOR THE DEGREE OF

MASTER OF SCIENCE

IN AERONAUTICS AND ASTRONAUTICS

at the

MASSACHUSETTS INSTITUTE OF TECHNOLOGY

May1990

© Massachusetts Institute of Technology

Signature of Author_____
Department of Aeronautics and Astronautics, May, 1990

Certified by_____
Professor Edward M. Greitzer
Thesis Supervisor
Department of Aeronautics and Astronautics

Accepted by_____
Professor Harold Y. Wachman
Chairman, Department Graduate Committee

MASS. INST. TECH.
JUN 19 1990
LIBR

INVESTIGATION OF MIXING IN A MULTISTAGE AXIAL COMPRESSOR

by

Sasi K. Digavalli

The work described in this thesis consists of an experimental investigation of mixing in a three stage axial compressor, in particular its evolution through the machine. A tracer gas is used to measure the mixing rates. The variation in mixing rates with position in the machine is examined. The effects of injection probe geometry and external flow parameters on the results are also investigated.

It is found that mixing across all three stators is very similar, as it is across all three rotors and across all three stages. There is little evidence of any evolution of the mixing process. Radial and circumferential flow distortions generated in one blade row do not affect mixing in the next blade row to any significant degree. Secondary flows contribute to mixing only near the end walls. At increased loading there is increased mixing in both stators and in rotors.

Thesis Supervisor : Dr. Edward M. Greitzer
Title : Professor of
Aeronautics and Astronautics

ACKNOWLEDGEMENTS

The completion of this thesis would not have been possible without the advice, help and encouragement of many people at the GTL.

First, I would like to express my respect and appreciation to Prof. E. M. Greitzer for his supervision and encouragement. His constant emphasis on data interpretation rather than on data taking has greatly broadened my vision of experimental investigation and understanding of fluid mechanics. Dr. C. S. Tan's criticism and advice have been very constructive and helpful.

Mr. Victor Dubrowski's patient and immaculate work during restaggering the low speed compressor and in the machine-shop will never be forgotten. Mr. Jim Nash and Mr. Roy Andrew have been very helpful in setting up the rig for running the compressor and moving around gas cylinders. Mr. Dave Dvore's work in replacing the computer system in the laboratory was very efficient and made the computer more user friendly.

A wealth of software left behind by Dr. P. L. Lavrich and Dr. David Fink has saved me a lot of time. The comraderie and cheering-up of Mr. Tonghuo Shang have made the long working hours look much shorter.

Financial support for the work was provided by Pratt and Whitney Aircraft Government Products Division and it is greatly appreciated. The interest and helpful comments of Dr. S. Baghdadi and Dr. S. Koff are very much appreciated.

I am also thankful to the U.S. Government for giving me the opportunity to study in this country.

Finally the work would have been impossible without the constant encouragement of my parents, sister and brother.

LIST OF TABLES

LIST OF FIGURES

CHAPTER 1

INTRODUCTION

1.A INTRODUCTION

With the present trend in axial flow compressor design towards low aspect ratio, a greater fraction of the annulus flow is subjected to end-wall effects. Although one might expect the losses at the end-walls to produce increasing temperature and velocity defects in this vicinity as the flow progresses through the machine, this phenomenon in fact does not occur after the first one or two stages [Ref. 1]. Measurements of flows in multi-stage compressors show the existence of a repeating stage condition, where the velocity profiles upstream and downstream of a stage are almost identical. Such a repeating stage condition indicates the existence of a radial mixing mechanism which causes the end-wall losses to be mixed out towards the mid-span and prevents steepening of velocity profiles. Measurements [Ref. 2] indicating higher efficiency near end-walls than those predicted have lent further evidence to the hypothesis that radial mixing plays an important role in flow through multi-stage axial compressors.

This thesis examines the mechanisms that cause the mixing, their

relative importance and the variation of mixing rates as flow progresses through a multi-stage axial compressor.

1.B BACKGROUND

Considerable research has gone into understanding the mechanisms of fluid migration and radial mixing in a multi-stage compressor and a brief outline of these developments is given below.

Based on the higher measured efficiencies at tip than predicted by through-flow calculations and the idea that this was due to radial mixing, Adkins and Smith [Ref. 2] postulated that the mechanism driving radial redistribution was a large scale secondary flow. They devised a method of including this effect in a through-flow calculation. Their model used inviscid, small-perturbation secondary flow theory to obtain radial velocities, which were used to calculate spanwise mixing coefficient. Flow properties were then redistributed radially by solving an equation which models a diffusion process. Inclusion of their spanwise mixing model in compressor through-flow calculations led to computed results that were in good agreement with radial profiles of total temperature observed during compressor tests.

Gallimore and Cumpsty [Ref. 3] examined this concept using a tracer gas technique. They measured mixing in two multi-stage compressors and concluded that the convective model of [Ref. 2] did not include the main source of the mixing, because the dominant mixing mechanism was a "turbulent diffusion" process. They found that the levels of mixing were high all the way across the span, and that the idea of separate end-wall boundary layers bounding a

free stream is not appropriate. Local spanwise mixing coefficients were derived by assuming that the tracer gas diffuses from a point source into uniform flow. Like Adkins and Smith [Ref. 2] they used their mixing coefficients in a through-flow calculation to obtain radial profiles of flow properties in a compressor. Their predicted spanwise distributions of total temperature also agree with experimental results, particularly away from end-walls.

It is reasonable to state, based on the results reported in [Ref. 2,3] that regardless of the underlying mechanism, inclusion of a mixing coefficient into through-flow calculation of an axial compressor improves the predicted results. A relevant comment is that made by Wennerstrom [Ref. 4]. It is,however, it important to understand the mechanisms that contribute to radial mixing, and further insight into this problem has been provided by Wisler et al [Ref. 5]. They investigated the relative importance of convection by secondary flows and diffusion by turbulence as mechanisms responsible for spanwise mixing in the third-stage of a four stage axial compressor. They concluded that away from the end-walls diffusion is the dominant mechanism, whereas close to the end-walls contributions to mixing from secondary flows and turbulence are of the same magnitude.

Li and Cumpsty [Ref. 6] have investigated mixing across several stages of a multistage compressor. Their measurements indicate that the level of mixing does not change appreciably from one stage to the next. They also stated that contribution to mixing by secondary flows is appreciable only close to the end walls.

Though the mixing levels predicted by [Ref. 2,3] agree with experi-

ments, they are based on two fundamentally different mechanisms and more data is needed before one can lend support to either of these hypotheses. A brief outline of the focus of the present research, the motivation, and the main findings of the investigation is given in the next section.

1.C RESEARCH OBJECTIVES

As stated earlier a complete understanding of all the mechanisms that generate radial mixing is far from complete. The consensus seems to be that turbulent diffusion dominates the mixing process through most of the span away from the end-walls and that contributions from secondary radial flows are significant only near end-walls. One of the objectives of this thesis is to clarify the relative importance of secondary flows and turbulent diffusion for radial mixing.

The results that have been reported so far, except for Li and Cumpsty [Ref. 6], are confined to radial mixing across a single blade row, in each case. Wisler et al [Ref. 5] studied extensively the third stator in a four stage compressor, but no other blade row. Adkins and Smith [Ref. 2] applied their theory mostly to a single blade row in each machine they picked for demonstration. Gallimore and Cumpsty [Ref. 3] measured mixing coefficients for a stator, in each of the two compressors they studied. An additional question is how the mixing level evolves through the compressor. Another goal of this thesis, therefore, is to carry out detailed mixing measurements for each blade row in a multi-stage compressor to understand how the mixing process evolves, as flow passes through the compressor. (Results from Ref. 6 were not available when this research effort began.)

It is also intended that the effect of Aspect Ratio on mixing be defined. As Aspect Ratio is decreased, secondary flows will increase in significance, the assumption of parallel stream tubes will be less valid and consequently mixing should increase. Mixing measurements will be available from four compressors (two from [Ref. 3], the third from [Ref. 5]), so a comparative study between mixing levels and Aspect Ratio will be possible.

Finally, Gallimore and Cumptsy [Ref. 3] used different kinds of probes for injecting the tracer gas. There are effects of probe shape and relative size on mixing of the injected fluid with external flow. We have thus documented the effects of external flow velocity and turbulence on mixing of an injected fluid with the external flow.

1.D SCOPE OF THE THESIS

The following chapter describes the principle of the tracer gas technique, used in the mixing measurements. A brief account of the operation of a Flame Ionization Detector which is a fundamental part of the tracer gas experiments is also included. Chapter 3 details methods for estimating mixing coefficients by using results from tracer gas experiments. Effects of external flow parameters and injection probe geometry on mixing coefficient are also discussed. Chapter 4 discusses the instrumentation and the experimental techniques used in this work. Chapter 5 describes a detailed experiment carried out to study mixing in a three-stage axial compressor. Chapter 6 presents conclusions and suggestions for further research.

CHAPTER 2

TRACER GAS TECHNIQUE

2.A DESCRIPTION OF THE TECHNIQUE

The principal idea behind the tracer gas technique is similar to that behind flow visualization methods. A tracer gas is injected into the stream of air that is being studied. As the tracer gas is carried downstream by the main stream it is detected either by direct visualization, as is the case if the tracer gas is smoke, or by measuring some property of the fluid (e.g. concentration or conductivity), which is affected by the presence of the tracer gas. For example, Kerrebrock and Mikolajczak [Ref. 7] used helium and a conductivity probe to study the migration of rotor wakes inside a stator row.

The method that we used to investigate the flow in a multi-stage compressor was first adopted to mixing analysis by Denton and Usui [Ref. 8]. Ethylene was chosen as the tracer gas since it has almost the same density as air. A small steady stream of ethylene is injected into the main flow from an injection probe, with the flow rate monitored by a flowmeter. The air, mixed with ethylene, is then sampled downstream at a constant rate using a sampling probe connected to a Flame Ionization Detector (FID). The voltage output of the FID is then converted to concentration in parts per million of ethylene.

These concentration measurements can be used to obtain mixing rates.

2.B FLAME IONIZATION DETECTOR (FID)

The concentration of tracer gas is measured using a commercially available FID. The FID employs a hydrogen flame in air to detect the presence of ions produced by combusting the hydrocarbons present in the sample. It has high sensitivity, being able to detect mass flow rates of ethylene as low as 10^{-10} gm/s, or concentrations of a few ppm. The FID used was Beckman Industrials model #400A. The gas detector system is comprised of the following components connected as shown in Fig. 1.

1. FID
2. Tracer gas injection probe
3. Sampling probe
4. Suction pump
5. Flowmeters
6. Flow control valves
7. Hydrogen, Ethylene and Air cylinders.

Fig. 2 shows a diagram of the FID combustion chamber.

As shown in Fig. 1, air containing a small quantity of tracer gas, is sucked into a sampling probe inserted into the flow being studied. After passing through a flowmeter and a valve the sample is mixed with a stream of hydrogen. This gas mixture enters the flame chamber of the FID. When ignited, the hydrogen burns and maintains a steady flame. Within the flame, the

hydrocarbon components of the sample stream undergo an ionization process that produces electrons and positive ions. Polarized electrodes collect these ions, causing current to flow through an electronic measuring circuitry. The burner jet and the collector function as electrodes. Current flow is proportional to the rate at which carbon atoms enter the burner. The ionization current is amplified twice, first by a preamplifier and then by a post-amplifier after passing through a filter.

It is important that the flow rates of all the gases going into the FID be kept constant during the experiment since the response of the FID varies with all these flow rates. Their relative values should be chosen so that peak response and maximum flame stability are achieved. In addition, the hydrogen used for flame generation was mixed with helium (40%) to prevent burner overheating. In the experiments (chapter 3&5) the sample flow rate was matched with local external velocity. The time taken by the FID to reach a steady output and the flame stability depend on the sample flow rate. When the sample flow rate was too high for the flame to be stable a by-pass was used.

Fig. 3,4 and 5 show how FID response (output measured in volts) varies when input pressures of sample, fuel and air flow were varied, respectively. Fig. 6 shows the linearity between FID output and the concentration of sample when ethylene samples of known concentrations were used.

Some FID models, used mainly in automobile exhaust studies, are fitted with heated sample-lines to prevent condensation of heavy hydrocarbons on the

walls of the tubing. To find out whether a heated line was necessary when the sample is ethylene, an experiment was conducted using a heated FID. The FID was fed with an ethylene sample of known concentration and its output was measured, once with sample-line heat switched off and another time with the heat on. A comparison of these two measurements is shown in Fig. 7. The difference between these two readings was within the margin of accuracy of the machine, so it was concluded that for ethylene a heated line was unnecessary.

CHAPTER 3

ESTIMATION OF MIXING COEFFICIENTS

3.A INTRODUCTION

It was mentioned in chapter 1 that mixing rates will be determined from the tracer gas concentration measurements taken on the multi-stage compressor (presented in chapter 5). If the mechanism is turbulent diffusion, these mixing rates imply eddy mixing coefficients, and analyses are presented in the next section for estimating these eddy diffusion coefficients from the concentration measurements. One of these analyses, originally developed by Towle and Sherwood [Ref. 9] has been used by Gallimore and Cumpsty [Ref. 3]. In this approach the injector is modelled as a point source. Another approach described here, is a simplified version of a method given in Hinze [Ref. 10] where the injection source is modelled as a jet. The author views the latter as a better approximation because the representation of the injection source is closer to the actual situation. In addition to these calculations, experiments to determine the influence of injection probe and external flow parameters on eddy diffusivity will be descussed.

3.B METHODS FOR PREDICTING THE MIXING COEFFICIENT

i) MODEL#1 : Point Source Model:-

The mean velocity of the turbulent flow is considered to be a constant Vx, in the direction of x. A point source with constant volume flow rate S is located at (x,y,z) = (0,0,0). The amount of the matter released by the source is small enough such that its effect on the turbulence may be neglected. It is assumed that the diffusion of the injected gas is defined by a diffusion constant or an eddy diffusivity constant ϵ. The mean concentration P of the injected species at a point (x,y,z) is identical with the probability of finding a particle of the species at that point. The differential equation for this mean concentration is :

$$V_x \frac{\partial P}{\partial x} = \epsilon \nabla^2 P \quad \ldots\ldots\ldots\ldots\ldots \quad (1)$$

The solution is [Ref. 10] :

$$P(x,y,z) = \frac{S}{4\pi R} \exp\{-V_x(R-x)/2\epsilon)\} \quad \ldots\ldots\ldots \quad (2)$$

where,
$$R^2 = x^2 + r^2$$
$$= x^2 + y^2 + z^2$$

The ratio of species concentration C at (x,y,z) to that at (x,0,0) is given by :

$$C = x/R \; exp\{-V_x(R-x)/2\epsilon)\} \quad \ldots\ldots\ldots\ldots\ldots\ldots \quad (3)$$

Approximating $x/R \simeq 1$, which, for our measurements, is accurate to within 2%, we find that :

$$C = exp\{-V_x r^2/4x\epsilon\} \quad \ldots\ldots\ldots\ldots\ldots\ldots \quad (4)$$

The effect of the presence of the probe is to produce greater mixing close to the probe than would otherwise be expected. The result is that the ethylene could be interpreted as originating from somewhere upstream of the injection probe position. A discussion of this phenomenon can be found in

Moore and Smith [Ref. 11], who proposed a correction for the position of the imaginary source position by introducing an empirical constant x_0. Thus

$$C = exp\{-V_x r^2/4(x-x_0)\epsilon\} \quad \ldots\ldots\ldots\ldots\ldots\ldots \quad (5)$$

This constant depends on the probe geometry, and a of a method for determining it is included in the next chapter.

ii) MODEL#2 : Free Jet Model :-

This approach models the mixing coefficient for a species injected in the form of a round free jet into a general turbulent stream of constant velocity. Fig. 8 shows the general case of injection and the notation followed. The outside turbulent stream has a velocity Us. The jet issues with a velocity Up and concentration Cp from an orifice of diameter 'd'. Cylindrical coordinates (x,r) are used with the axial coordinate 'x' along the jet axis, and x=0 is the plane of the orifice.

The equation for transport of species concentration, after applying the approximations associated with free turbulence [Ref. 10], is :

$$\bar{U}_x \frac{\partial \bar{C}}{\partial x} + \bar{U}_r \frac{\partial \bar{C}}{\partial r} = -\frac{1}{r} \frac{\partial}{\partial r}\left(r\epsilon \frac{\partial \bar{C}}{\partial r} \right) \quad \ldots\ldots\ldots \quad (6)$$

Similarity methods discussed by Abramovich [Ref. 12] provide the solution of equation (6). For region $U_1/U_p \ll 1$, $U_r/U_p \ll 1$ and $r/x \ll 1$ the solution simplifies to :

$$C = exp\{-U_s r^2/6(x+a)\epsilon\} \quad \ldots\ldots\ldots\ldots\ldots\ldots \quad (7)$$

where C is the ratio of concentration at (x,r) to that at (x,0) and a is the distance between the geometrical origin of similarity and the origin of the

coordinate system. We will take 'a' to be the same as the negative of 'x_0' of model #1. Its value is evaluated in the next chapter.

3.C INFLUENCE OF PROBE AND FLOW PARAMETERS ON MIXING

It was stated earlier that understanding of the factors influencing the level of mixing in a tracer gas experiment is important. Because of this, investigations were carried out to define the effects of : size and shape of the injection probe, turbulence level of the main stream, difference in speed between main stream and injected gas, and streamwise large eddy length scale of the main stream. To calibrate the mixing coefficient against these parameters a uniform flow of known turbulence and length scales was needed. A preliminary experiment on a wind tunnel was conducted to test suitability for this purpose.

Using square meshes, flows of different turbulence levels were generated. The largest length scales in the flow field are determined by the spacing between the rods of the grid in use. Experiments were conducted with meshes of 1" and 1/2" spacing and rod diameters ranging from 1/12" to 1/2". Fig. 9 shows that at about 30 diameters downstream into the wake of the grid the flow attains a uniform turbulence level, in accordance with with results obtained in [Ref. 13]. The maximum turbulence, however, was less than 5%, as shown in Fig.10, which corresponds to a mesh of solidity 0.5 and rod diameter 1/2". Typical turbulence levels in axial compressors are roughly 7–10%, [Ref. 14]. Meshes with larger rod diameter, needed for higher turbulence levels, give a uniform turbulence only farther downstream. As an example Fig. 11 shows the nonuniform turbulence field measured at 20 rod diameters downstream of a screen. Meshes with larger rods could not be used due to lack of test section

space. In addition, increasing solidity beyond 0.5 can lead to jet coaliscence instability as discussed in [Ref. 13]. Thus we did not pursue the wind tunnel calibration experiments further.

Several other schemes [Ref. 15,16] were then considered and it was found that free (round) jet give a wide range of turbulence levels from zero, in the potential core, to about 25% in the self-preserving region. In that region the turbulence level remains constant for roughly 10 diameters so that this configuration is useful to provide the external flow for the calibration experiment.

The calibration experiments were carried out using a 1" diameter free jet. Hot wires were used for all velocity measurements. Before starting the investigation on ethylene spreading several tests were run to ensure that the flow issuing from the jet confirmed to measurements documented in the literature [Ref. 12,17]. Fig. 12 shows measurements of the jet velocity profiles at several axial locations. Fig. 13 shows the variation of jet centerline velocity as a function of distance from the orifice and fig. 14 gives the turbulence level on the centerline of the jet. Turbulence intensities along lines that make constant angles with the jet axis also are shown in Fig. 14. All these measurements are consistent with those reported in the literature cited.

The integral length scale λ in a turbulent flow with an average velocity U and a fluctuating component of u' is given by :

$$\lambda = U \int_0^\infty f(\tau)\, d\tau \quad \ldots\ldots\ldots\ldots\ldots\ldots (8)$$

where the function $f(\tau)$ is the autocorrelation at time τ given by :

$$f(\tau) = \frac{\overline{u'(t)u'(t+\tau)}}{\overline{u'(t)u'(t)}} \quad \ldots\ldots\ldots\ldots \quad (9)$$

Autocorrelations were measured at four locations on the axis of the jet at x/d = 25, 29, 33, 37. Fig. 15 shows $f(\tau)$ as a function of τ at x/d = 25. The same figure also includes the integral length scale λ as a function of distance from the jet orifice. In the region investigated the length scale changes only by less than 10% (from 5cm. to 5.5cm).

Probes for injecting and sampling ethylene were made from high strength steel tubing of several different diameters. The tube was heated and bent 90 degrees to give an 'L' shaped probe. Care was taken to ensure that a proper radius was given at the bend to avoid excessive contortion of the passage. According to [Ref. 3] 'L' shaped probes were as good as any other probes they tested so that other shapes were not investigated.

Ethylene was injected into the jet along its centerline through probes of different diameters and streamwise arm lengths. The ethylene was sampled 2" downstream (typical rotor and stator chords in the multi-stage compressor are roughly 2 and 1.2 inches). The sample was fed into a flame ionization detector (FID), and concentration curves were plotted.

Concentration and velocity profiles of the injected ethylene were measured 2" downstream with the jet shut off. The ratio of their half widths was calculated to be 1.22, which gives a turbulent Schmidt number of 0.67; the generally accepted value of this number for gases is 0.7, [Ref. 17]. This test was necessary to ensure that the half concentration widths measured in the experiment were sufficiently accurate to be used in the following

calculations of mixing coefficients.

I) EFFECT OF INJECTION PROBE DIAMETER ON SPREADING:-

Fig. 16 shows the observed ethylene spreading for injection probes of three different diameters. The peak concentration observed was different in each case, the widest probe giving the maximum. However, when the radial variation of ethylene concentration is normalized by its peak, the spreading rates collapse to essentially a single curve, as would be expected. This result confirms that the nature of spreading is independent of injector diameter if the latter is small compared to the transverse scale of the external flow.

Data presented in Fig. 16 show some scattering of the concentration measurements at 0.909 and 1.0 inches from the axis. This is because of the insufficient time interval over which output from the FID was averaged, 1 minute for this run. In subsequent runs the averaging time was increased to 2 minutes which proved to be sufficient.

II) EFFECT OF PROBE STREAMWISE ARM LENGTH:-

Four probes of the same diameter but of different arm lengths were tested. Though the radial variation of spreading is identical the peaks differ slightly as shown in Fig. 17. The peak given by the smallest (0.125") probe is about 4% higher than that by the largest (1"). This difference can be attributed to the thicker wake the longer probe generates and consequent higher mixing. These two results conclude that the spreading can be regarded as independent of the probe length or diameter to a good approximation.

The effect of finite diameter and length of the injector is to make the tracer gas appear as if it is originating further upstream than the actual location of the injection probe. The apparent origin was located by two methods. One was by tracing the half concentration width at several locations downstream and extrapolating towards the injector to find the point of zero half width, which is the apparent origin. The second was by measuring and extrapolating the peak concentration to give the point of 100% of injected concentration. From the first method the apparent origin was calculated to be 1.7 radii upstream of its actual position. This equals roughly 2% of spreading distance. The second method gives 1.1 radii. In mixing coefficient calculations the result from the first method was used, as it was thought to be more accurate than the other.

The effects of external velocity and turbulence levels on the spreading level were next investigated. In these measurements an injection probe of 0.041" inner diameter, 0.059" outer diameter and 0.50" arm length was used. Ethylene was injected at 2.05 lit/min which gives an exit speed of 40 m/s based on the inner diameter of the injecting probe, or 19.5 m/s when based on the outer diameter of the probe. The term "injection velocity" will refer to the latter speed (19.5 m/s).

III) EFFECTS OF EXTERNAL TURBULENCE LEVEL:-

Ethylene was injected into the jet at four axial locations.

i) At 2.25 jet diameters downstream of the orifice where the turbulence

level is roughly 3%. This region is in the potential core of the jet. As shown in Fig. 18 the spreading here is affected very slightly by external jet velocity. The observed turbulence intensity of 3% is consistent with the measurements reported by Antonia and Bilger [Ref. 18].

ii) At 10.25 diameters downstream where the local turbulence is roughly 10%. The halfwidth of concentration curves in this case is larger and spreading is sensitive to external jet velocity variations as shown in Fig. 19.

iii)&iv) At 18.25 and 28.25 diameters downstream where the local turbulence levels are roughly 18 and 25%. Again the half width increases with turbulence and is sensitive to external jet velocity changes as shown in Fig. 20 and 21.

IV) EFFECTS OF EXTERNAL STREAM VELOCITY

To investigate the effects of external jet velocity on spreading, jet velocity was varied between 5 and 60 m/s in case (iv), while the injection rate was kept constant. The half width was a minimum when the jet speed was closest to that of injection. It increases with the difference in velocities of injection and the jet, (nondimensionalized by the jet velocity). The results are shown in Fig. 21.

ESTIMATION OF MIXING COEFFICIENT:-

Mixing coefficients were calculated from equations (5) and (7) using

the half concentration widths as the measure of the radius of spreading. Fig. 22 shows the calculated mixing coefficient as a function of local jet turbulence level for two different jet velocities. Both plots show mixing coefficients, calculated from the point source model and the free jet model, as a function of external turbulence level, for values ranging from 3 to 25%.

Effects of changing the external velocity on the mixing coefficient are shown in Fig. 23. This plot gives the mixing coefficient as a function of the difference between external velocity and the injection velocity nondimensionalized by the latter, i.e. $(V_{ext} - V_{inj})/V_{inj}$.

SUMMARY OF RESULTS :-

Effects of probe characteristics on mixing were investigated. Probe diameter and streamwise arm length have no appreciable influence on mixing levels. External flow velocity and turbulence levels, however do affect the rate of spreading of the tracer gas. A free jet model has been proposed for relating tracer gas spreading to mixing coefficient.

CHAPTER 4

INSTRUMENTATION AND EXPERIMENTAL TECHNIQUES

This chapter describes the experimental facility, instrumentation, data acquisition and reduction techniques. Measurements of compressor speedline, flow angles and turbulence levels are also reported.

4.A COMPRESSOR AND RIG DESCRIPTION

The test compressor is a three stage, low speed compressor originally used to research blading concepts for Pratt and Whitney. It is described in detail by Christianson [Ref. 19] and Gamache [Ref. 20]. The compressor has a constant annulus flow path with inner diameter of 21.12 inches, outer diameter of 24 inches (hub to tip radius ratio of 0.88). Aspect ratio averages 0.8 for the rotors and 1.2 for the stators. Specifications for the design performance and blading are included in Tables 1 and 2.

All the tracer gas experiments were carried out in the build #4 configuration of the compressor. Specifications of this build are included in Tables 1 and 2. A complete description of the facility is available in either reference, and only a brief explanation is provided here.

Fig. 24 shows the compressor rig assembly. Room air enters a bellmouth through a foreign object damage screen (FOD), located approximately one compressor radius upstream of the IGV entrance. The flow passes through the compressor, out through a constant height annular section about two compressor radii in length. Downstream of this a conical throttle is used to control mass flow rate. After the throttle, the flow enters a dump plenum, and flow straighteners (consisting of two screens and a honeycomb section) before encountering an orifice plate used to measure overall flow rate. The flow then exits through a 90 degree elbow, and an exhaust fan. The fan was off and its rotor locked in all the tests described in this thesis.

4.B DATA ACQUISITION SYSTEM

The data acquisition and control system used in this thesis effort consists of several distinct parts. These are :

1) Computers : An LSI-11/23 and a Microvax-II were used to control all data acquisition, drive the two traversers and reduce and plot the results.

2) A/D Converter : A Data Translation DT2752 12 bit analog-to-digital converter was used to digitize analog data on line. Analog data were not recorded. An onboard programmable gain amplifier allowed resolution of the converter to vary between 0.5mV and 4mV depending on the type of measurement being made. All instrument calibrations were performed at same gain level as the actual measurements.

3) Real-Time Clock : A Data Translation DT2769 programmable real time clock

was used as a time base generator for the A/D conversions.

4) Filters : TSI Model 1057 signal conditioners were used to filter the high response data.

5) Traversing Unit : Two L.C. Smith trversing units were used to allow computer-controlled positioning in radial, circumferential and yaw angle motions of the hot wire sensors, cobra pressure probe and tracer gas sampling probe. This allowed a fairly automated high and low response data acquisition process. Accuracy of positioning using this unit was ±0.004 inches in radial motion and ±0.2 degrees in circumferential motion and yaw angle positioning.

6) Baratron Pressure Unit : All pressure calibrations were referenced to a high accuracy MKS Baratron electronic pressure measurement system. The differential pressure head has a range of 100 torr (1.93 psi) and pressure could be read to an accuracy of ±0.0005 inches of water. The Baratron unit had a digital output read directly by the computer.

7) Scanivalve : A scanivalve unit was used to acquire most of the pressure measurements made on the compressor. A single Spectra strain gage type transducer was mounted in the unit with a pressure range of ±5 psi. The standard deviation of its calibration was 0.05 inches of water. This corresponds to roughly 1.5% of mean dynamic pressure in the compressor.

8) Temperature Multiplexer : An Analog Devices uMAC-4000 temperature multiplexer was used to acquire all thermocouple measuremenants. Type K

thermocouples were used for temperature measurements.

9) Torque Meter : A Lebow 1105-5K skip-ring torque meter is used for torque measurement. The meter is an integral part of the drive train, located between the compressor and the output of the speed increasing drive belt assembly. The torque meter also contained a sixty tooth gear used to measure RPM of the compressor.

4.C EXPERIMENTAL TECHNIQUES

1) HOT WIRE ANEMOMETRY

A single hot wire sensor was used to measure all the velocities and the correlations for length scale calculations on the free jet. An electronic linearizer was used to make the anemometer voltage output directly proportional to stream velocity, with the constant of proportionality determined through calibration.

One source of error in taking hot wire data is shifts in the calibration constant over a run time (typically 8 hours). These shifts are mainly due to dirt deposition on the wire. Typically calibration slope could shift by 7%, which introduces a $\pm 3\%$ error into velocity measurements. Temperature also affects hot wire calibration. At a typical overheat ratio of 2 (sensor operating at about 450^0F), a 20^0F temperature rise corresponds to a 1% drop in indicated velocity. Corrections to measured velocities were made by assuming that any shift in the calibration constant was linear with time.

2) MASS FLOW CALIBRATIONS

Although it is possible to use a calibrated inlet to measure flow rate while the test compressor is operating unstalled, it was more convenient to use the orifice plate pressure drop. The calibration procedure for this method was documentd by Lavrich [Ref. 21]. The form of the calibration is :

$$C_x = C_{\sqrt{}} \frac{\overline{\Delta P \rho_{op}}}{\rho} \quad \ldots\ldots\ldots\ldots\ldots\ldots \quad (10)$$

where

C_x = average axial velocity in the compressor annulus
C = Reynolds number dependent calibration constant
ΔP = the orifice plate pressure drop
ρ_{op} = the air density in the duct
ρ = the ambient air density.

3) ENSEMBLE AVERAGING

Ensemble averaging was required for all velocity measurements taken with high response instrumentation. This averaging must be done judiciously in order to not throw away important information. A signal from a probe is composed of three distinct parts. The first one is the D.C. value of the signal, the next one is a sum of all signals that occur at distinct frequencies and the last is the noise and random event portion of the signal. The third part includes turbulence and other unsteadiness of random nature. Averaging is performed to increase signal-to-noise ratio for a given measurement.

For measurements on the free jet, where the second part of the signal is absent, the difference between the total signal and the average gives the

instantaneous randomly fluctuating component (turbulence) of the velocity. However the second component was present for measurements in the compressor in the form of rotor wakes at blade passing frequency. Calculation of turbulence in this case required that along with the D.C. component this frequency be also subtracted from the total signal. A more detailed discussion can be found in [Ref. 22].

4.D COMPRESSOR PERFORMANCE

Locations of the instrumentation used in the following measurements are shown in Fig. 25. Inlet and exit total pressures were measured with rakes of kiel head total pressure probes at four circumferential locations. Inlet and exit static pressures were measured at both inner and outer radii at four circumferential positions. Interrow static pressure taps were located on the outer wall at a single circumferential location. Temperatures were measured with type K thermocouples at 50% span at each interblade position. All pressure measurements were made using the scanivalve unit. Overall performance was also measured by a direct differential pressure measurement with the Baratron unit.

Inlet total to exit static pressure difference, normalized by mean blade dynamic pressure, is a useful performance measure. The total to static pressure coefficient is defined as :

$$\psi_{ts} = \frac{P_{s9} - P_{t2}}{0.5\rho U^2} \quad \ldots\ldots\ldots\ldots\ldots\ldots\ldots \quad (11)$$

where the numbered subscripts refer to axial measurement stations shown in Fig. 25.

Normalizing data by this factor, for low tip Mach numbers, the data at different speeds collapse sufficiently to a single curve. Total to static pressure rise coefficient versus flow coefficient data is shown in Fig. 26. Data were taken at three different rotational speeds : 1200, 1800, 2400 RPM giving a Reynolds number range of 0.83×10^5 to 1.66×10^5 based on average blade chord, and a tip Mach number range of 0.11 to 0.22.

Flow angles behind each rotor were measured using a self-nulling cobra probe at several spanwise locations. The cobra probe consists of three total pressure taps. The outer two holes are perpendicular to each other and the middle one bisects the angle between them. The pressure difference between the two outer probes is sensed by a pressure transducer and an actuator rotates the probe until the pressure difference is nulled. Fig. 27 and 28 show the flow angles at design point flow and at a higher loading.

Turbulence levels (the fluctuating part of the velocity signal as defined in the ensemble averaging technique) were measured in front of each of the three stators and the IGV at mid-pitch locations. Fig. 29, 30 and 31 show the turbulence levels for design point flow and at a higher loading upstream of the three stators respectively.

A detailed description of the results of the tracer gas experiments in the compressor is included in the next chapter.

CHAPTER 5

TRACER GAS EXPERIMENT

This chapter describes the tracer gas experiment carried out on the low speed compressor. Measurements were taken at design point (flow coefficient = 0.5) and at an increased loading (flow coefficient = 0.42). These two points were marked on the compressor speedline in fig. 26.

5.A ETHYLENE INJECTION AND SAMPLING PROCEDURE

Ethylene was injected at selected locations in the compressor flow field and detected downstream. The sampling probe was traversed in a grid like network of span and pitchwise locations. The concentration output of the FID was then reduced to a set of contour plots, one set per each injection. The contour plots of constant ethylene concentration are used to display the spreading patterns of ethylene in the sampling planes.

As mentioned earlier, one aim was to investigate the evolution of the mixing process. This meant that spreading was to be observed across each of all three stators, all three rotors and all three stages individually. In each case ethylene was injected at various spanwise locations, some close to the endwalls and some in the mid-span region so that effects of both secondary flows and turbulence could be looked at. The pitchwise location of injection

was found to be unimportant when spreading across a rotor was investigated. For observations across stators and IGV, injection was done at several pitchwise locations.

The injection probe was mounted on a L.C. Smith actuator, driven by a computer, with radial and yaw motions. In all the cases discussed above injection was done 1mm upstream of the leading edge plane of the respective blade row and sampling was accomplished 1mm downstream of the trailing edge plane of the corresponding blade row. (For reference 1mm corresponds to roughly 3% of stator chord, 2% of rotor chord and 5% of IGV chord.) The sampling probe was mounted on a second actuator with radial, circumferential and yaw motions, though only two motions can be performed at any one time. This actuator was also automated.

At each injection location the direction of injection was adjusted to align with that of the local flow using a three head cobra probe discussed in chapter 4. The speed of injection was matched with the local flow speed. Local velocity was measured using the middle head of the cobra probe for total pressure and a linear interpolation between the outputs of the static pressure taps on the hub and the casing. Velocity matching was not possible for injections close to end walls (within 6% of the span), because at these velocities ethylene flow was smaller than that necessary for good FID and flowmeter resolutions.

Similar flow angle adjustments were made in sampling probe positioning also. The was not completely nulled owing to the large number of data points and time involved. Nulling typically takes about 10 iterations and 30 seconds.

Only the first two iterations were allowed during sampling. The sampling probe was connected to a suction pump and the suction rate was kept a constant for each injection. No velocity matching adjustments were made during sampling since the sensitivity of the FID changes with the sample flow rate as discussed in chapter 2. However, Wisler et al [Ref. 5] tested sampling at several different rates and reported that the suction speed did not significantly alter the measurements.

The settling time of the FID was greatly decreased compared to the free jet experiments, because the FID could be placed much closer to the sampling probe, and thinner tubing could be used to carry the sample from the probe to the FID. Settling time was roughly about 15–20 seconds.

The probes used for injection and sampling were picked from those tested in chapter 3. As mentioned in that chapter all the probes were 'L' shaped. The probe selected for injection had a streamwise arm length of 1/8 inches, inner diameter of 0.023 inches and a wall thickness of 0.01 inches. The sampling probe was of the same arm length and had a diameter of 0.033 inches and a wall thickness of 0.012 inches. Volume flow rate, based on outer diameter, is denoted by injection speed, or sampling speed.

The sizes of the radial and circumferential movement increments of the sampling probe were dictated by the relative change of ethylene concentration with position. If the ethylene concentration increased or decreased rapidly, sampling probe movement increments were decreased in length; this was necessary in the vicinity of maximum ethylene concentration.

5.B DATA REDUCTION PROCEDURE

Data for concentration contour plots were acquired by recording the voltage output from the FID and the radial and pitch positions of the sampling probe relative to a reference point. The voltage output of the FID was converted into concentration using a calibration curve. One contour plot was made for each injection point, requiring roughly an hour of data taking. The contours were plotted on a background grid which is in the shape of a passage between two adjacent blades in a blade row. (Note that the pitch differs from one blade row to another.) All contours were plotted on a grid of 100 units in span and 100 units for convenience. A polynomial interpolation routine was used in plotting to generate points of desired concentration.

At flow speeds in the compressor, and distances over which spreading was observed, molecular diffusion of ethylene into air can be assumed to be negligible [Ref. 23]. (The diffusion length is roughly 0.5% of the convected distance.) Thus, the movement and spreading of ethylene are solely due to the action of the compressor flow and turbulence.

5.C RESULTS OF ETHYLENE TRACING MEASUREMENTS

Fig. 32 and 33 show contour plots for spreading across the first stator, at design point and at increased loading respectively. The next two figures, 34 and 35, show the contour plots for the first rotor at the two flow conditions. Since these contour plots are similar to those of the other rotor stator rows (as will be shown) we can discuss them as representatives of the situation throughout the compressor.

Consider the spreading due to injection at mid-span, mid-pitch location in front of the first stator at design point in Fig. 32. The contours are almost circular with centers moved towards the suction side by roughly 2% of the pitch. This movement of the core, though small, is present in all three stators. It is probably due to the pressure difference between the pressure and suction surfaces of the adjacent blades. The symmetric spreading of ethylene can be attributed only to turbulent diffusion. Contour plots due to injections at 25% and 75% of span at mid-pitch are also remarkably symmetric. Thus it seems that in the mid-passage region only turbulence is the cause of ethylene spreading.

Contours close to the blade surfaces or to the end walls are distorted. One can not say, just from the contours, whether the distortion is due to secondary flows or anisotropies in turbulence. A qualitative analysis can however be provided by scaling the one-dimensional diffusion equation. The differential equation is :

$$u\frac{\partial u}{\partial x} = \epsilon\frac{\partial^2 u}{\partial y^2} \quad \ldots\ldots\ldots\ldots\ldots\ldots \quad (12)$$

where 'u' is the velocity in a direction 'x', which is perpendicualar to 'y' and 'ϵ' is the diffusion coefficient.

For a fluid particle, whose motion can be described by this equation, the time ' t ' taken to diffuse through a transverse distance 'y', during which it would have travelled a distance 'u' in the 'x' direction , is given by :

$$t = o(x/u) \quad \ldots\ldots\ldots\ldots\ldots\ldots \quad (13)$$

and also

$$t = o(y^2/\epsilon) \quad \ldots\ldots\ldots\ldots\ldots\ldots \quad (14)$$

Equations (13) and (14) applied to the contours for mid-pitch and mid-span location imply a mixing coefficient of 0.0035 m^2/s. According to Fig. 22 this corresponds to a 8% turbulence level. This number is in reasonable agreement with the measured turbulence level for this location, which from Fig. 29 is 6%. The analysis is consistent with measurements, and the implication is thus that, at this location, spreading is due to turbulent diffusion.

These arguments can be applied to a set of distorted contours, say 90% span and 45% pitch. These yield a mixing coefficient of 0.008 m^2/s. According to Fig. 22, based on the free jet model discussed in chapter 4, this corresponds to a 18% turbulence level. However, the measured turbulence level for this location, from Fig. 29, is 10-11%. This implies that some other mechanism (secondary flows and/or anisotropies in turbulence) must be involved to account for the mixing at this location. In other words, at this location contributions from turbulence and other effects are of similar magnitudes.

At increased loading the wakes become thicker and the turbulence level increases. Contours at increased loading show increased spreading as seen in Fig. 33. This is true for both the more symmetric and the distorted

contours. The growth of the symmetric contours can be attributed to a rise in the overall turbulence level in the compressor, which increased by about 4% to 10%. At increased loading secondary flows also become stronger, e.g. more tip leakage due to higher blade loading, thicker hub and casing boundary layers. This results in increased distortion of the tracer gas contours.

Fig. 34 and 35 show contour plots for injection in front of the first rotor. These contours show more spreading pitchwise than spanwise primarily because of the rotation of the blade row. Secondary flows seem to have less effect on spreading across a rotor than for a stator even for injections made fairly close to the end walls.

Fig. 36 to 43 show contour plots for the second and third stators and rotors at design point and at the increased loading. We will come back to these figures shortly, but we now examine fig. 44 and 45, which are contour plots for injections made in front of the IGV at design point and increased loading, respectively. Spreading across the IGV is less (evidenced by smaller contours) than that across stators due to its smaller chord and a lower turbulence level. At increased loading mixing increased; this was unexpected. This is presumably due to larger potential disturbances from the downstream rotor.

To see how the process of mixing evolves from one stage to the next as the flow progresses through the machine spreading of the tracer gas was observed across all the blade rows of the next two stages also. These contour plots are presented in Fig. 36–43. Spreading was measured across each of the three stages also (i.e., injection was done in front of each of the three

rotors and sampling was done immediately downstream of the corresponding stator). Fig. 46–51 show these contour plots.

The central point shown by all these figures is that spreading across all the three stators looks very similar, as does spreading across all three rotors. There is little evolution of mixing from one stage to the next. Further the same conclusion can be drawn from contours plotted for spreading across a whole stage. This conclusion was independently drawn by Li and Cumpsty [Ref. 6] where it was shown that the spreading across first and second stators was similar and that the mixing coefficients were roughly the same. Note that the distortions observed in stator related contours appear to be less prominant in these plots, because they are now combined with a more uniform spreading pattern. The distortions themselves diffuse out as the flow progresses through the rotor.

Based on the contour plots, a mixing coefficient was calculated for each injection. First the average distance (radius) of each contour from its core (maximum concentration point) was calculated. Next a least square fit was obtained between concentrations of the contours and their average radii. In obtaining the least square fit each contour was wighted by the number of data points it contained. One set of points from this fit was used in equations (5) and (7) for ' C ' and ' r '. Mixing coefficients thus obtained were normalized by the product of axial velocity and the axial distance over which spreading was observed. The nondimensionalized coefficients were plotted in Fig. 52–61 as functions of span.

Fig. 62 shows the evolution of mixing in the compressor. In this figure

the mixing coefficient was plotted for four different cases for each blade row: at midspan and at end-wall for design point loading and at increased loading. The mixing coefficient was normalized independently for each blade row by local relative velocity and blade chord. (The author is grateful to Dr. Koff for this suggestion.) The difference in the magnitudes of the mixing coefficients for stators and rotors is smaller than using the previous normalization, but the rotors still have larger mixing coefficients. For reference mixing coefficients corresponding to 6% turbulence (the level measured in the mid-span mid-pitch region at design point loading) and 11% (measured near end-walls at design point loading) are also indicated.

In Table 3 normalized mixing coefficients and corresponding aspect ratios from [Ref. 10,11] were summarized along with our results. No clear trend in mixing as a function of aspect ratio can be oserved.

The next chapter gives a summary of the conclusions derived from this data. at is given. Some recommendations for future research in this field are also included.

CHAPTER 6

CONCLUSIONS AND SUGGESTIONS

The work described in this thesis consists of an experimental investigation of mixing in a three stage axial compressor. The evolution as flow progresses through the machine was examined. Research was also carried out to quantify the effects of injection probe geometry, turbulence level, injection and free stream velocity difference, and integral length scales on spreading rates of the injected species.

6.A CONCLUSIONS

Based on the tracer gas measurements the following trends in mixing in the multi-stage compressor can be inferred :

Fluid migration and mixing are the combined effects of turbulent diffusion and secondary flows. The relative importance of each of these mechanisms depends on the location in the machine.

In a stator row turbulent diffusion dominates in the midpassage region. However, near the end walls and close to the blade surfaces secondary flows can also make appreciable contributions to mixing.

Turbulence is more important in mixing across a rotor than across a stator. Thus effects of secondary flows are less noticeable in the rotor even close to end walls.

At increased loading there is more mixing in both stators and rotors. Contributions from secondary flows become more significant at increased loading.

Mixing across all three stators is very similar, as is mixing across all three rotors. There is little evidence of evolution of the mixing process. Flow distortions generated in one blade row do not affect mixing in the next blade row to any significant degree.

Mixing coefficients for rotors based on relative velocity and blade chord are in general larger than those for stators. (For the geometry examined they are roughly twice that for stators.)

Measurements of the effects of probe and external flow parameters on the spreading of the injected species show:

The length of the injection probe has little effect on the level of mixing, even when comparable to the distance over which the tracer gas was allowed to spread.

The diameter of the injection probe does not affect the spreading pattern.

Turbulence level of the external flow has a strong effect on the mixing coefficient.

The mixing coefficient changes with the velocity difference between the mainstream and the injection speed. Mixing is a minimum when both velocities are equal (with the injection velocity defined as the volume flow rate per unit area based on the outer diameter of the probe).

The integral length scale of the main stream does not affect the level of mixing strongly, at least within the range of the length scales that was investigated.

6.B SUGGESTIONS FOR FUTURE RESEARCH

The results of the present research provide some more insight into understanding the mixing process in multi-stage axial compressors. However some important issues remain unresolved. It is suggested that this process be investigated further as detailed below.

A detailed measuremnt of the secondary flow field in a blade row would be helpful in determining whether it is indeed the secondary flows that cause distortions in the tracer gas concentration contours. Once this is done a method needs to be devised to separate the effects of turbulence from those of secondary flows so they can be modelled separately, thus more accurately, using [Ref. 2] and equation (7). It is suggested that streamline tracing using three dimensional computational procedures would be useful in this regard.

The experimental results indicate that secondary flows generated in one blade row diffuse out (or mix out some other way) before the flow approaches the next blade row. Most of this must clearly be happening in the spacing between the two rows, similar to wake mixing. This process should be investigated to see how exactly this diffusion takes place and how it is affected by varying the inter-row gap.

Any kind of mixing introduces extra losses. But the mixing process in axial flow machines takes away high loss fluid from the end walls and redistributes it all over the annulus. Thus it decreases profile losses while introducing some losses of its own, the balance being to our benefit. This observation raises the question as to whether enhancing mixing by some artificial means would decrease the overall losses. If so, it is definitely worthwhile to find out by how much.

With the data presented in this thesis, mixing measurements are available for four machines. Emphasis should thus be shifted to analysis. Models that can compute the parametric dependence of the mixing coefficient on various flow parameters, e.g. loading level, blade-wake thickness, pressure gradient, etc. and machine parameters, e.g. aspect ratio, tip clearances, inter blade row gap, etc. should be investigated.

Efficient methods to incorporate mixing coefficient into through-flow calculations should devised.

Compressor Design Specifications (Bld 4)

Number of stages	:	3
Tip diameter [in]	:	24.0
Hub-to-tip radius ratio	:	0.88

Static Tip Clearance [in] (measured)

Rotor 1	0.032
Rotor 2	0.030
Rotor 3	0.034

Static Hub Clearance [in] (measured)

IGV	0.002
Stator 1	0.030
Stator 2	0.036
Stator 3	0.038

Design Average reaction	0.65
Design Flow Coefficient	0.50
Total Pressure Rise Coeff. (measured)	1.46

Table 1

Compressor Blading Design [Bld 4]

	No. of Blades	Chord [in]	Aspect Ratio	Camber [deg]	Stagger Angles
IGV	124	0.826	1.746	11.0	13.1
Rotor 1	54	1.779	0.811	17.0	44.3
Stator 1	85	1.235	1.168	27.0	26.0
Rotor 2	55	1.764	0.817	18.0	45.5
Stator 2	88	1.232	1.170	25.0	28.0
Rotor 3	49	1.996	0.722	20.0	46.6
Stator 3	90	1.235	1.168	53.0	20.5

Table 2

SUMMARY OF AVAILABLE MIXING DATA

Compressor Name	Cambridge	C106	Cranfield	General Electric	Deverson	MIT GTL Stator	MIT GTL Rotor
Aspect Ratio	2.0	1.75	1.5	1.45	1.34	1.2	0.8
Mixing Coeff. $\varepsilon/(V_a C)x10^3$	3.7	0.5	1.8	2.1	0.4	1.1	2.5

Table 3.

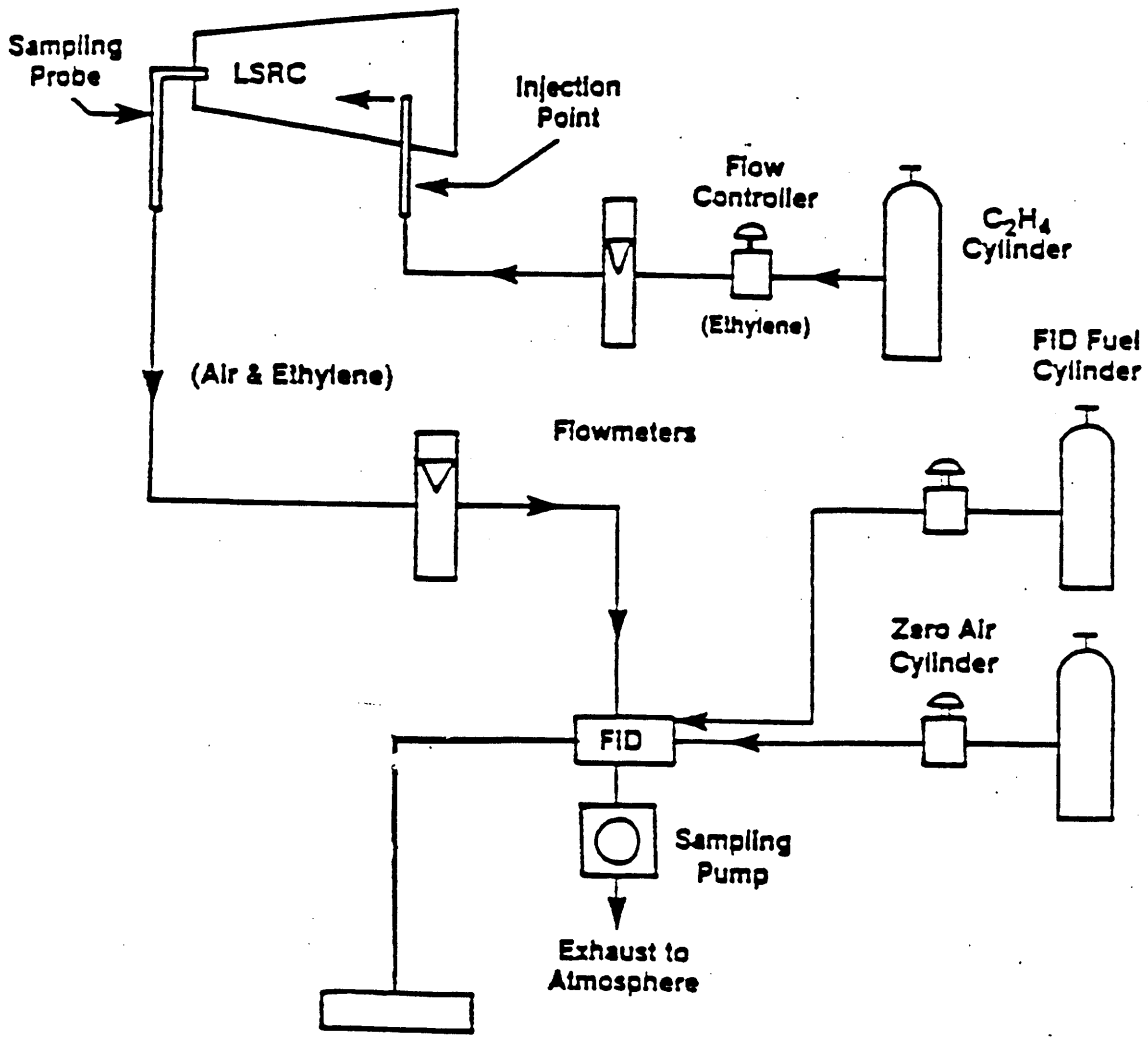

Fig. 1 Tracer Gas Detection System.

Acknwl. Denton and Usui [Ref. 6]

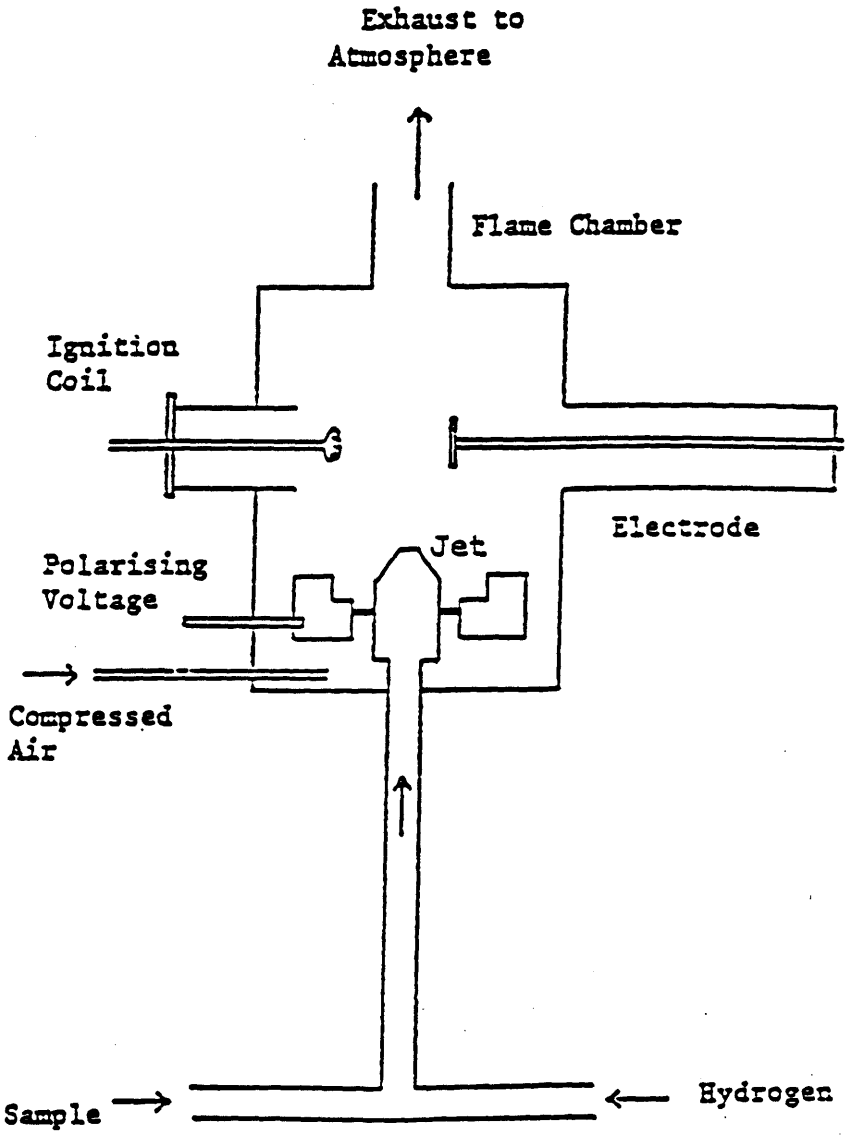

Fig. 2 Flame Ionization Detector.

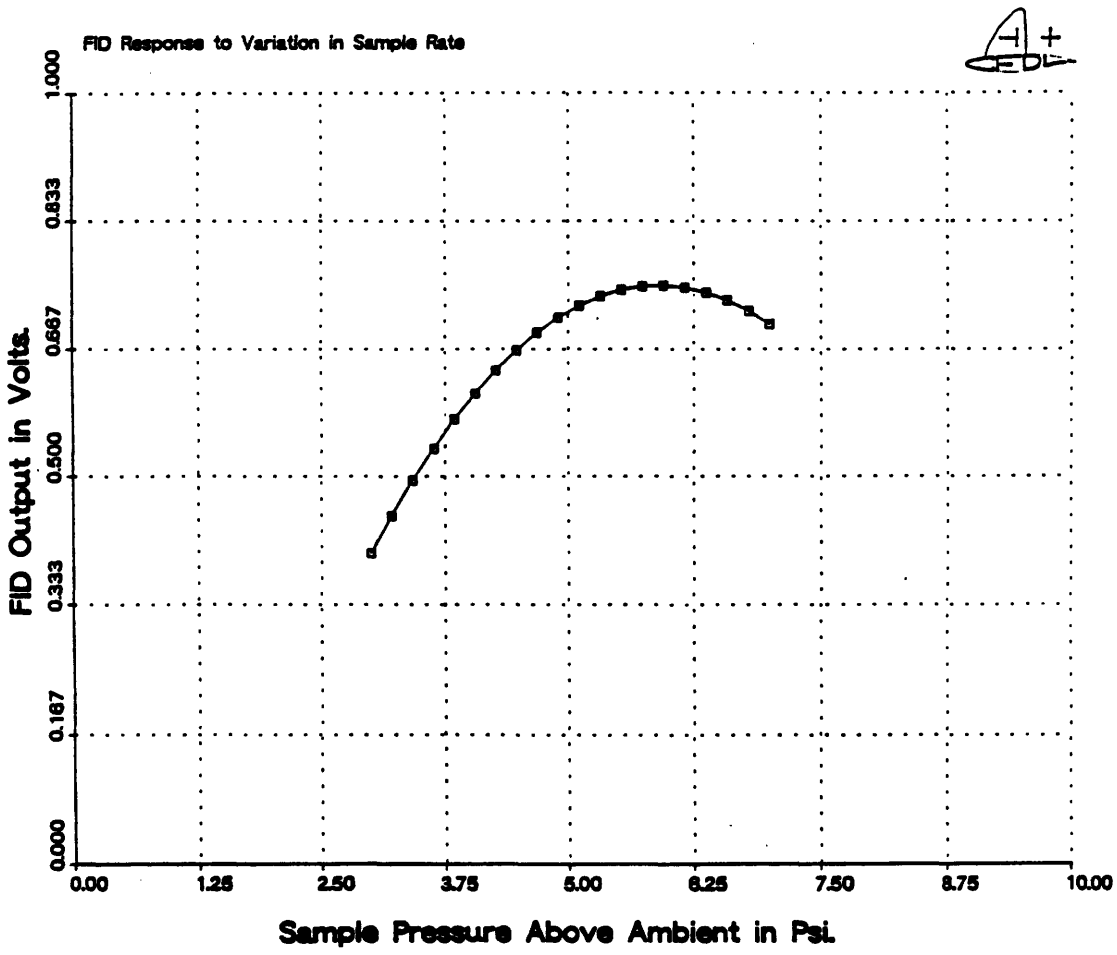

Fig. 3 FID Response to Sample Pressure Variations.

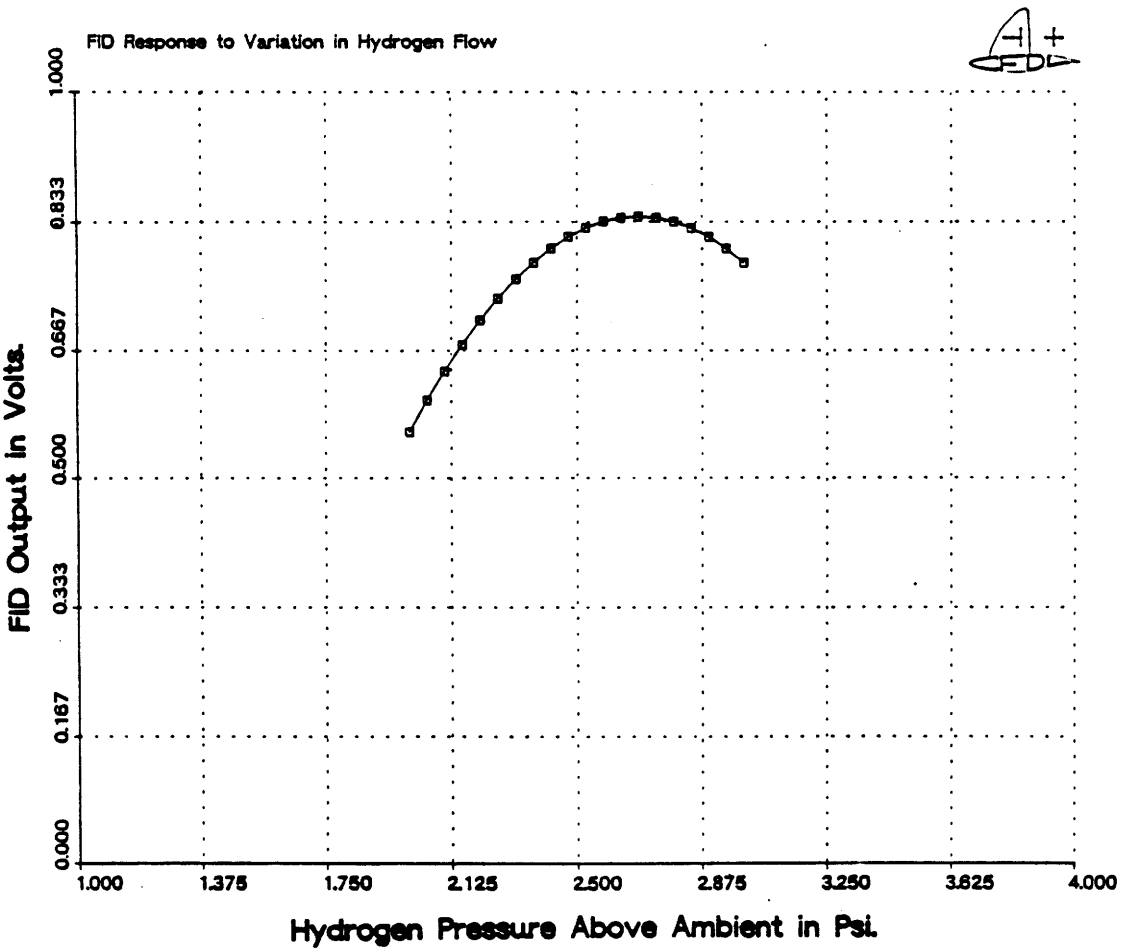

Fig. 4 FID Response to Hydrogen Pressure Variations.

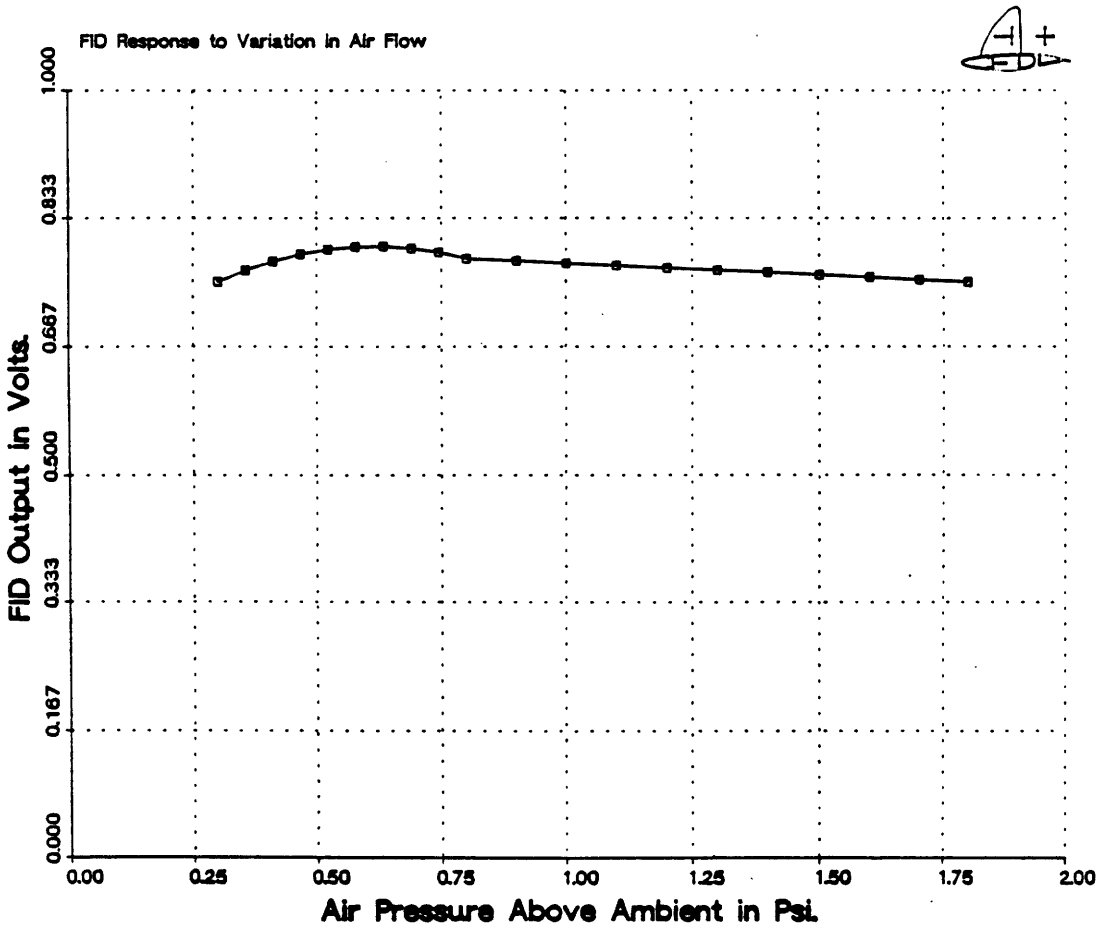

Fig. 5 FID Response to Air Pressure Variations.

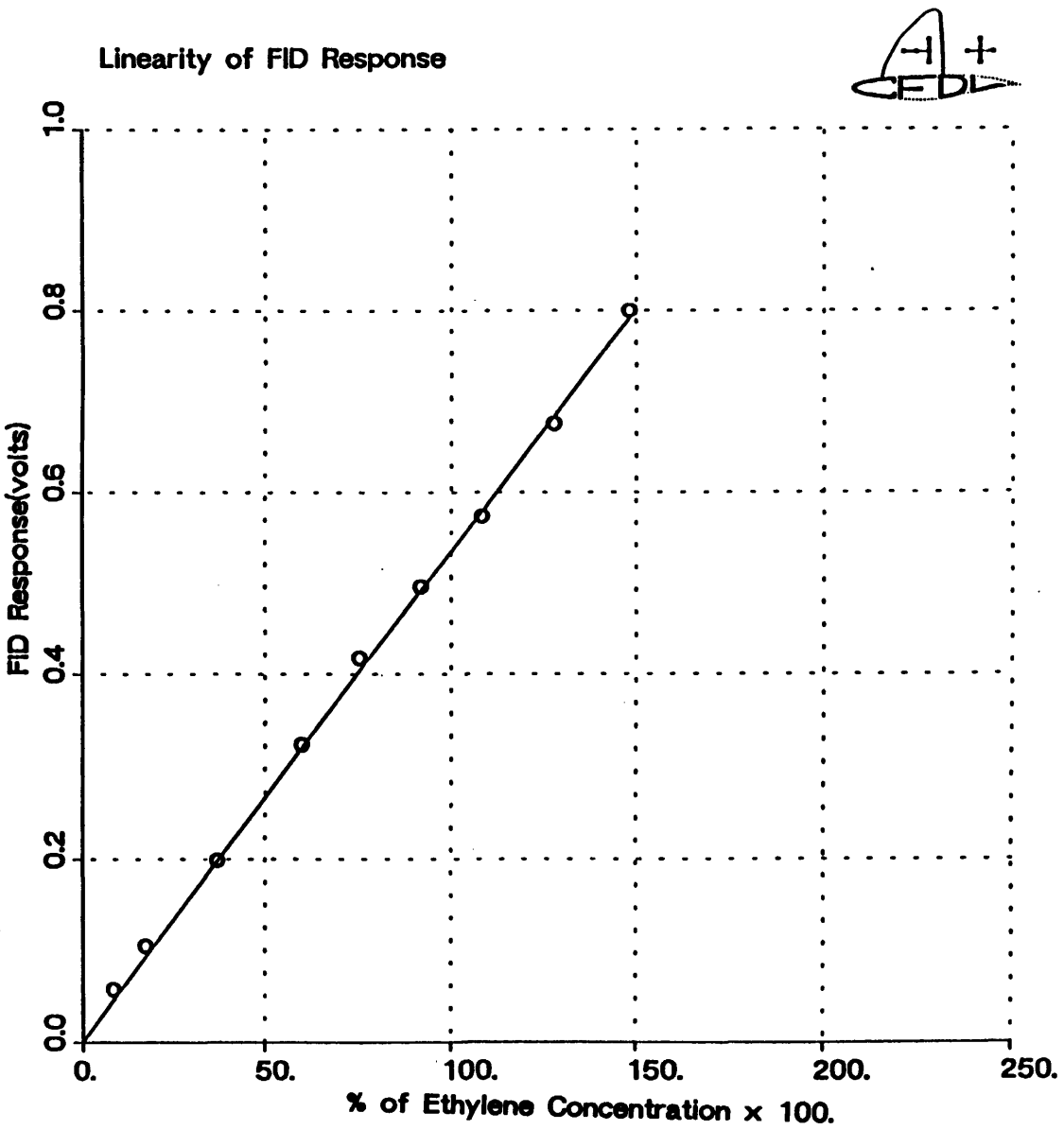

Fig. 6 Linearity of FID Signal.

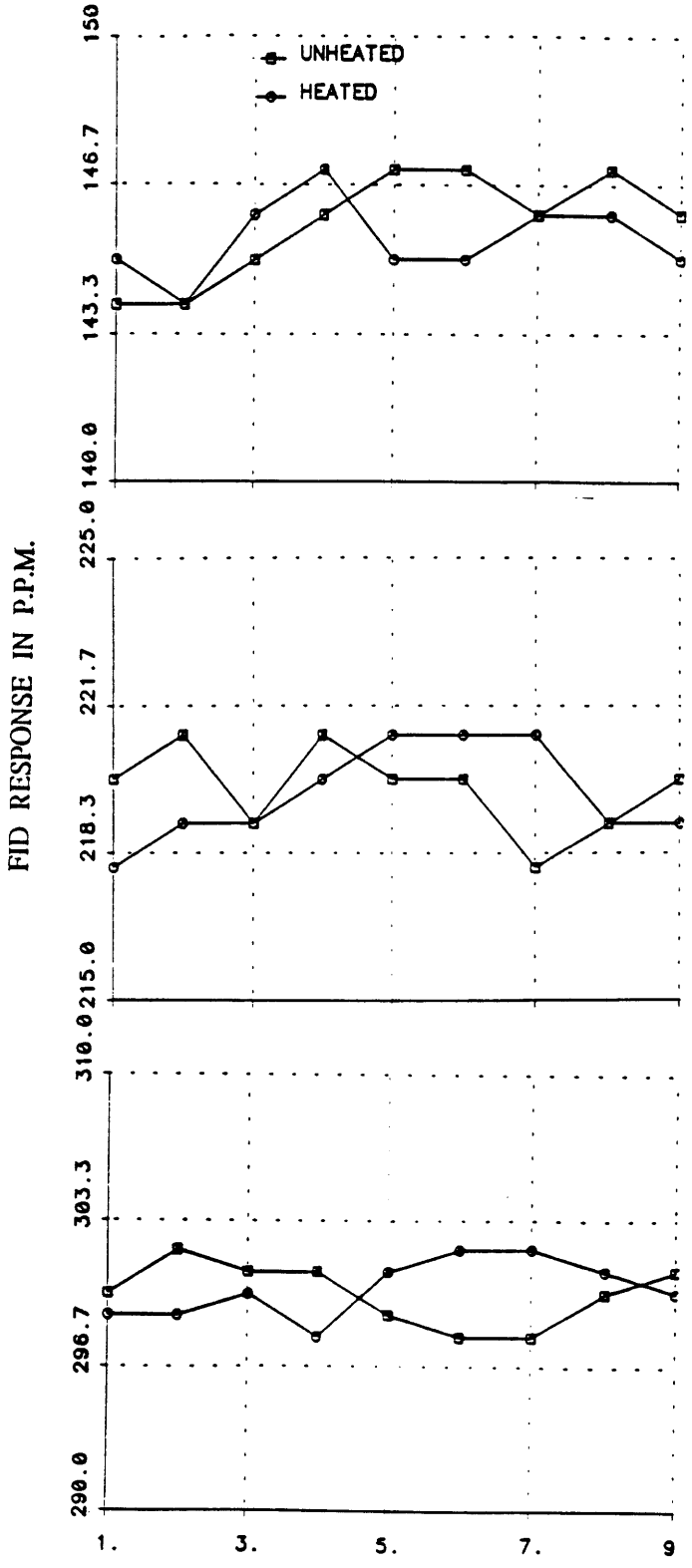

Fig. 7 *Effects of a Heated Sample-line on FID Output.*

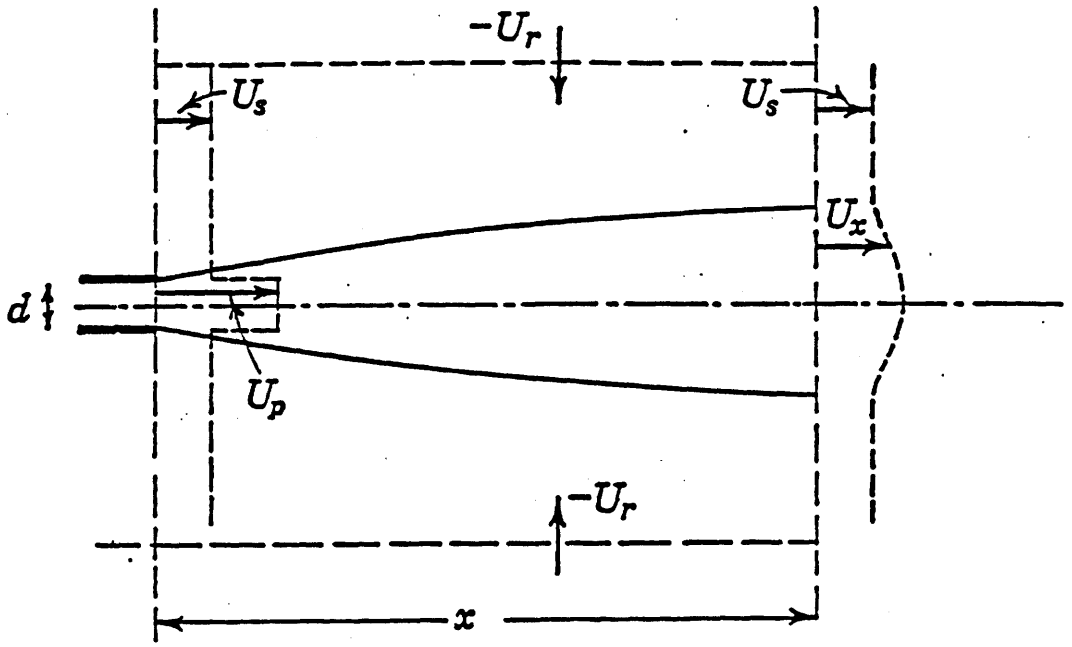

Up = *Injection Velocity*

Us = *External Stream Velocity*

Ux = *Total Axial Velocity*

Ur = *Radial Velocity*

d = *Jet Diameter*

Fig. 8 Schematic of Injection from a Jet into a Uniform Stream.

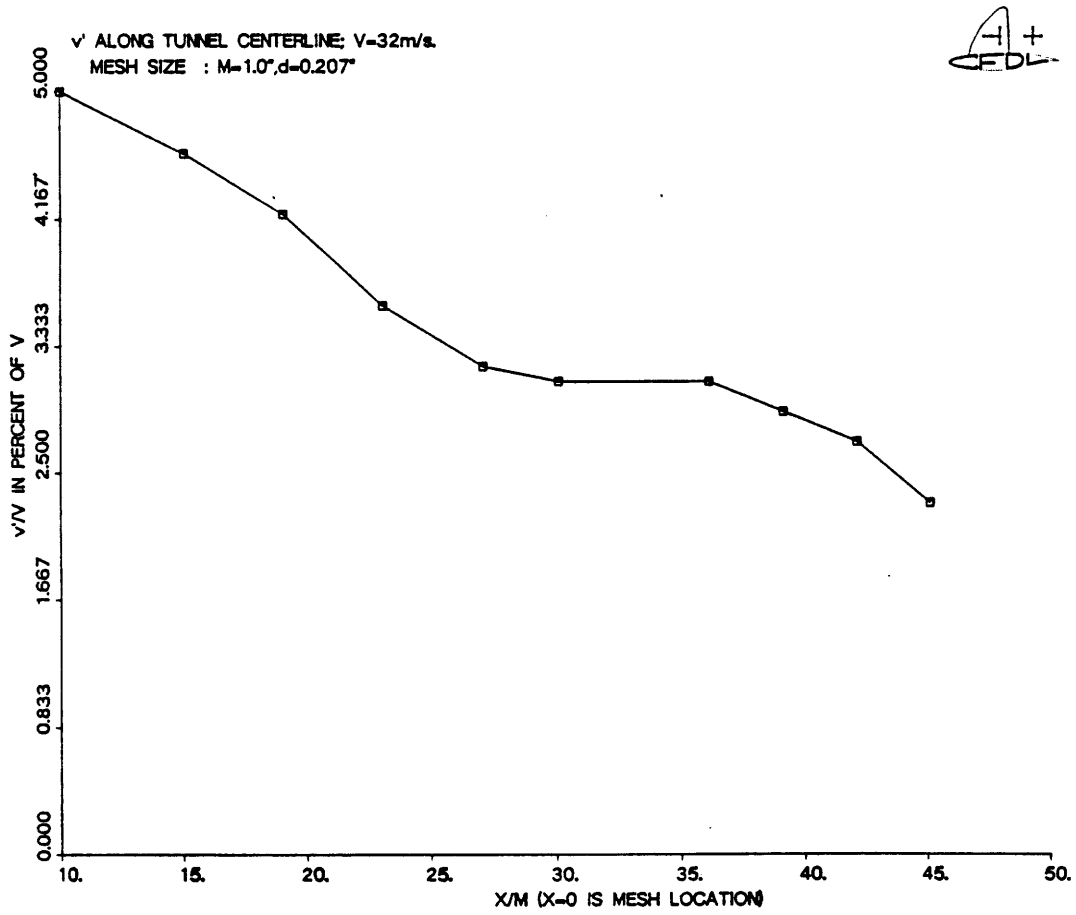

Fig. 9 Streamwise Variation of Turbulence Intensity in a Wind-tunnel Fitted with Screens.

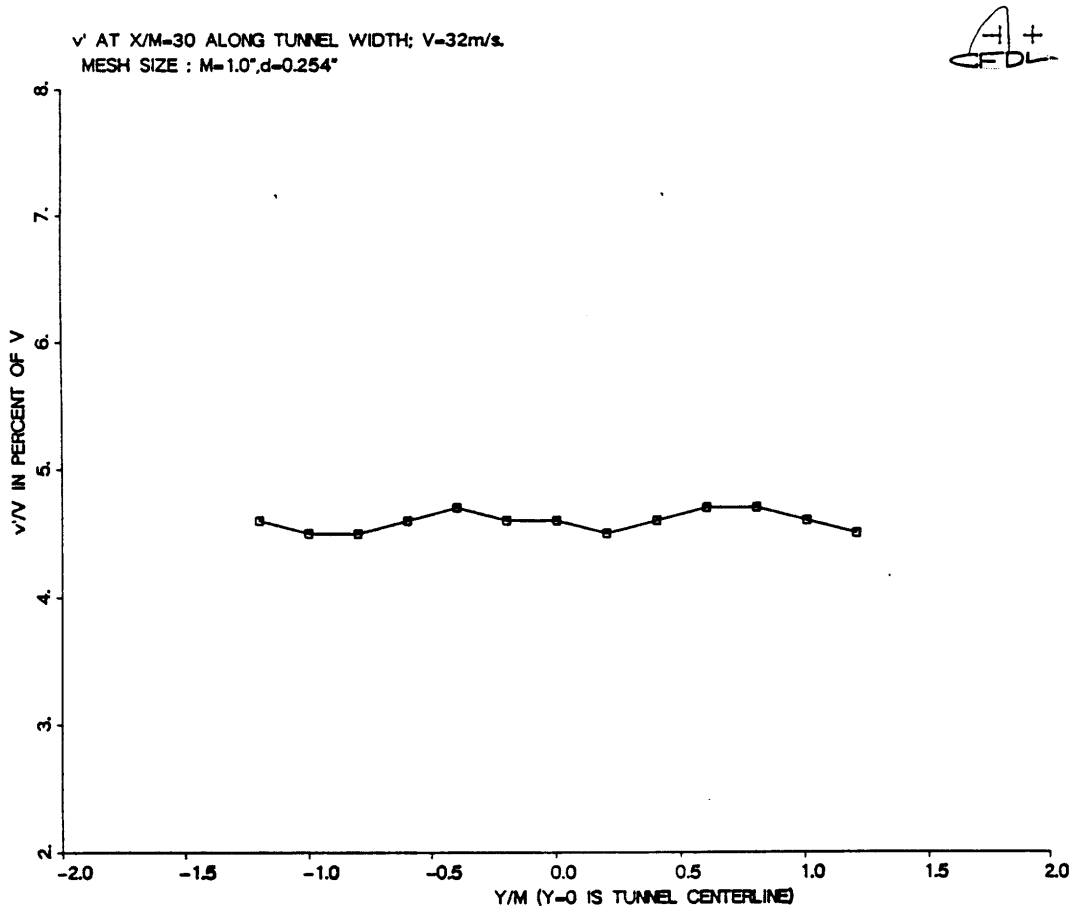

Fig. 10 Highest Turbulence Level Achieved in Wind-tunnel.

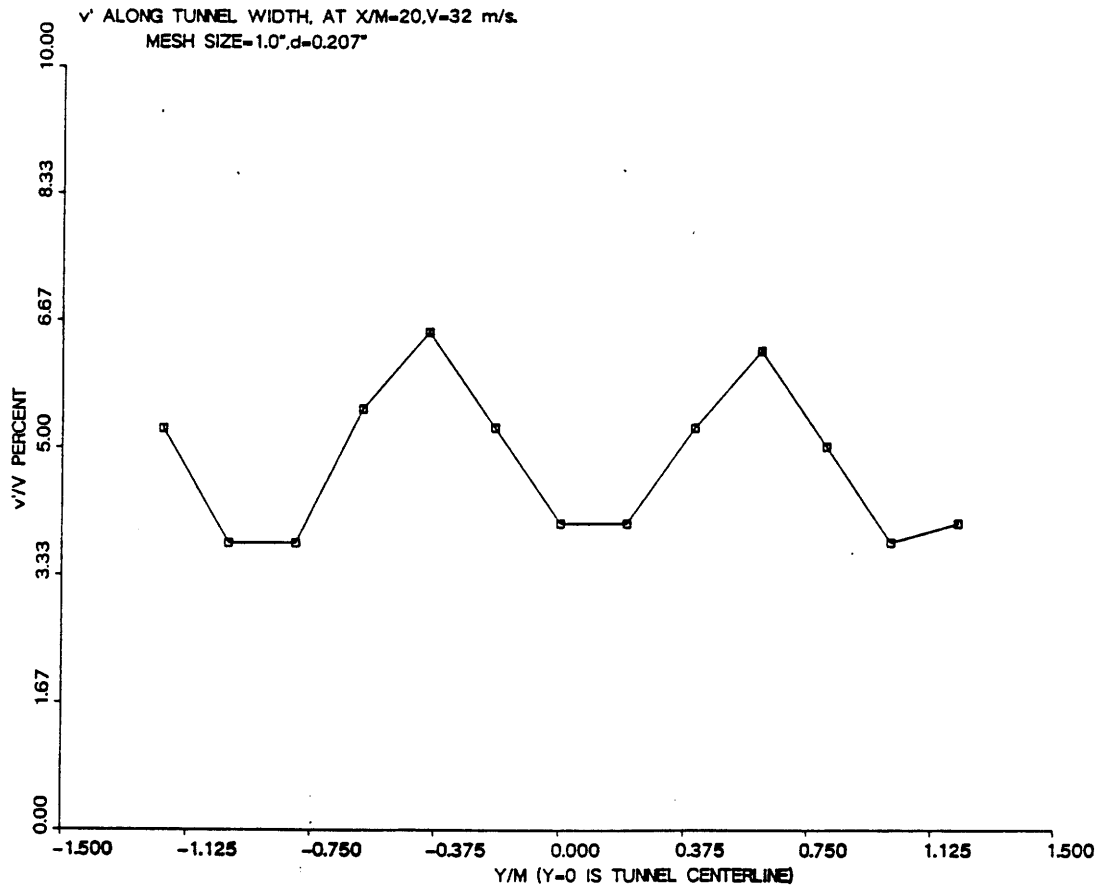

Fig. 11 Profile of Nonuniform Turbulence Intensity.

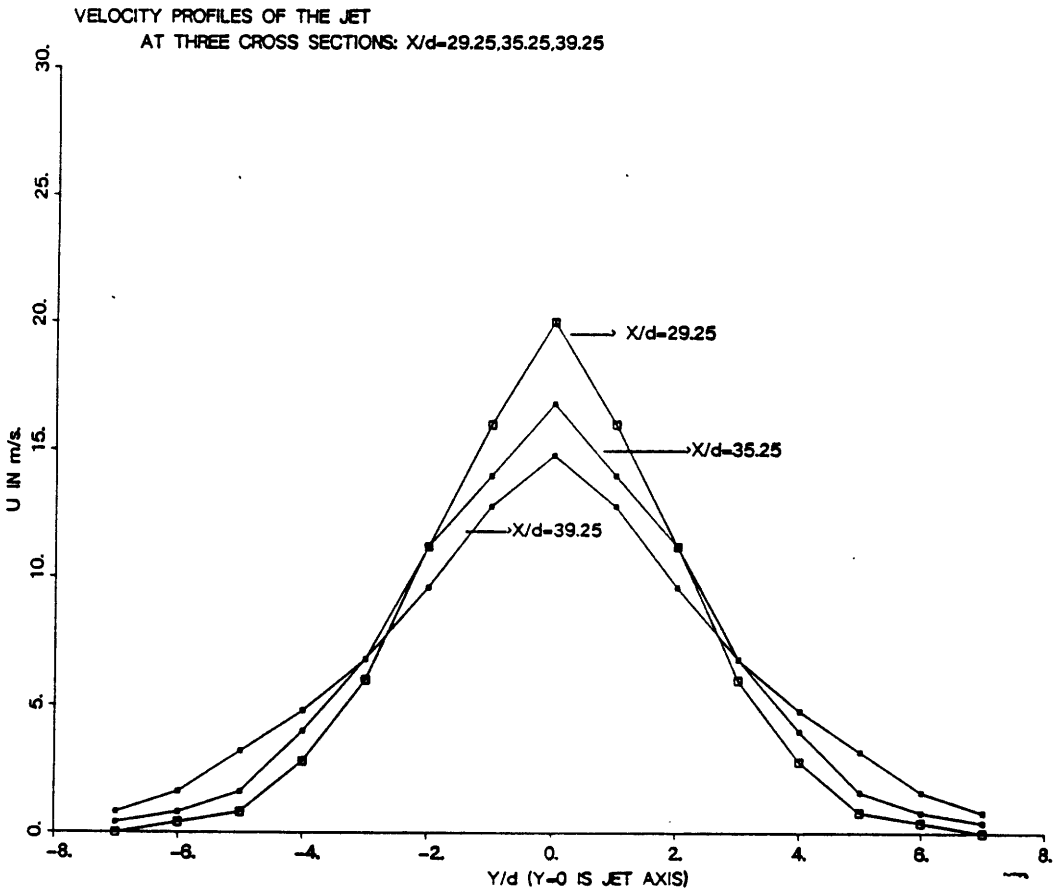

Fig. 12 Test of Symmetry of the 1" Round Jet.

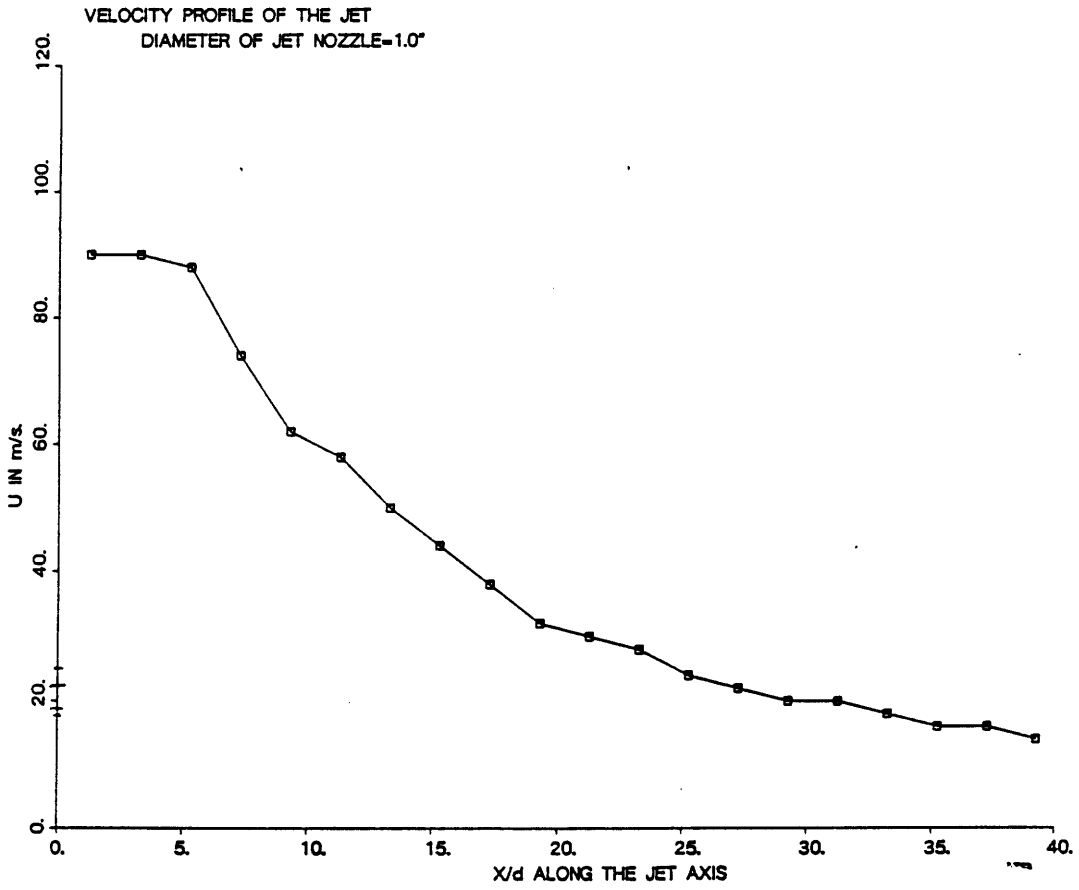

Fig. 13 Velocity Profile of the Jet.

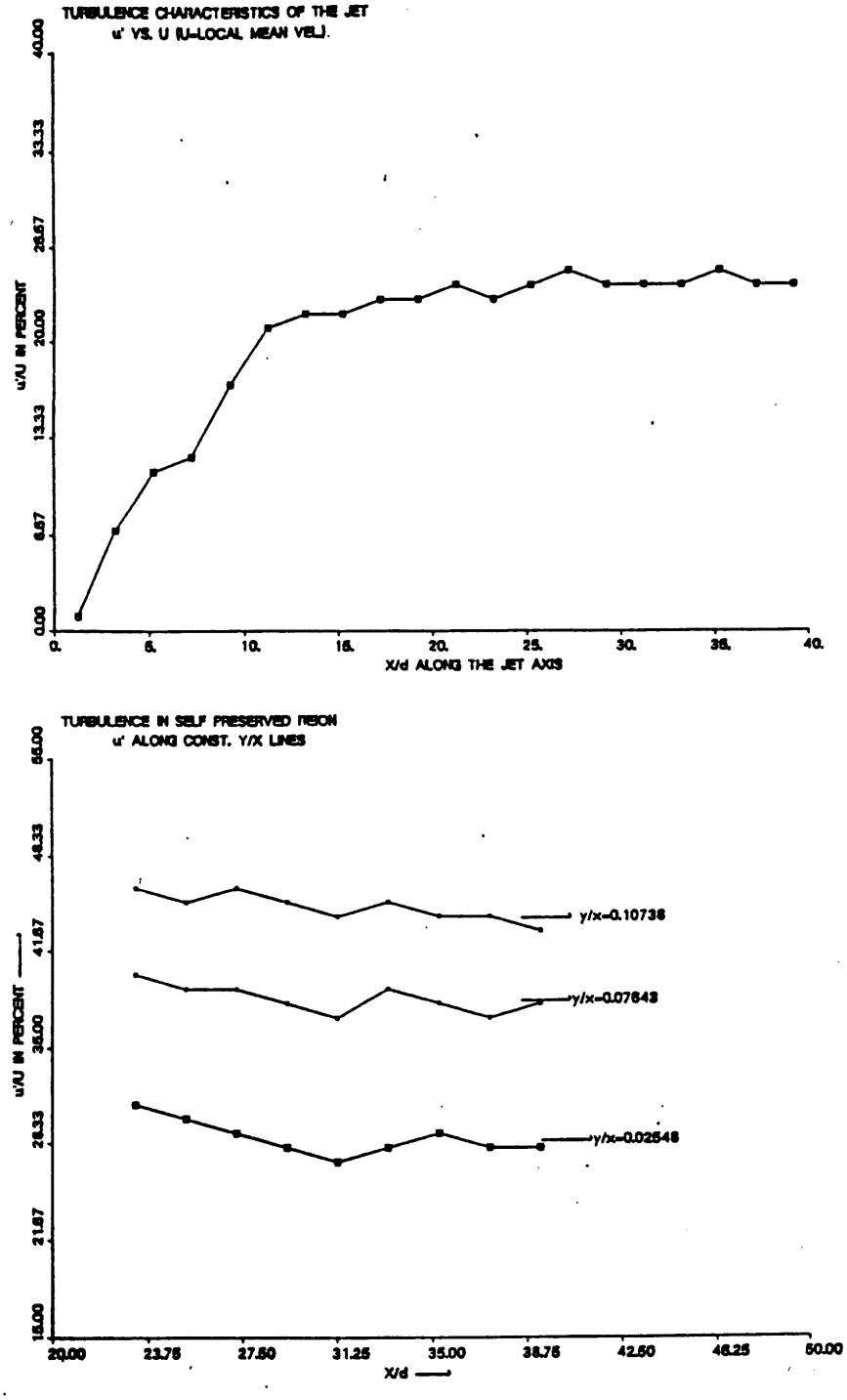

Fig. 14 Turbulence Intensity in the Jet.

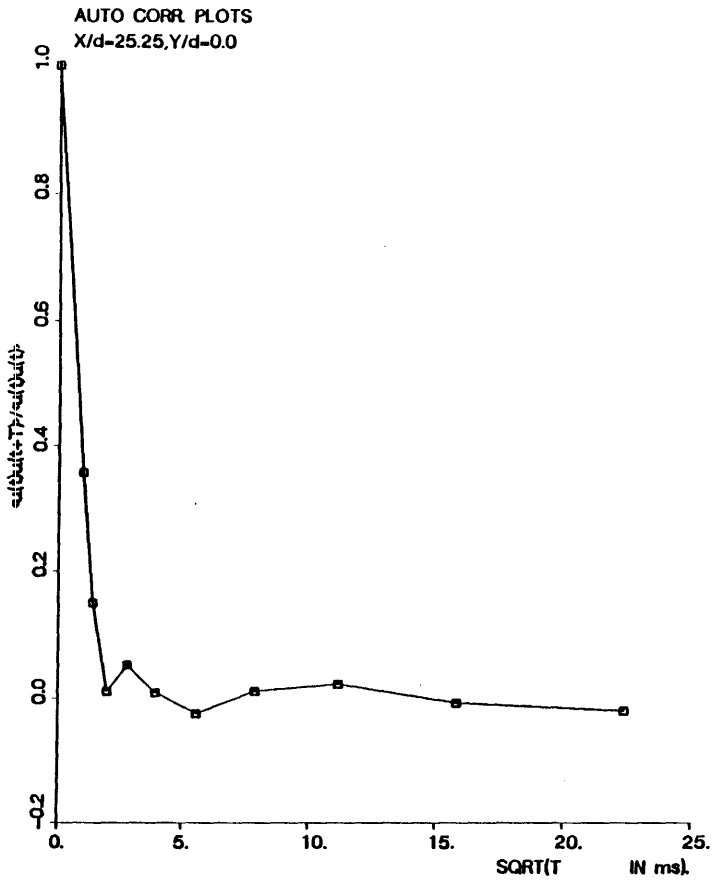

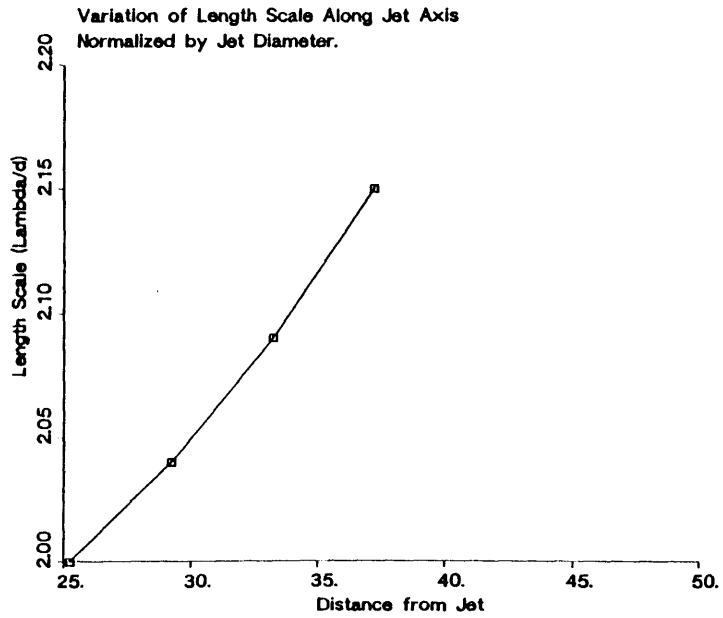

FIG. 15 Length Scales in Similarity Region of the Jet.

V(JET)=20M/S; V(INJ)=20M/S; X(INJ)/D=28.25; L(INJ)=0.5"

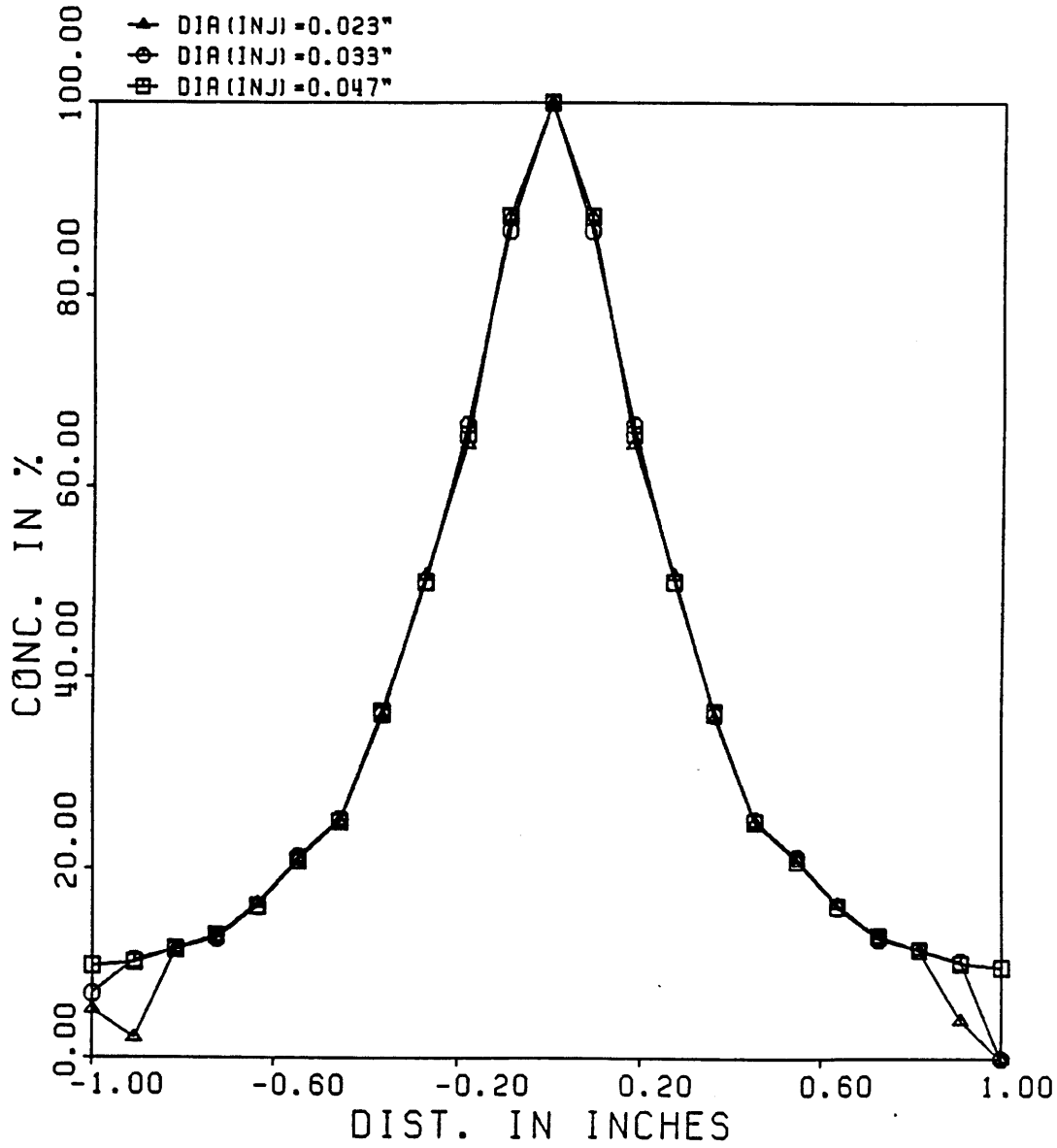

Fig. 16 Effect of Injection Probe Diameter on Tracer Gas Spreading.

V(JET)=20M/S; V(INJ)=20M/S; X(INJ)/D=28.25; DIA(INJ)=0.041"

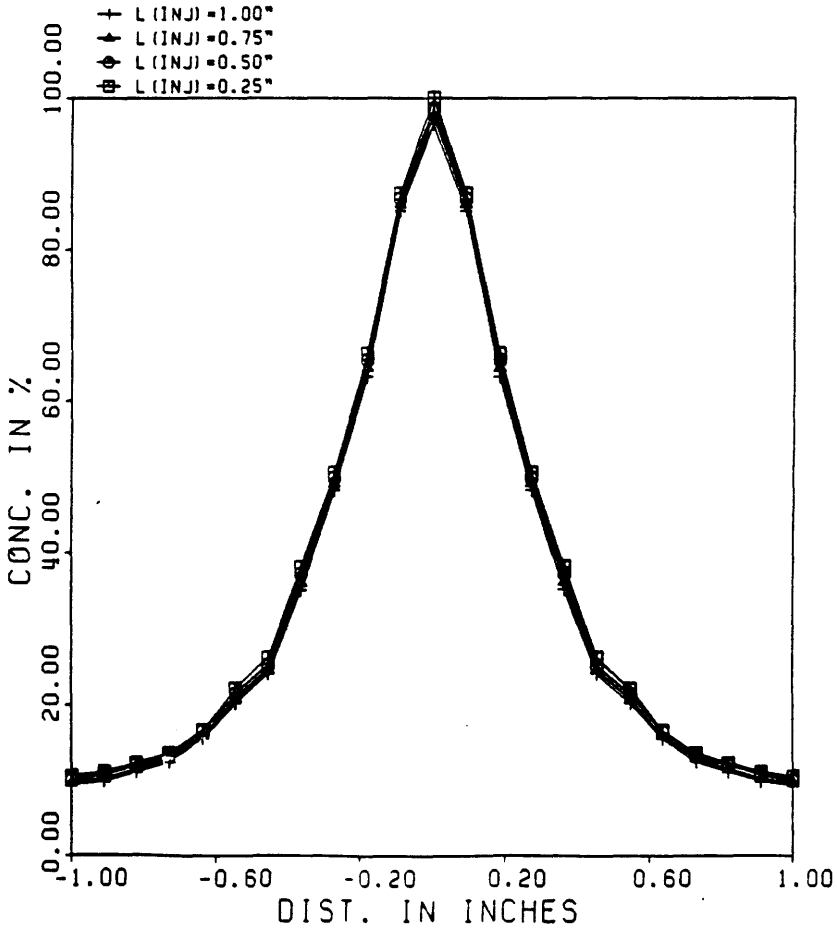

Fig. 17 Effect of Injection Probe Length on Tracer Gas Spreading.

Potential Case

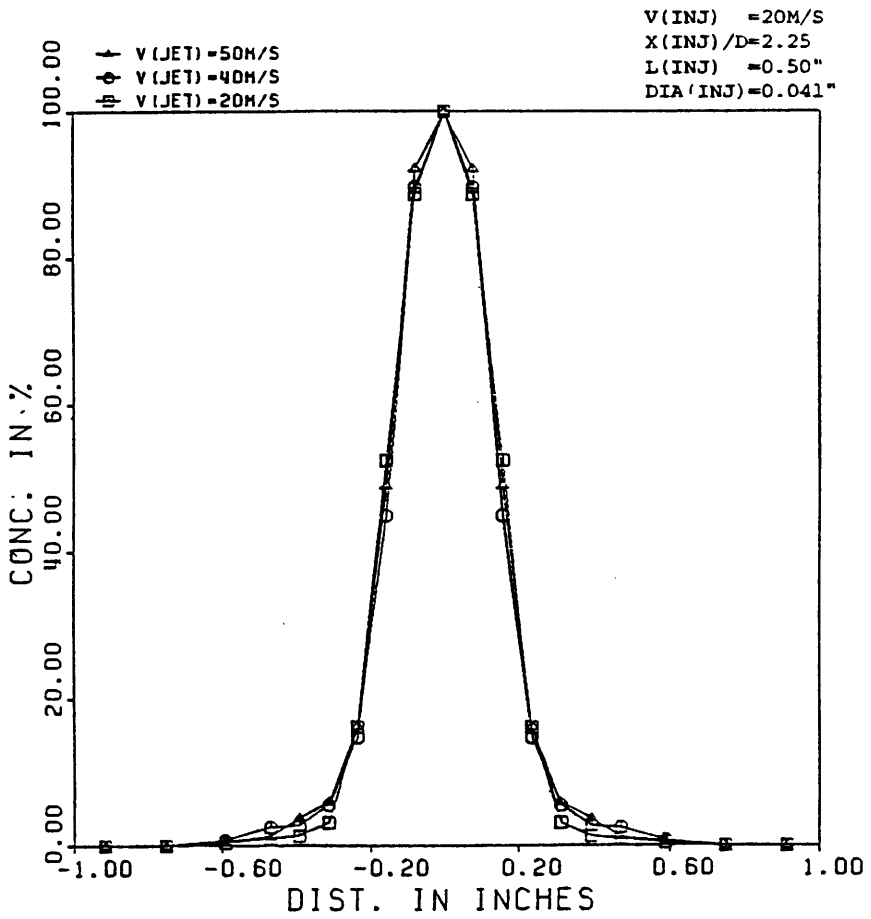

Fig. 18 *Effect of Turbulence on Tracer Gas Spreading; Case-I : Potential Flow*

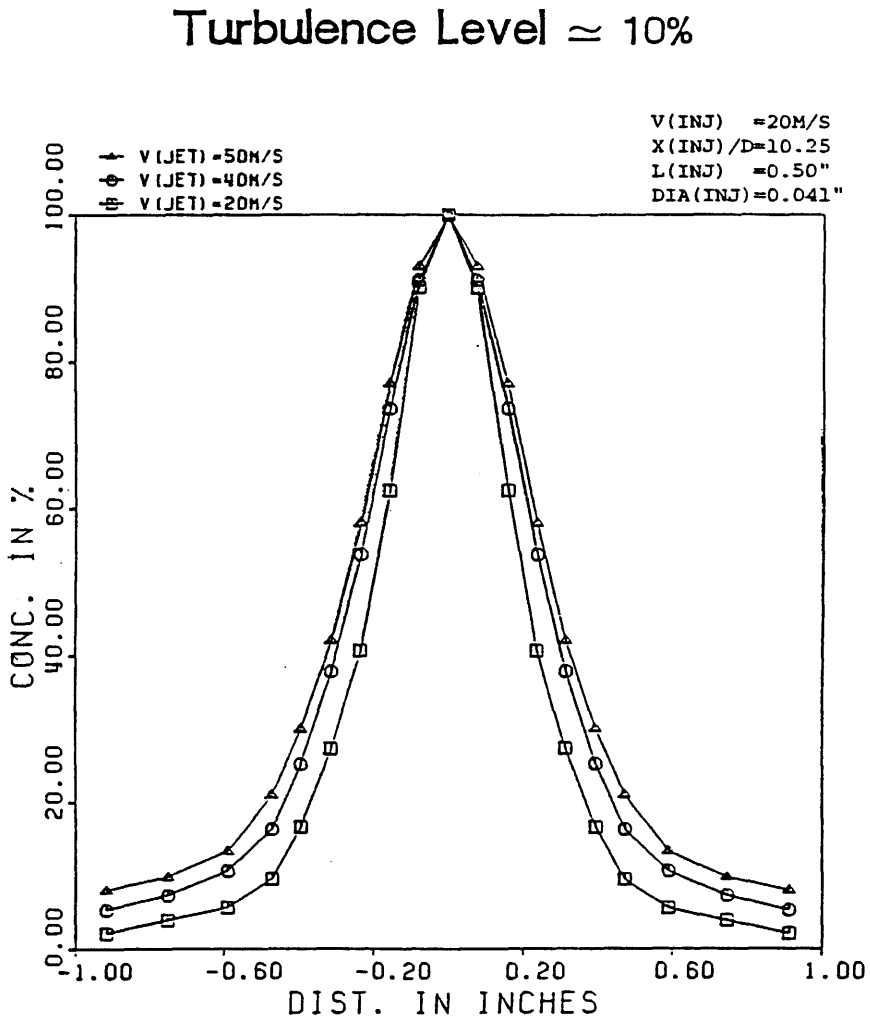

Fig. 19 *Effect of Turbulence on Tracer Gas Spreading; Case-II : 10% Turbulence*

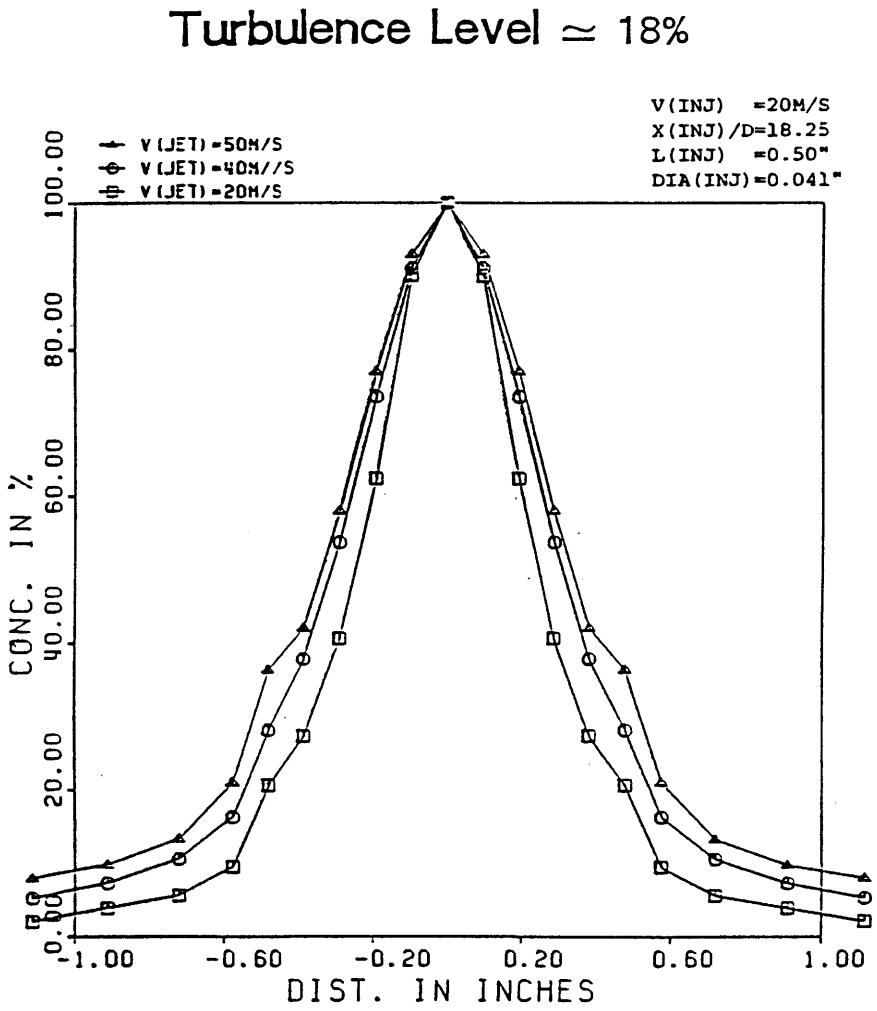

Fig. 20 *Effect of Turbulence on Tracer Gas Spreading; Case-III : 18% Turbulence*

V(INJ)=20M/S; X(INJ)/D=28.25; L(INJ)=0.50"; DIA(INJ)=0.041"

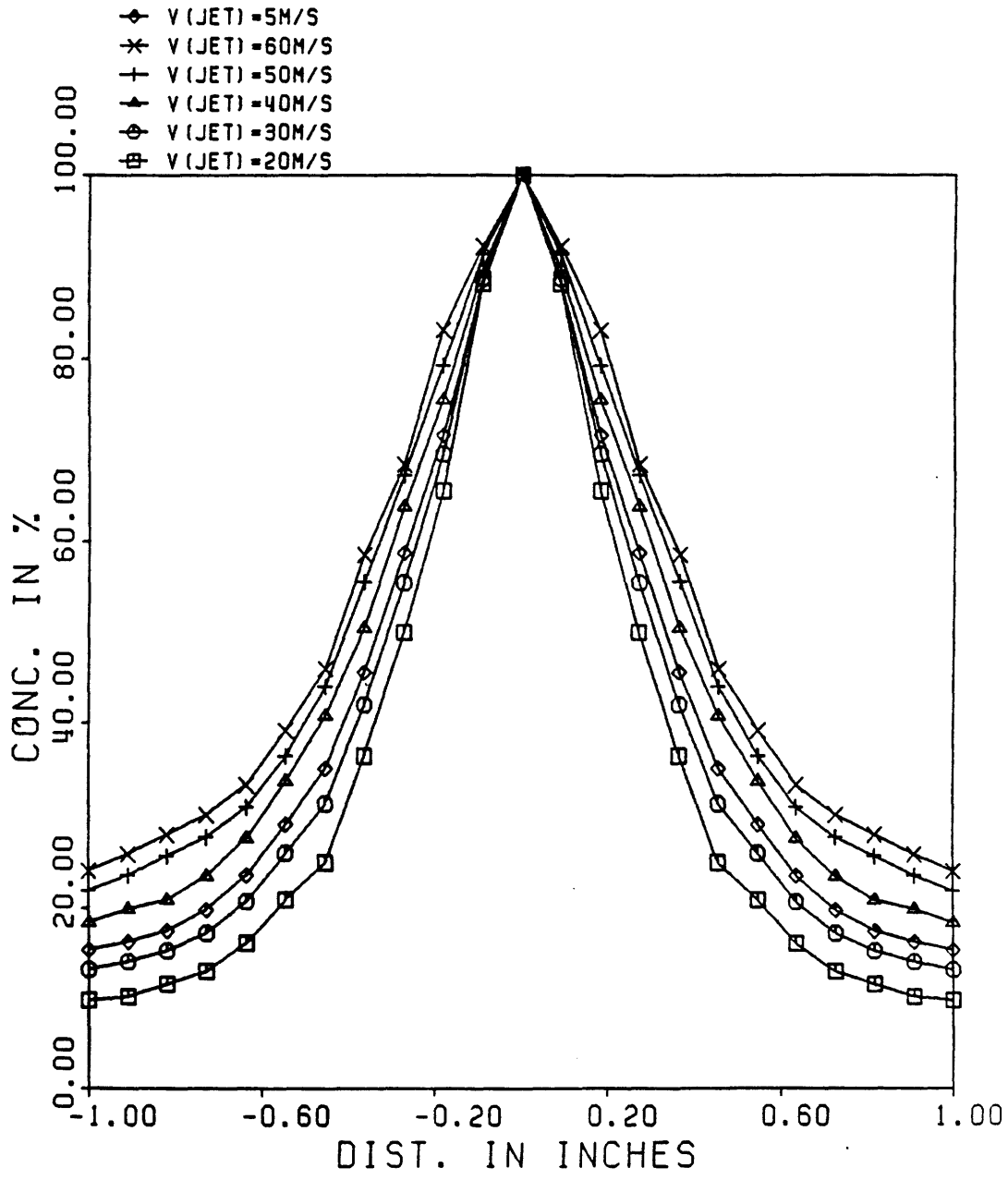

Fig. 21 *Effect of Turbulence on Tracer Gas Spreading; Case-IV : 25% Turbulence*

MIXING COEFFICIENT VS. TURBULENCE LEVEL

V (JET) =20M/S; V (INJ) =20M/S

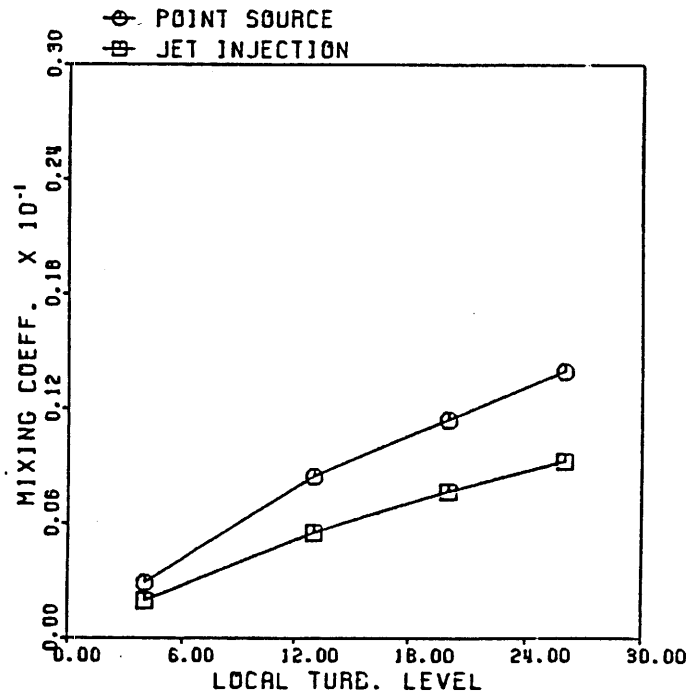

V (JET) =40M/S; V (INJ) =20M/S

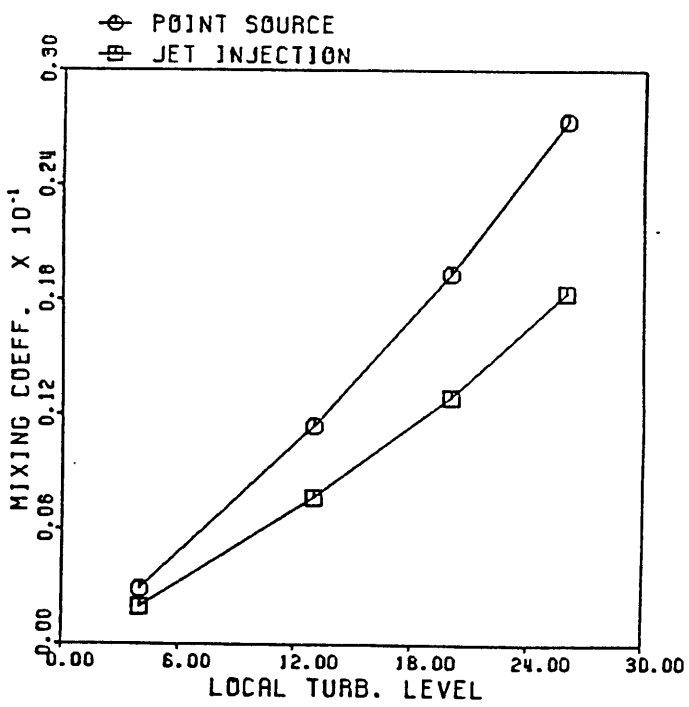

Fig. 22 Variation of Mixing Coefficient with Turbulence Level.

MIXING COEFFICIENT VS. VELOCITY DIFFERENCE
X(INJ) = 28.25; TURB. LEVEL = 25% FOR ALL POINTS

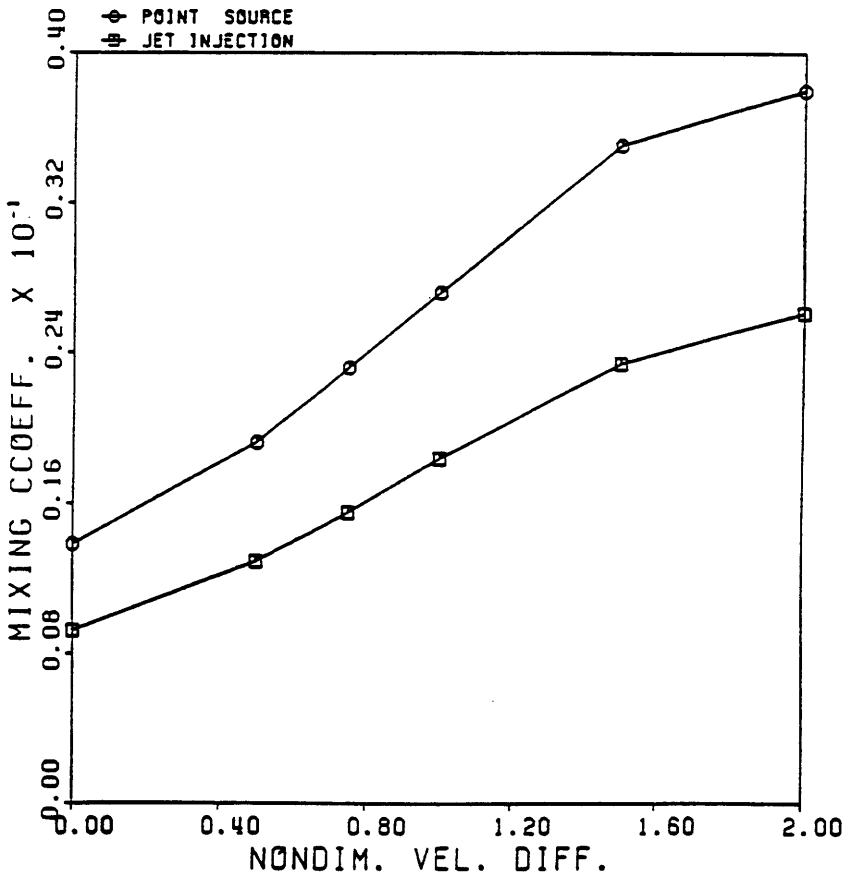

Fig. 23 Variation of Mixing Coefficient with Main Stream Velocity.

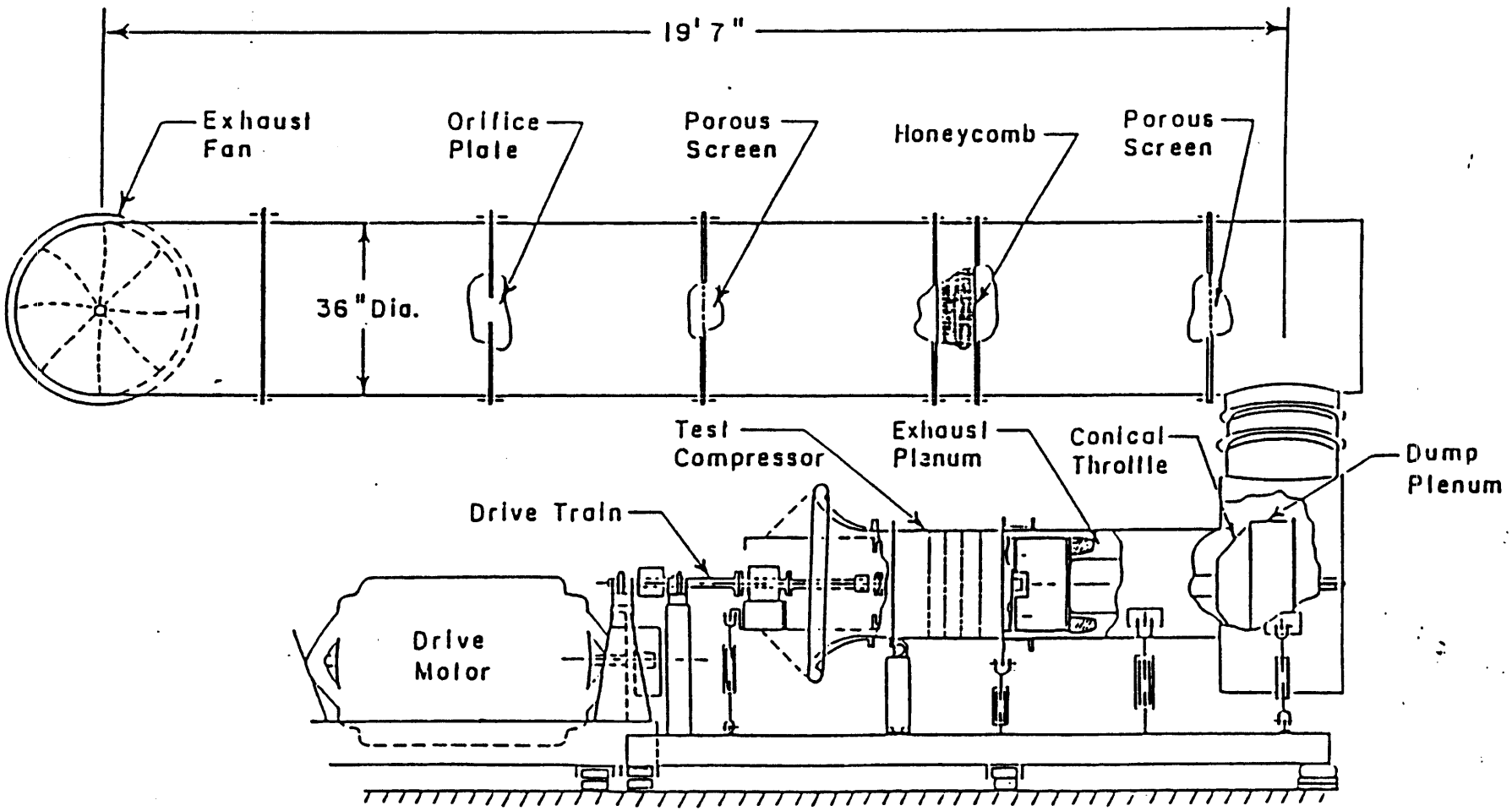

Low Speed Multistage Compressor Test Facility

Fig. 24 Low Speed Compressor Rig Schematic.

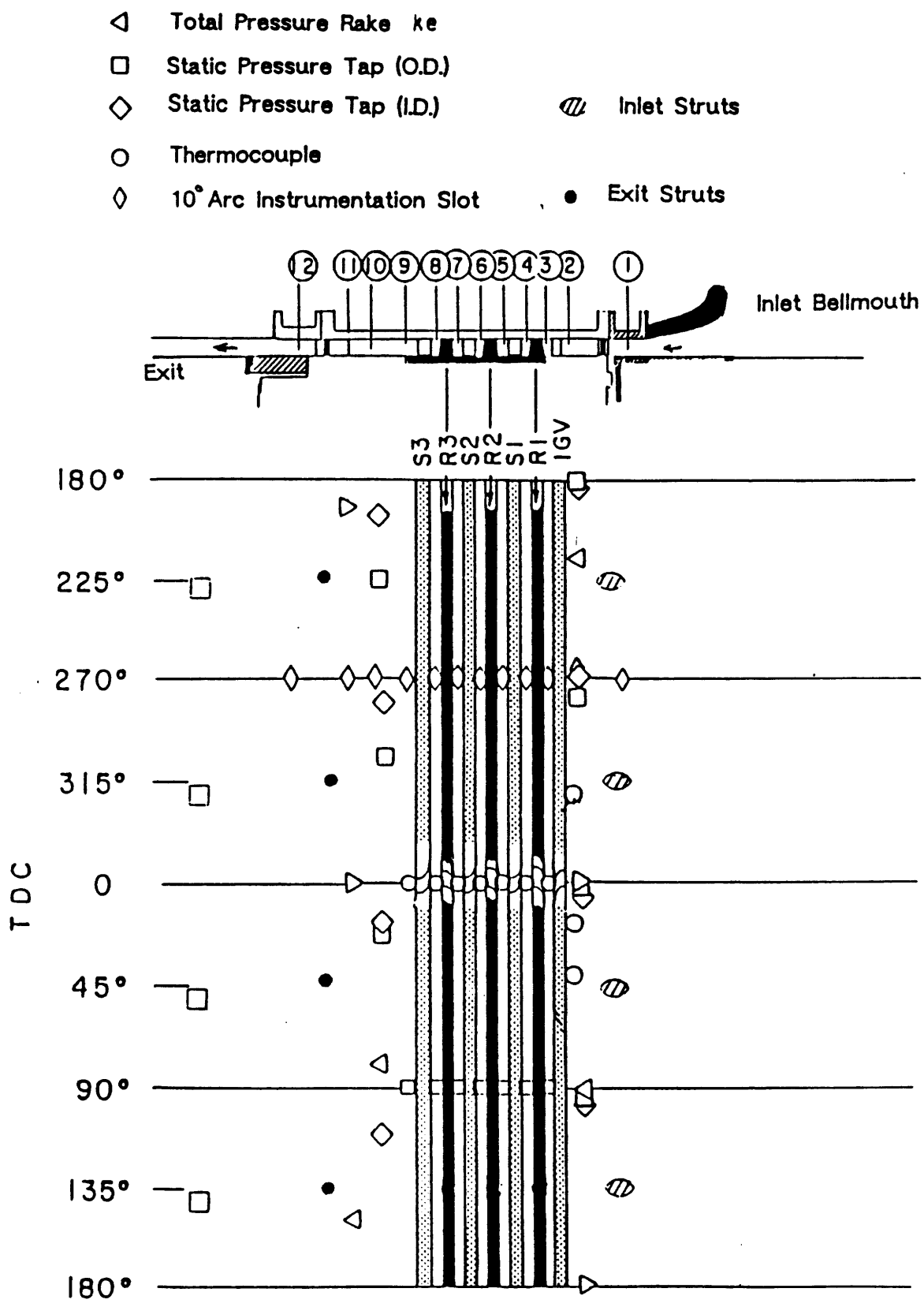

Fig. 25 Steady-state Measurement Locations.

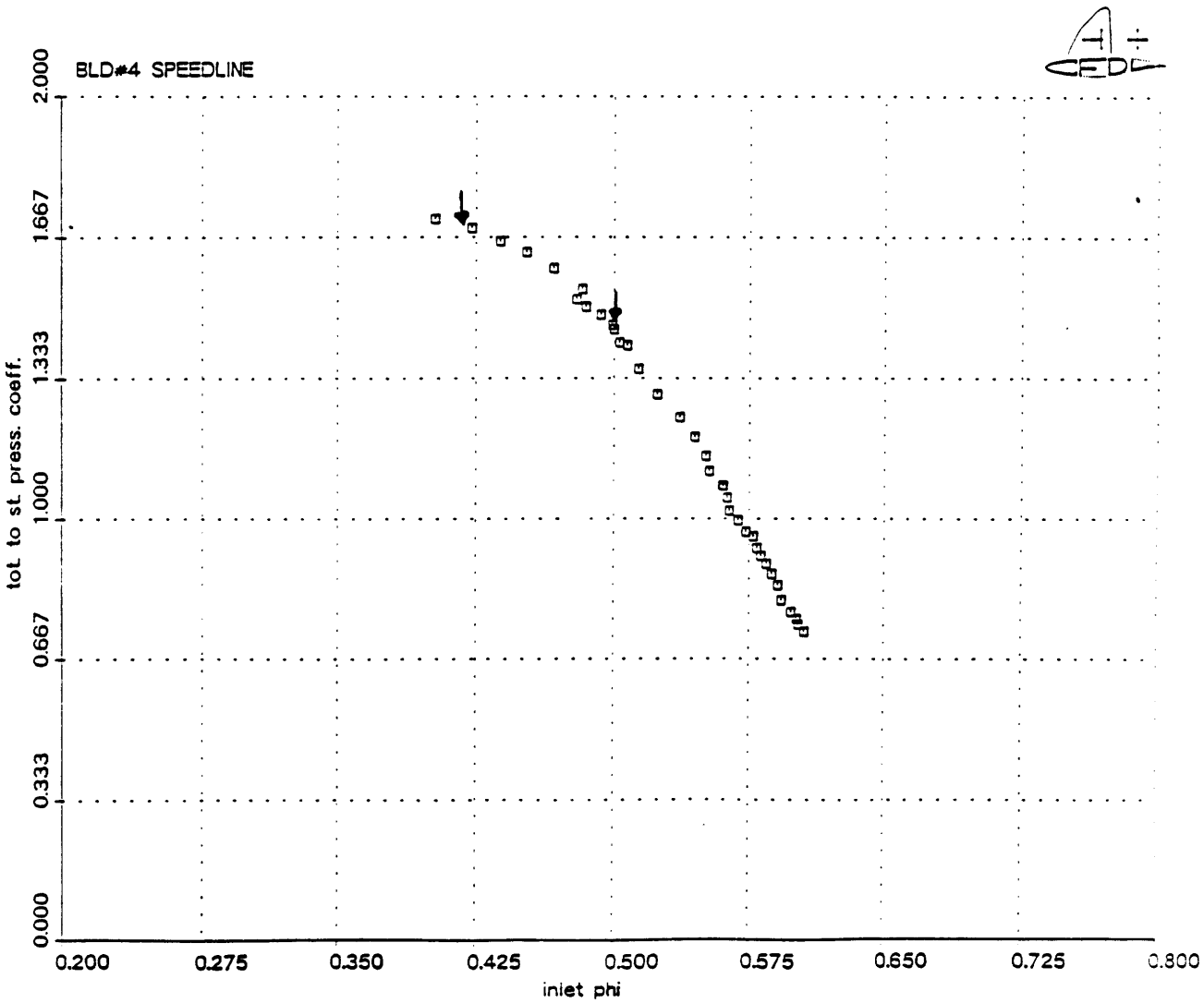

Fig. 26 Total to Static Pressure Performance.

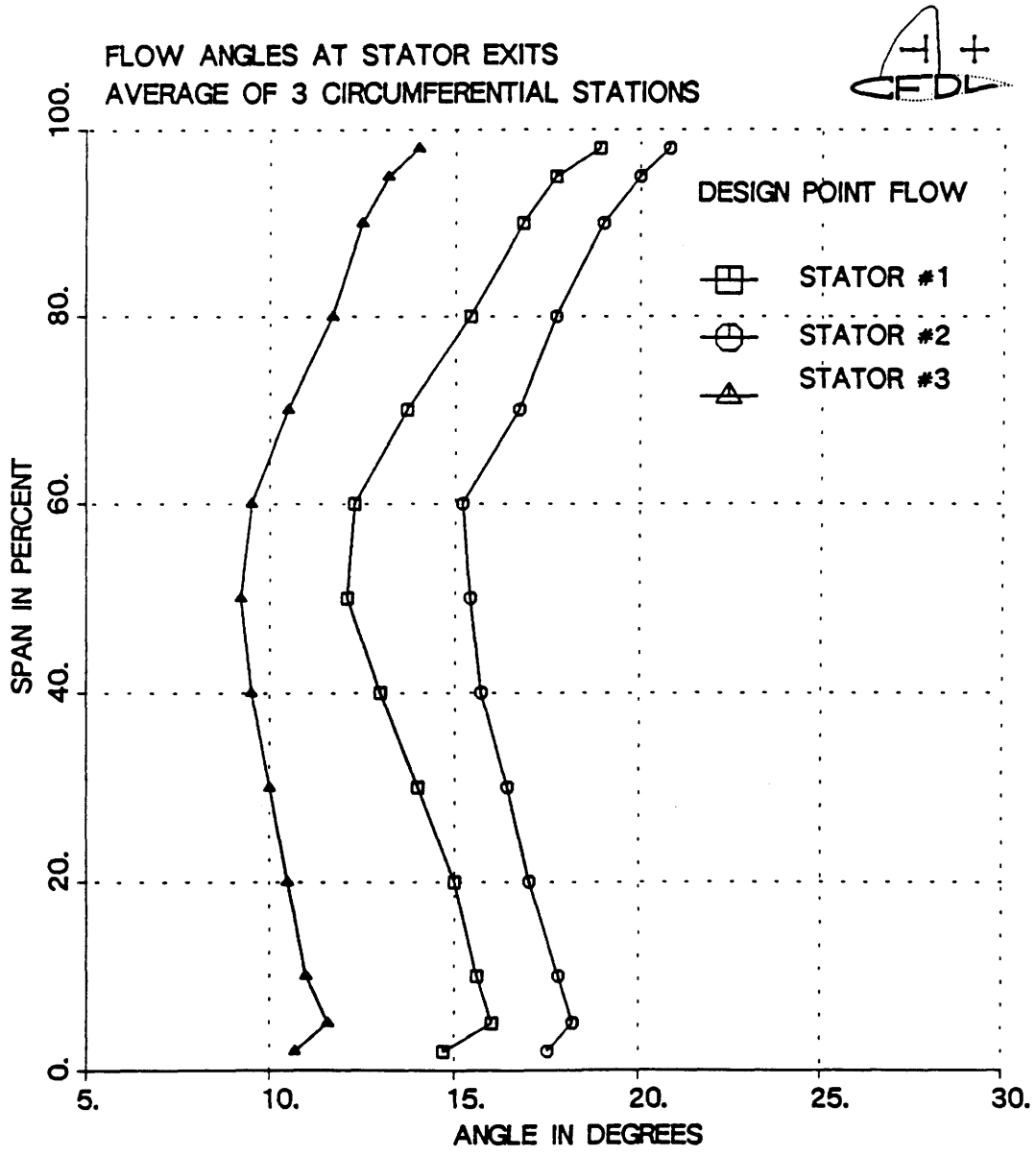

Fig. 27 *Stator Exit Flow Angles at Design Point Loading.*

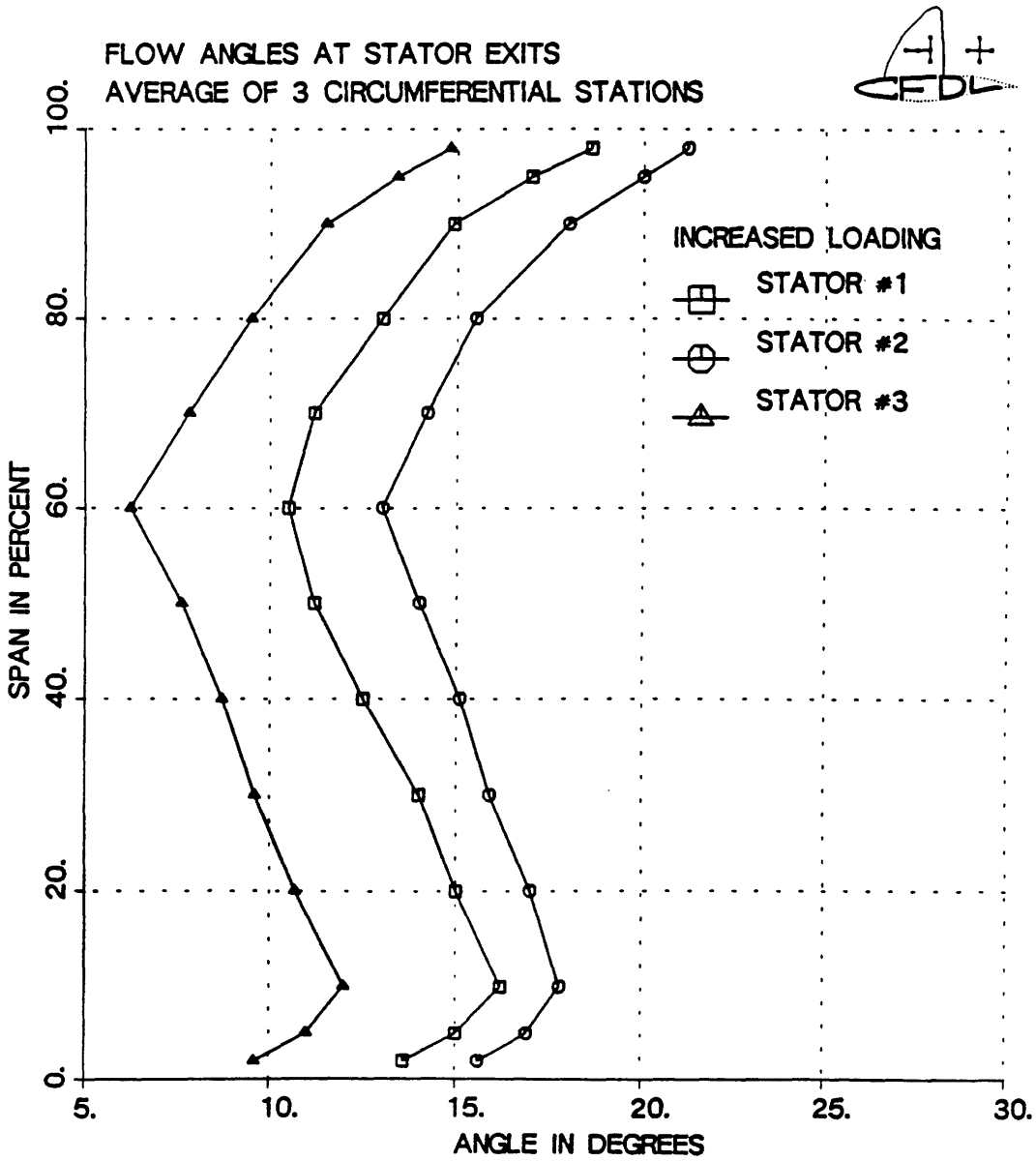

Fig. 28 *Stator Exit Flow Angles at Increased Loading.*

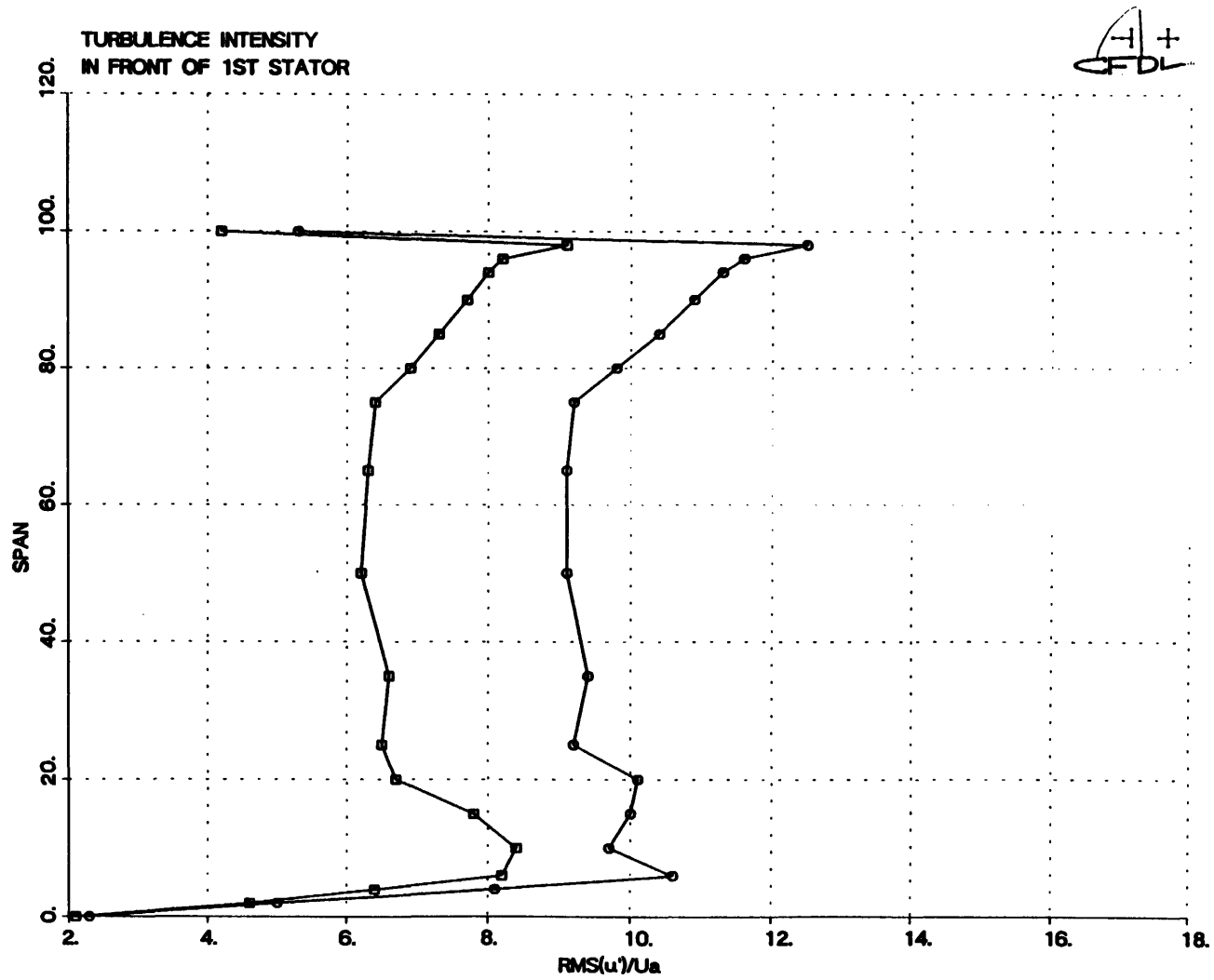

Fig. 29 Radial Variation of Turbulence Levels Upstream of 1st. Stator.

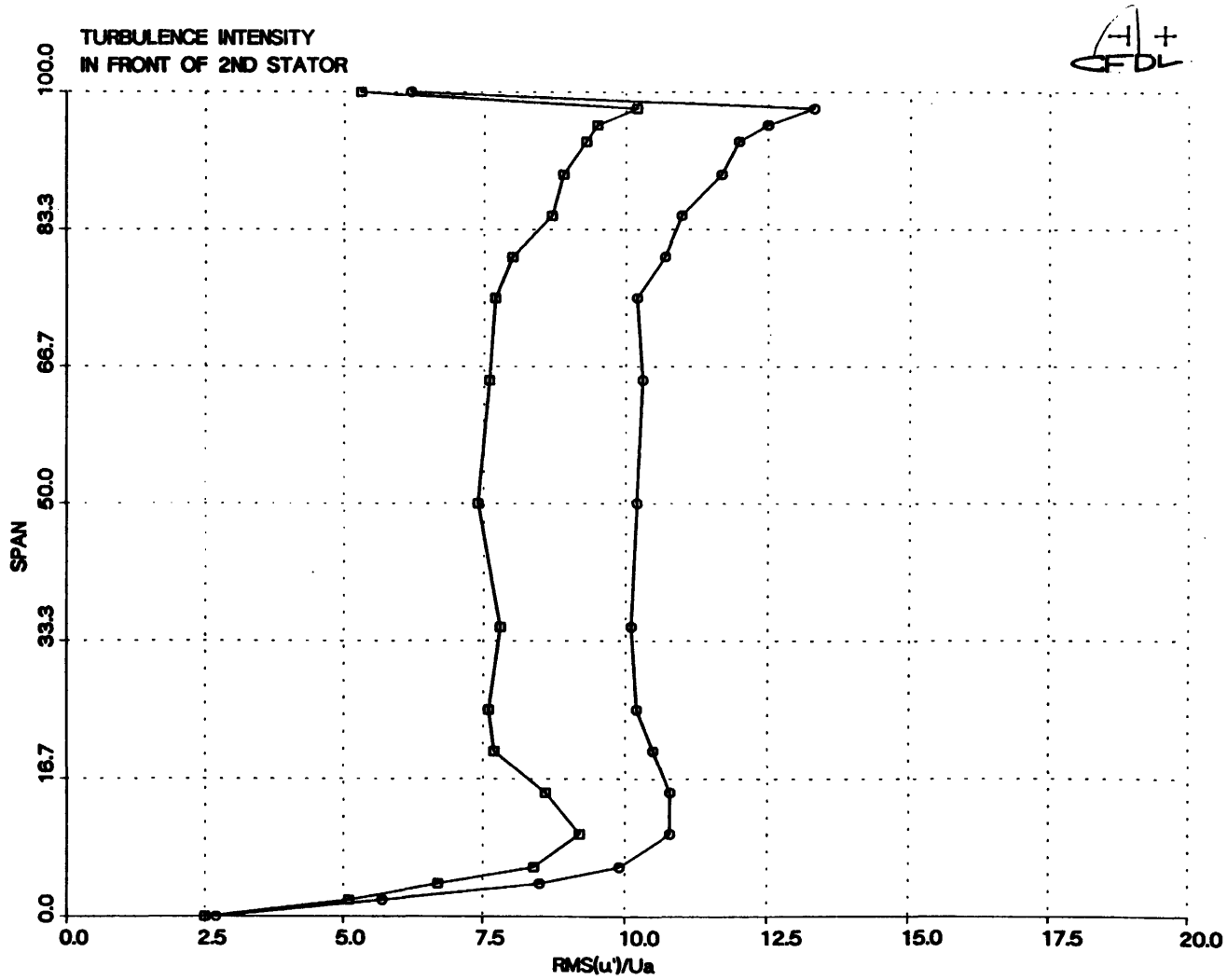

Fig. 30 *Radial Variation of Turbulence Levels Upstream of 2nd. Stator.*

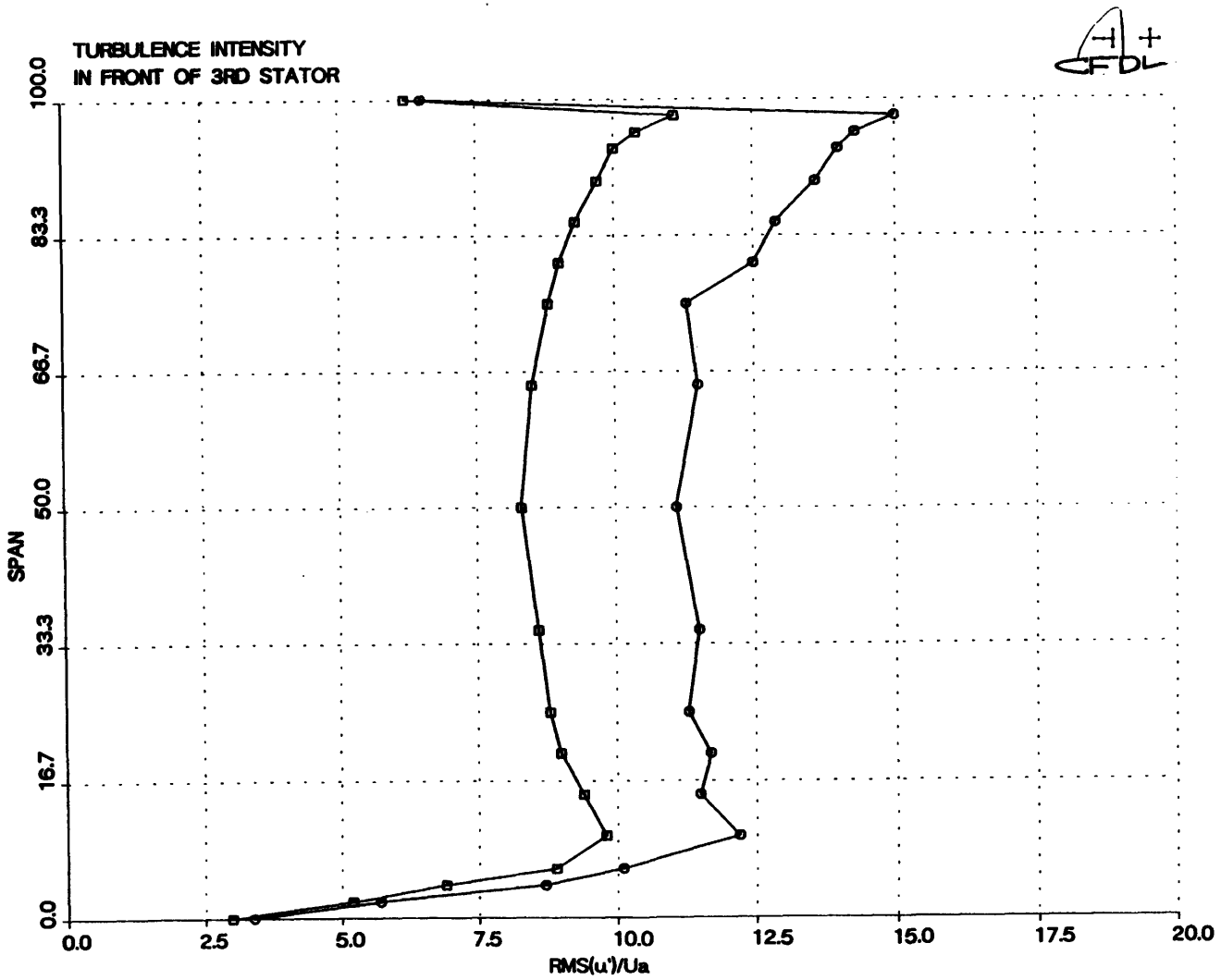

Fig. 31 Radial Variation of Turbulence Levels Upstream of 3rd. Stator.

DIAGRAM ILLUSTRATING THE COMPRESSOR PASSAGE USED IN CONTOUR PLOTS

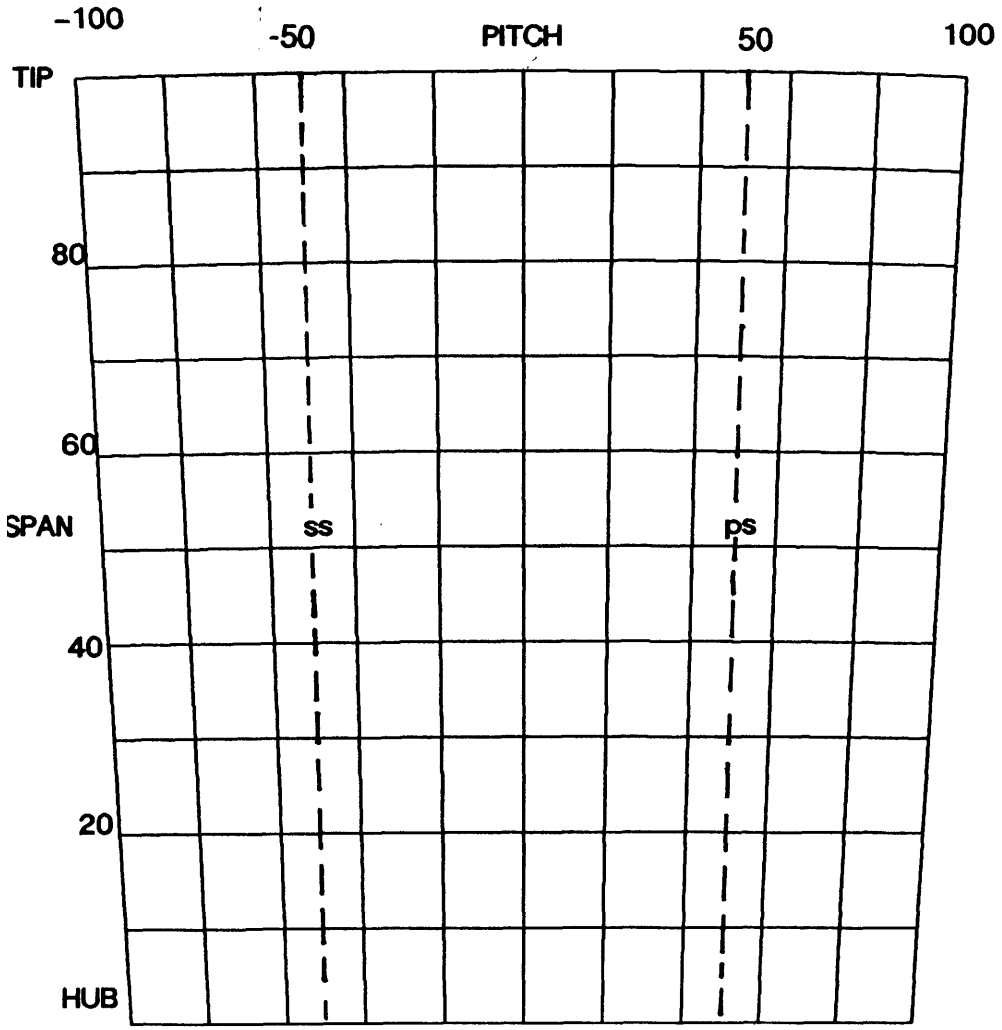

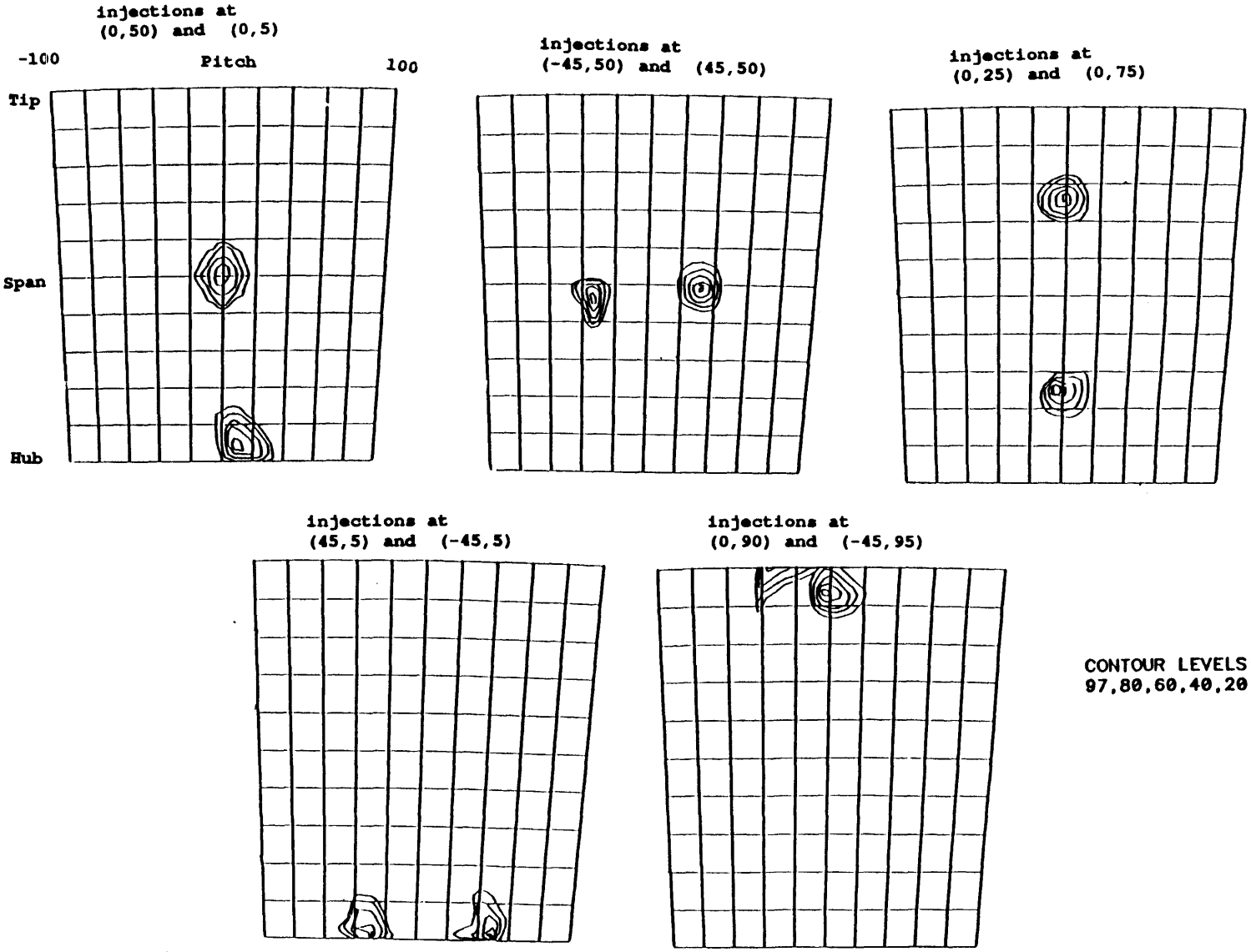

Fig. 32 *Contour Plots for Tracer Gas Spreading Across 1st. Stator at Design Point Loading.*

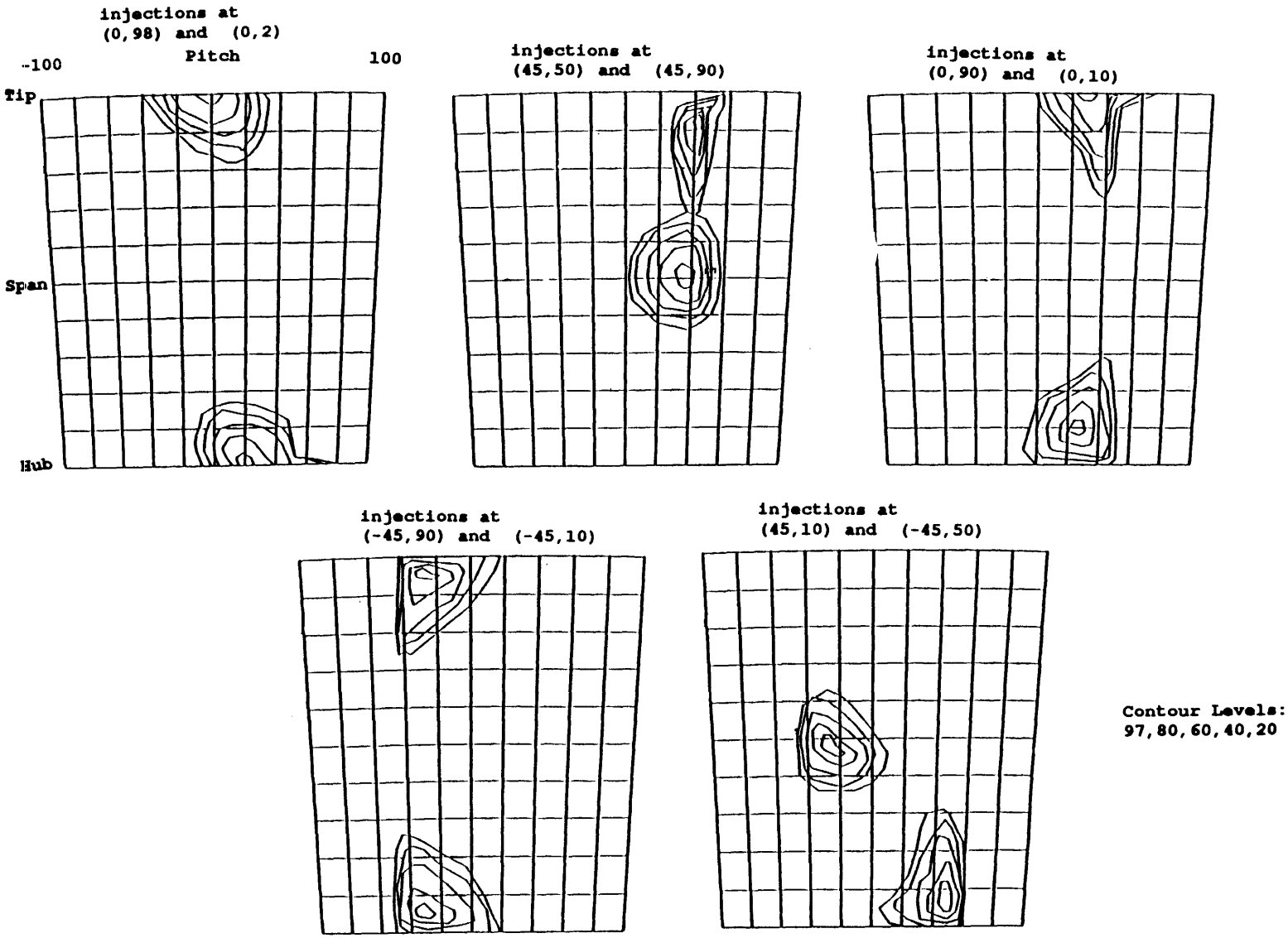

Fig. 33 Contour Plots for Tracer Gas Spreading Across 1st. Stator at Increased Loading.

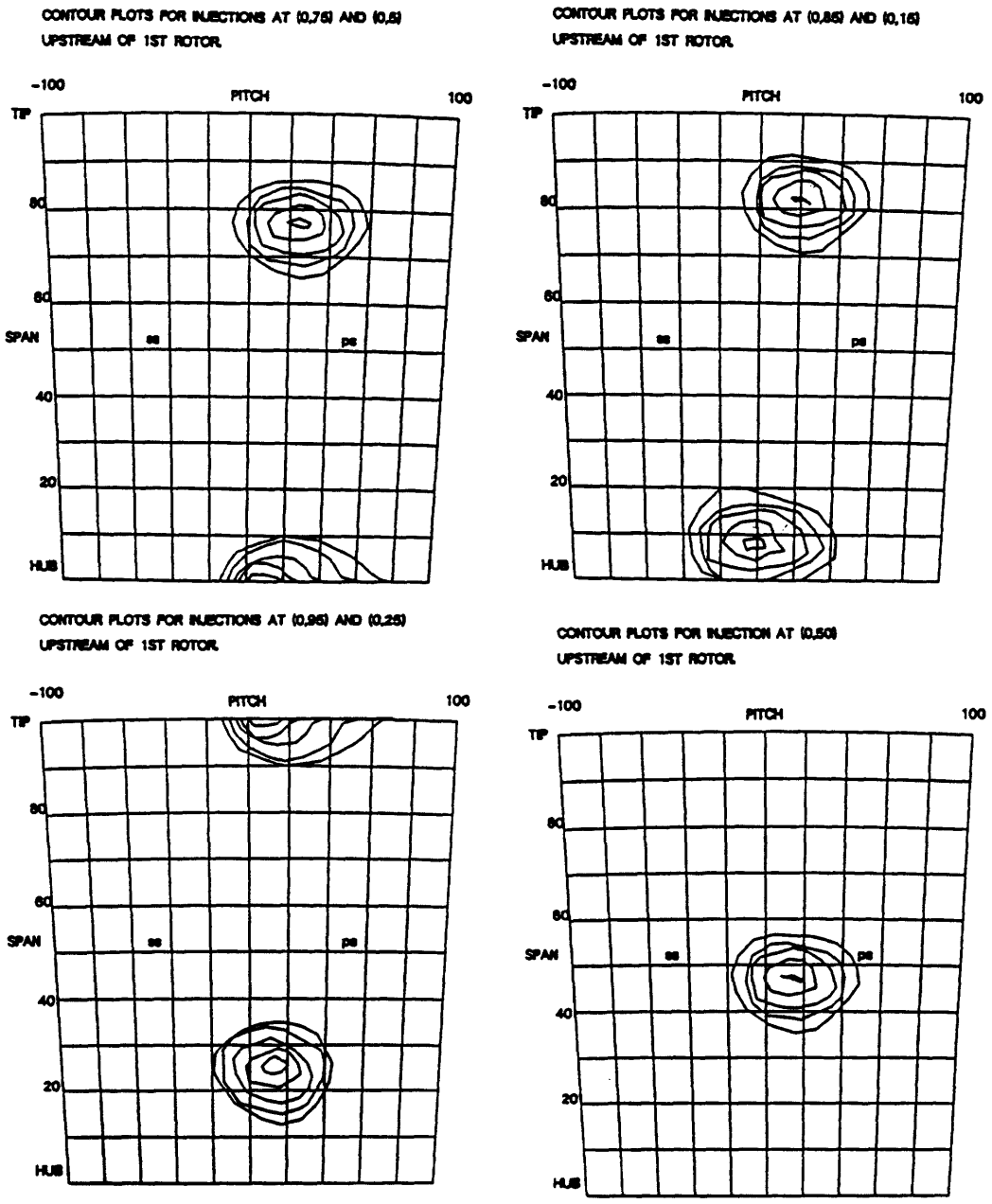

Fig. 34 *Contour Plots for Tracer Gas Spreading Across 1st. Rotor at Design Point Loading. Contour Levels : 97,80,60,40,20.*

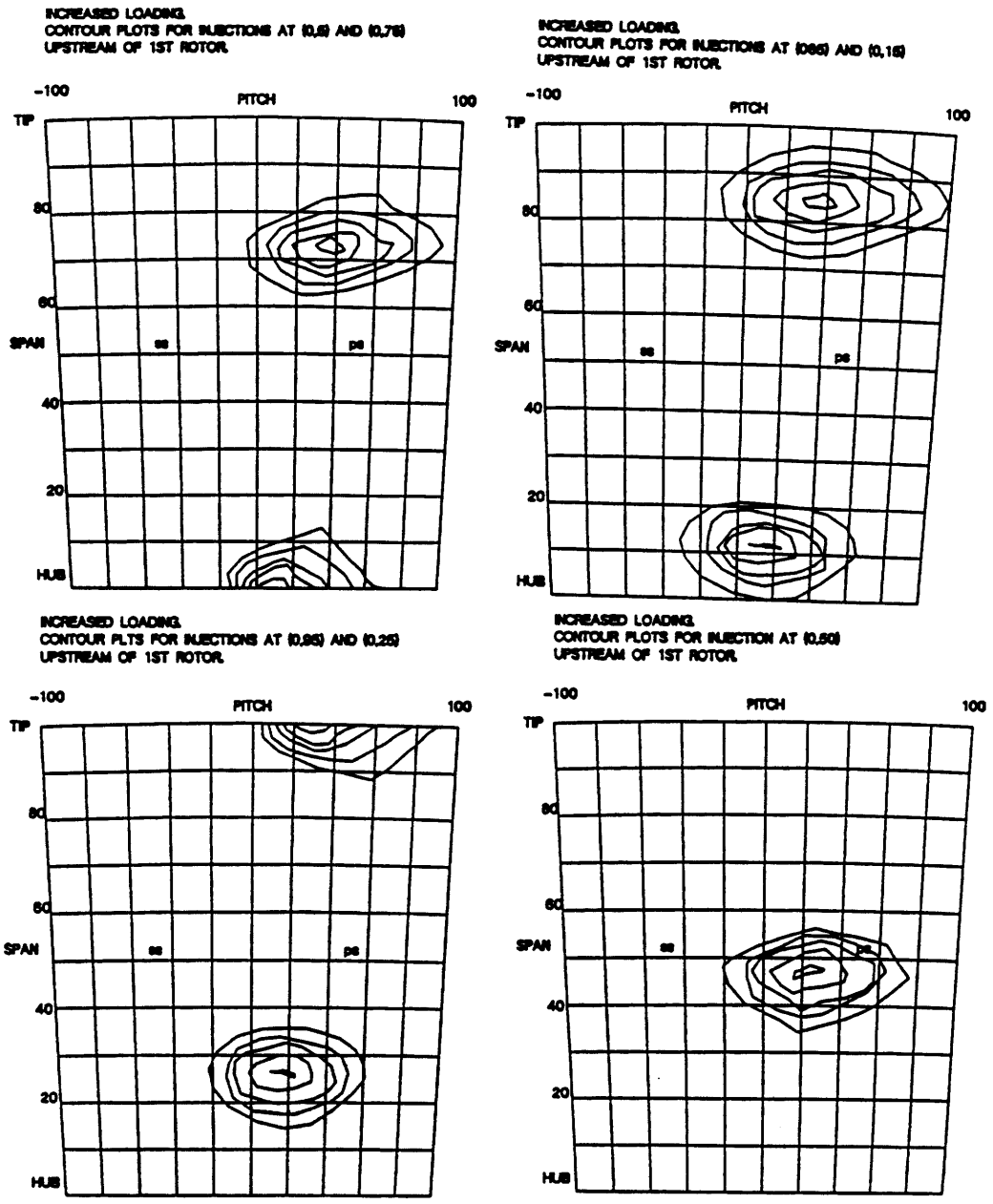

Fig. 35 *Contour Plots for Tracer Gas Spreading Across 1st. Rotor at Increased Loading. Contour Levels : 97,80,60,40,20.*

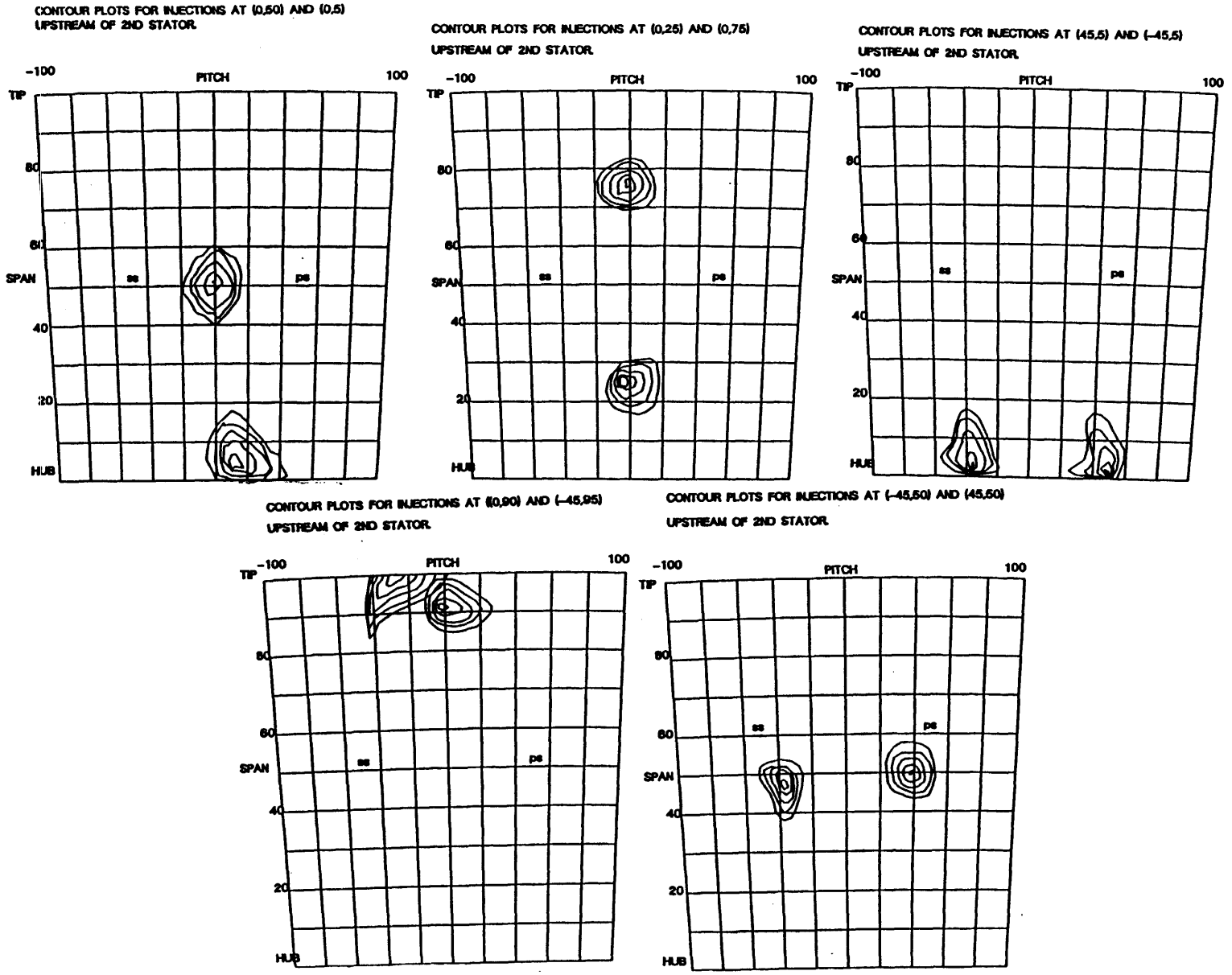

Fig. 36 *Contour Plots for Tracer Gas Spreading Across 2nd. Stator at Design Point Loading. Contour Levels : 97,80,60,40,20.*

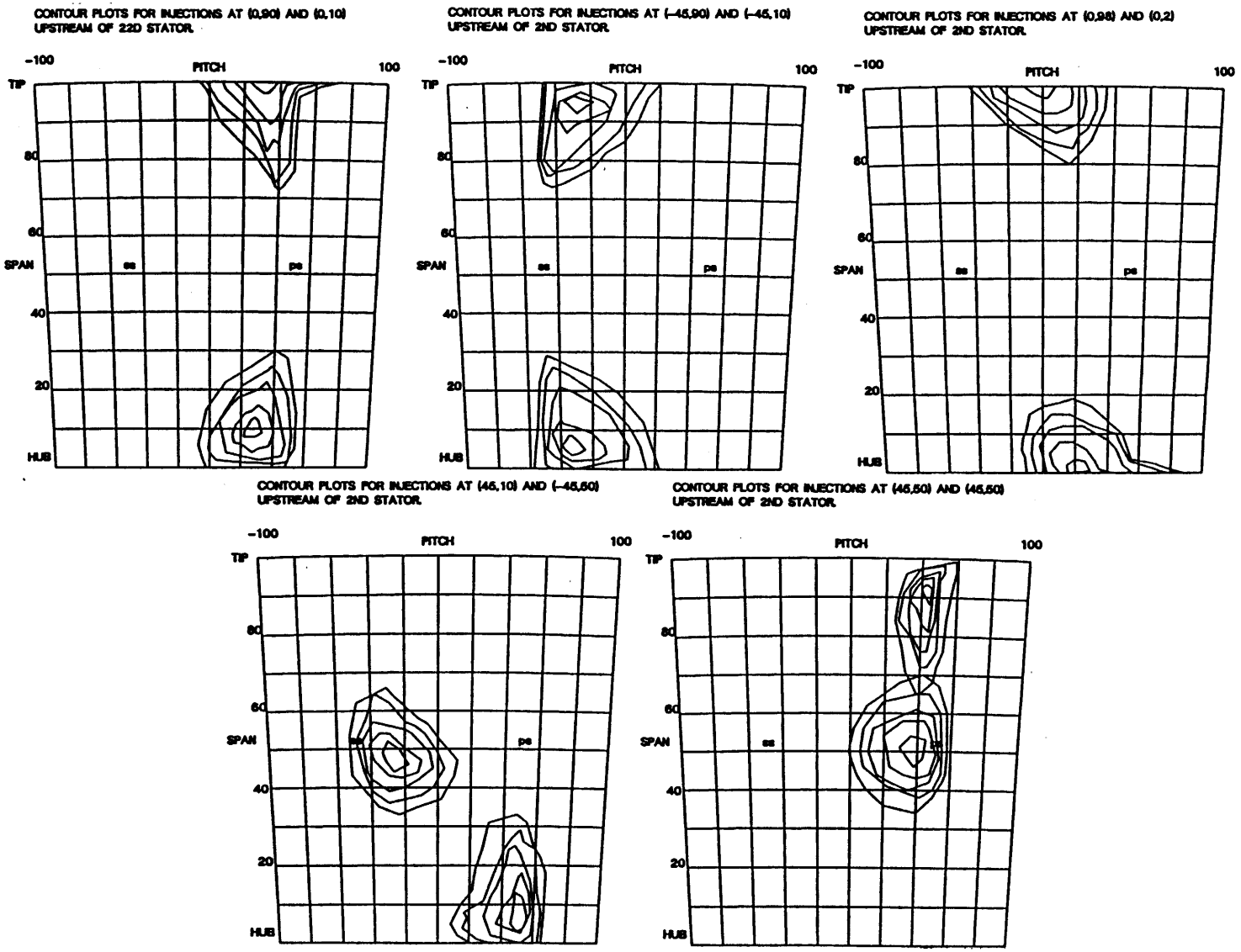

Fig. 37 *Contour Plots for Tracer Gas Spreading Across 2nd. Stator at Increased Loading. Contour Levels : 97,80,60,40,20.*

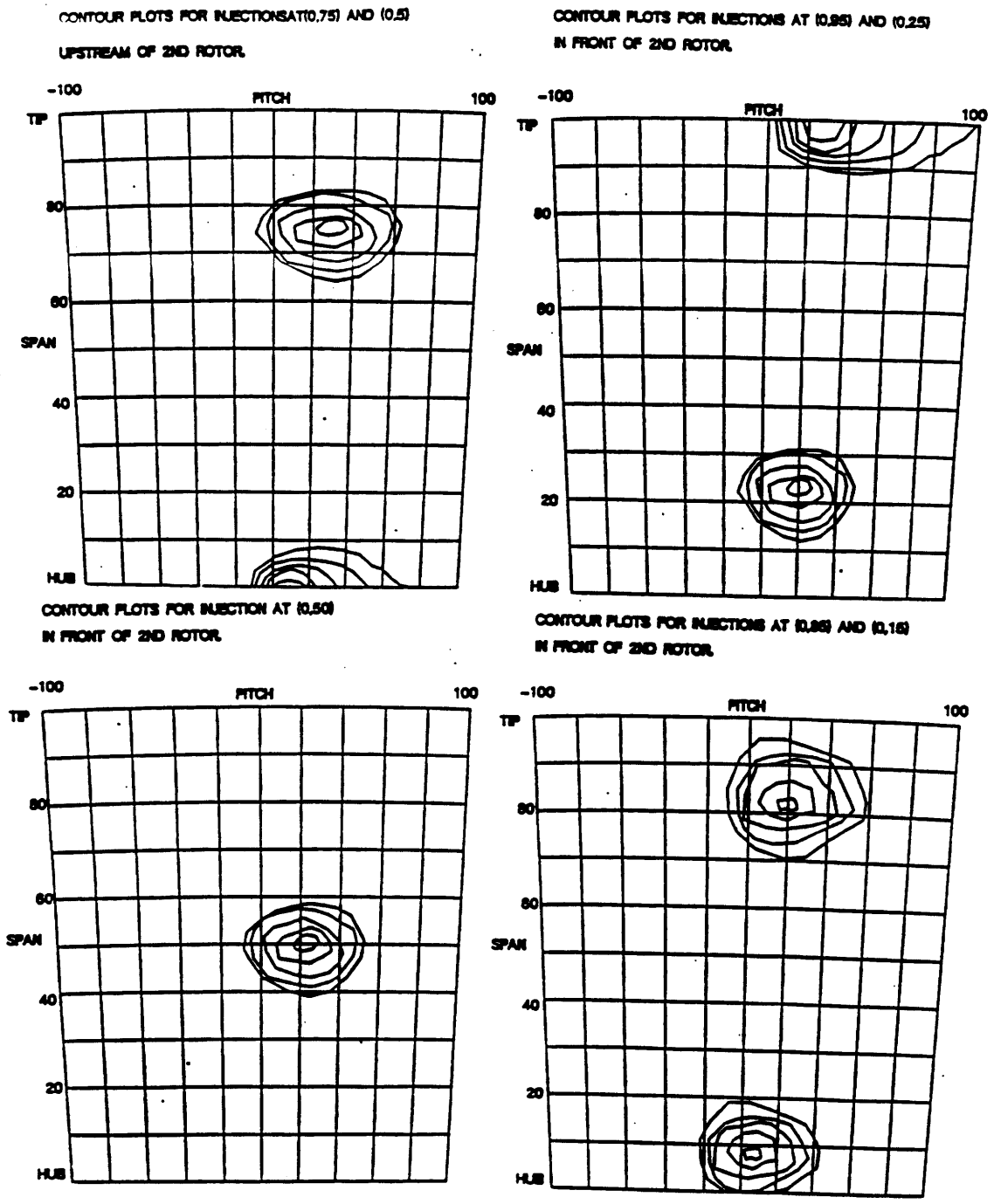

Fig. 38 *Contour Plots for Tracer Gas Spreading Across 2nd. Rotor at Design Point Loading. Contour Levels : 97,80,60,40,20.*

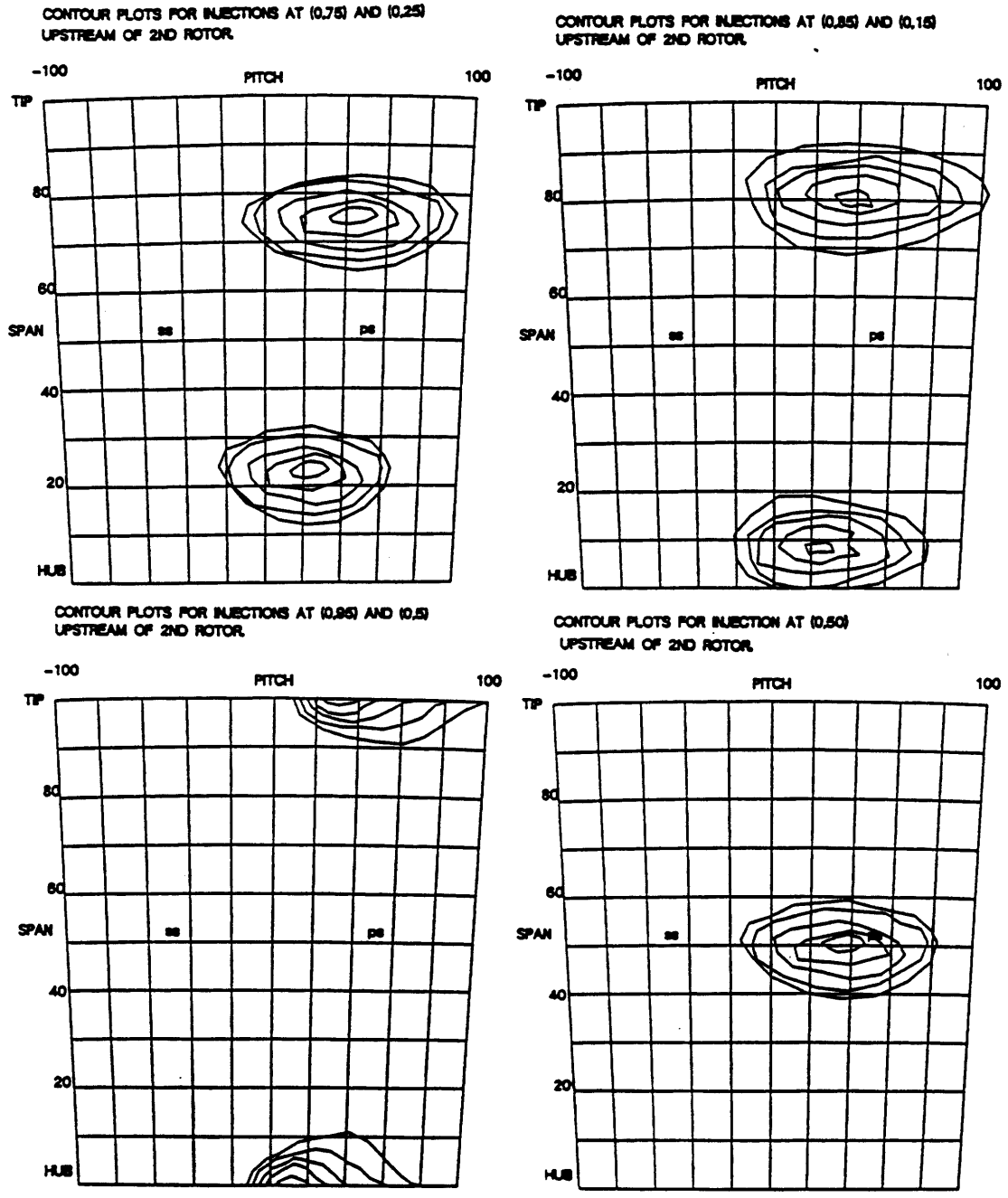

Fig. 39 Contour Plots for Tracer Gas Spreading Across 2nd. Rotor at Increased Loading. Contour Levels : 97,80,60,40,20.

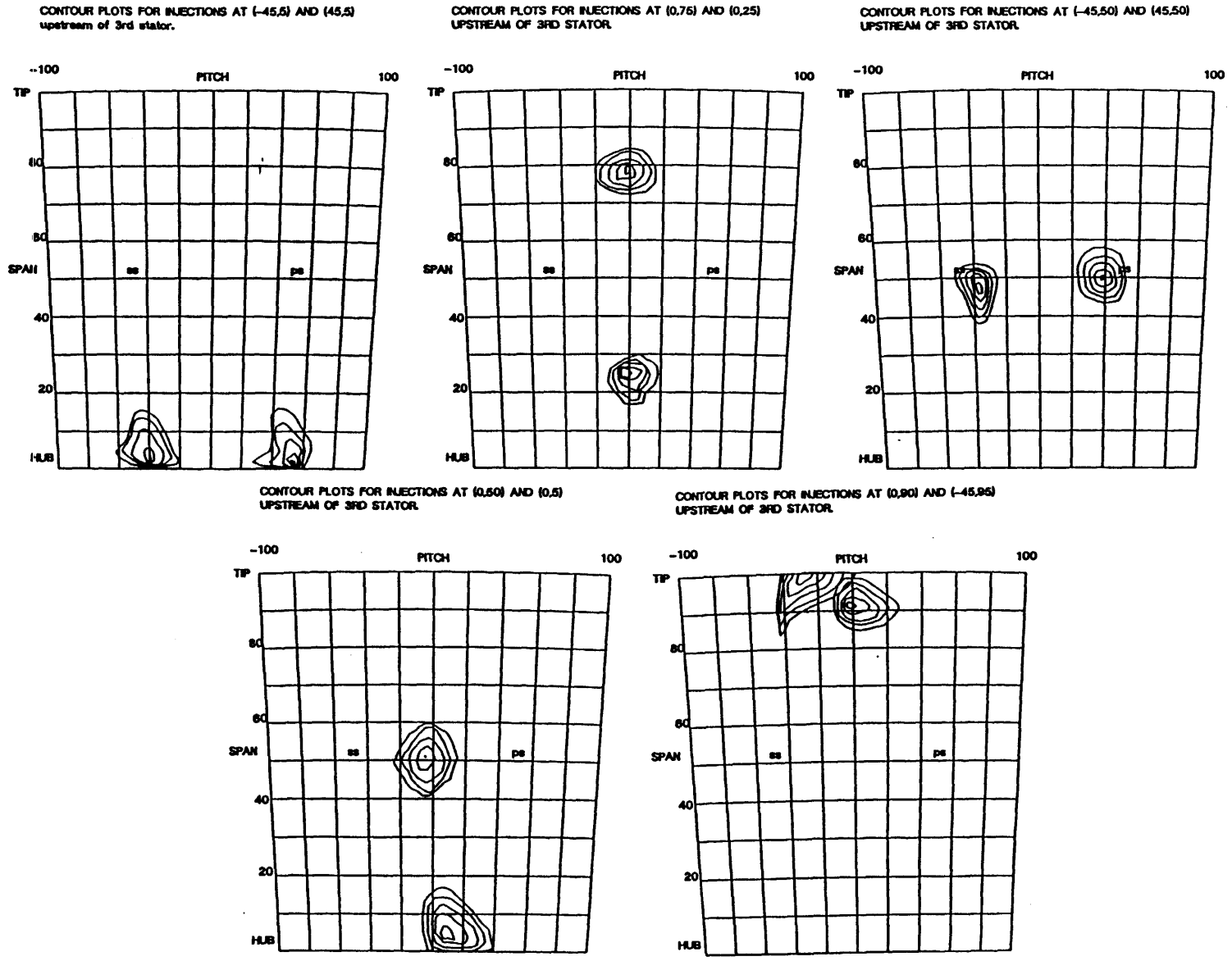

Fig. 40 *Contour Plots for Tracer Gas Spreading Across 3rd. Stator at Design Point Loading. Contour Levels : 97,80,60,40,20.*

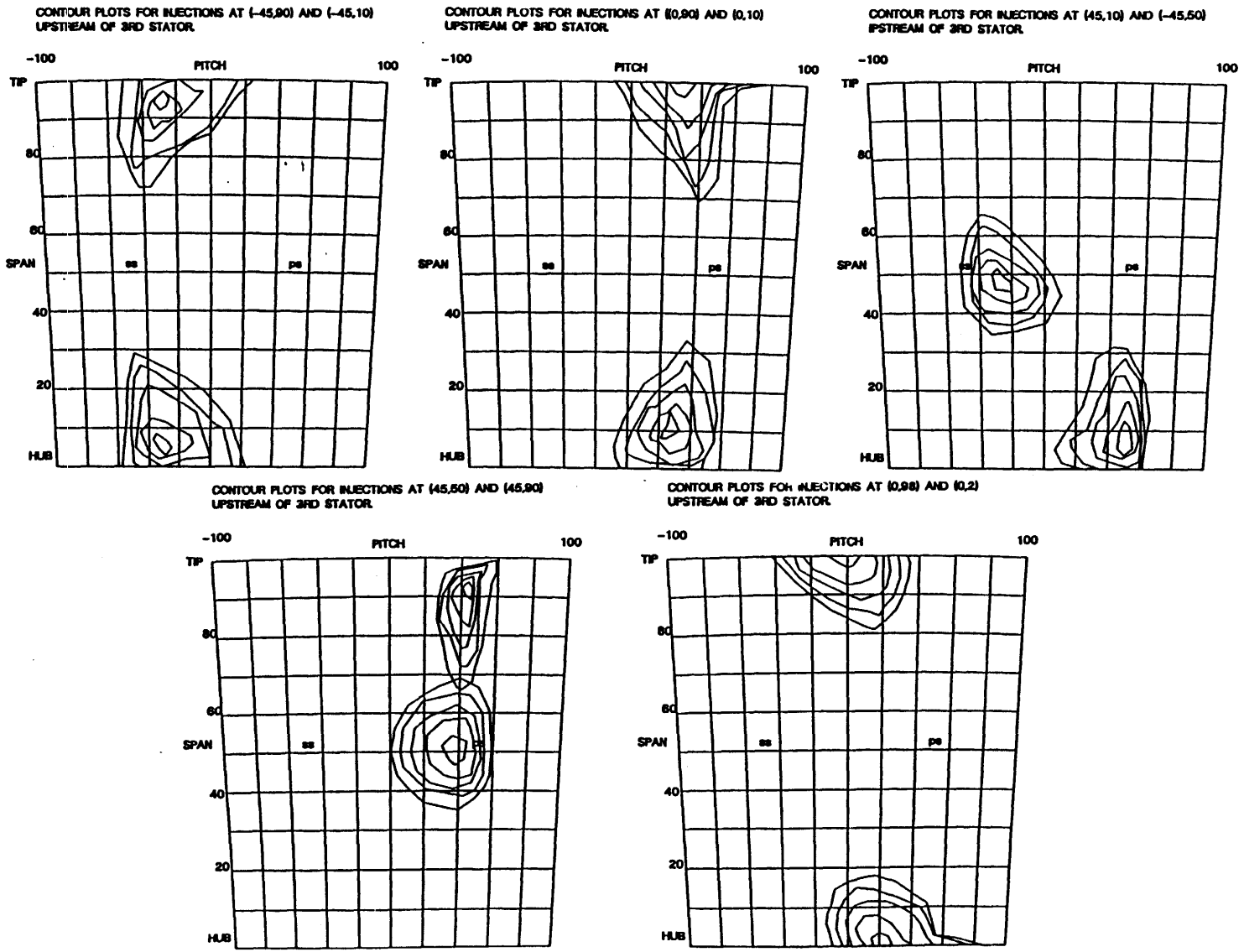

Fig. 41 *Contour Plots for Tracer Gas Sprea Across 3rd. Stator at Increased Loading. Contour Levels : 97,80,60,40,20.*

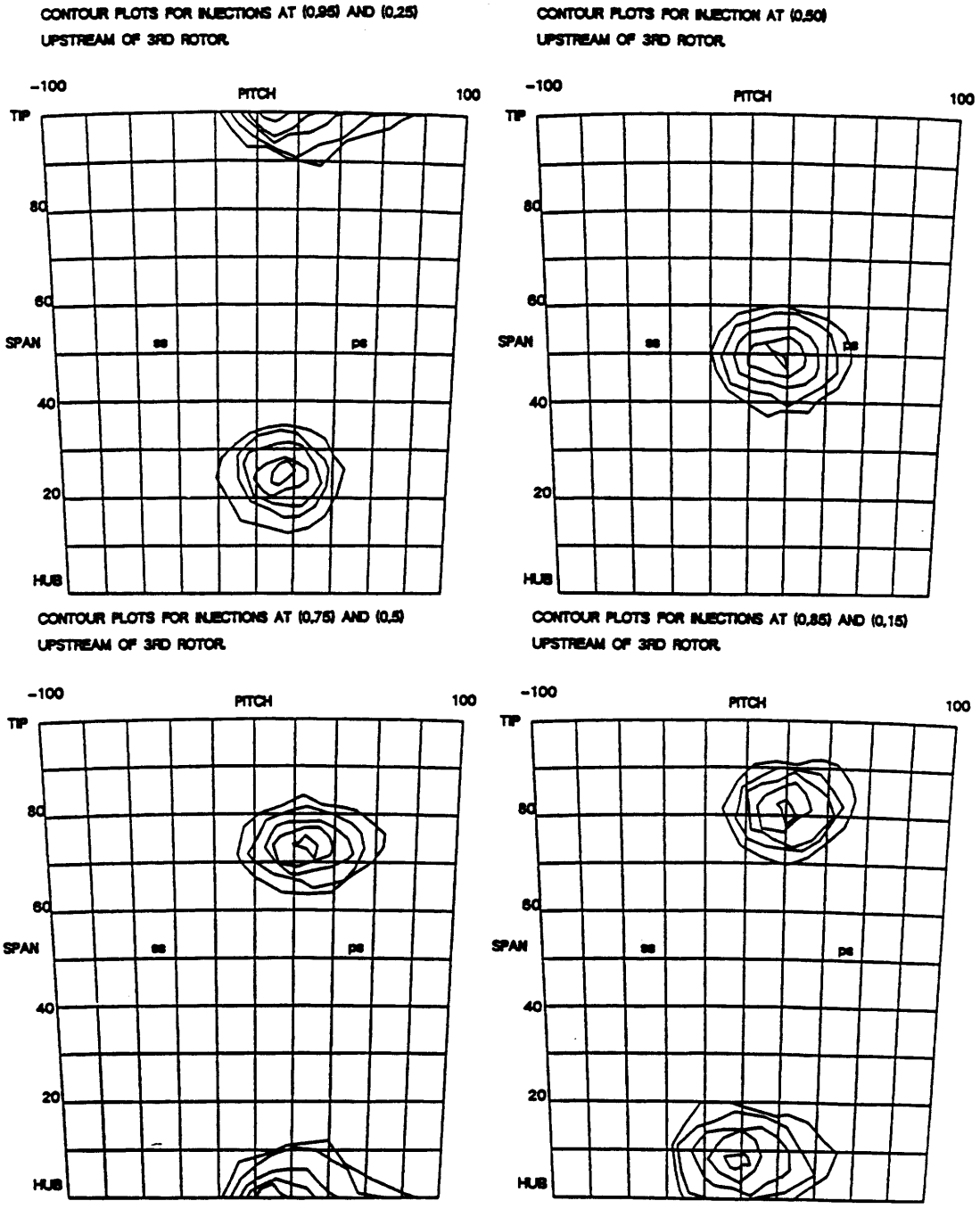

Fig. 42 *Contour Plots for Tracer Gas Spreading Across 3rd. Rotor at Design Point Loading. Contour Levels : 97,80,60,40,20.*

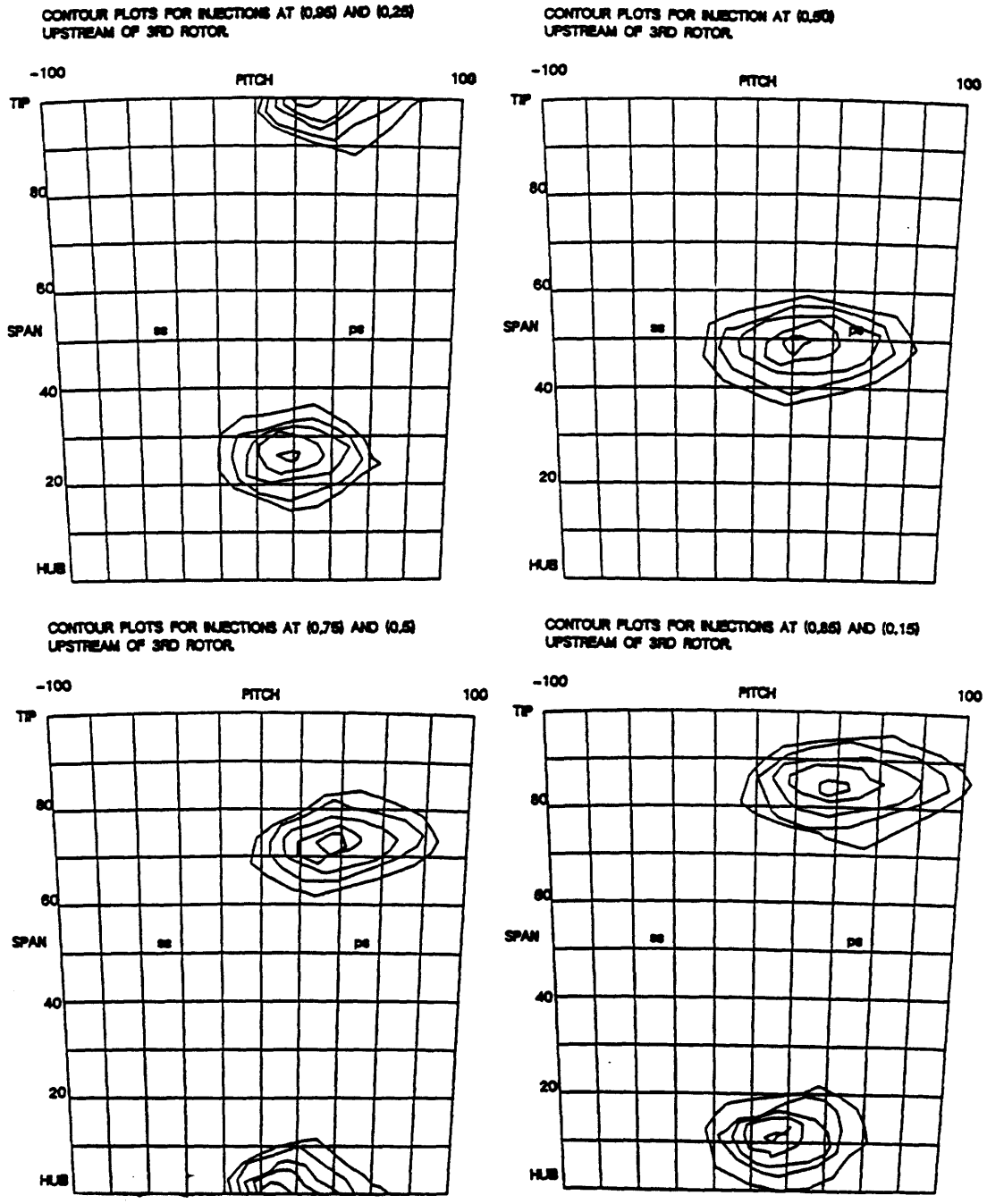

Fig. 43 *Contour Plots for Tracer Gas Spreading Across 3rd. Rotor at Increased Loading. Contour Levels : 97,80,60,40,20.*

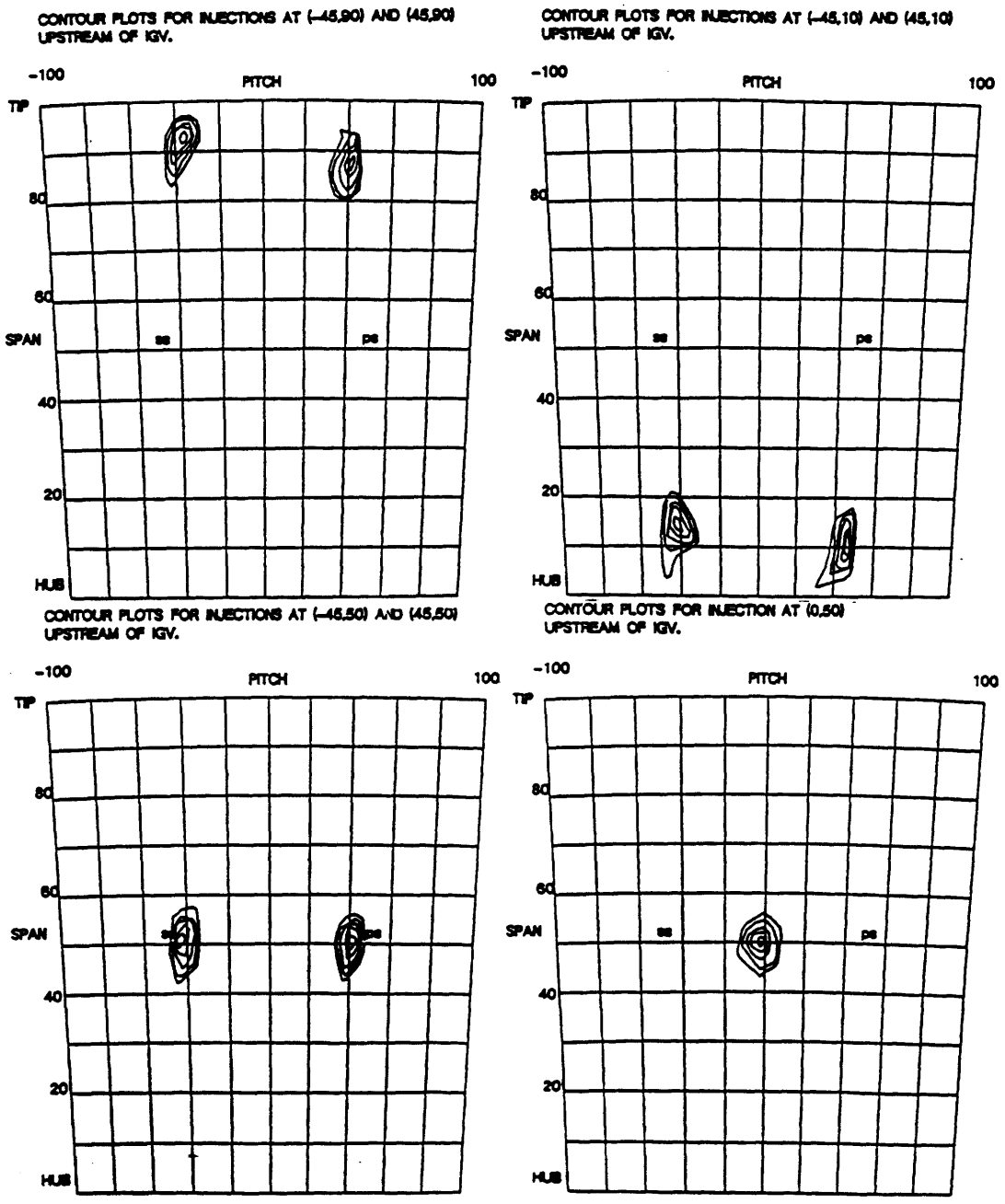

Fig. 44 *Contour Plots for Tracer Gas Spreading Across IGV at Design Point Loading. Contour Levels : 97,80,60,40,20.*

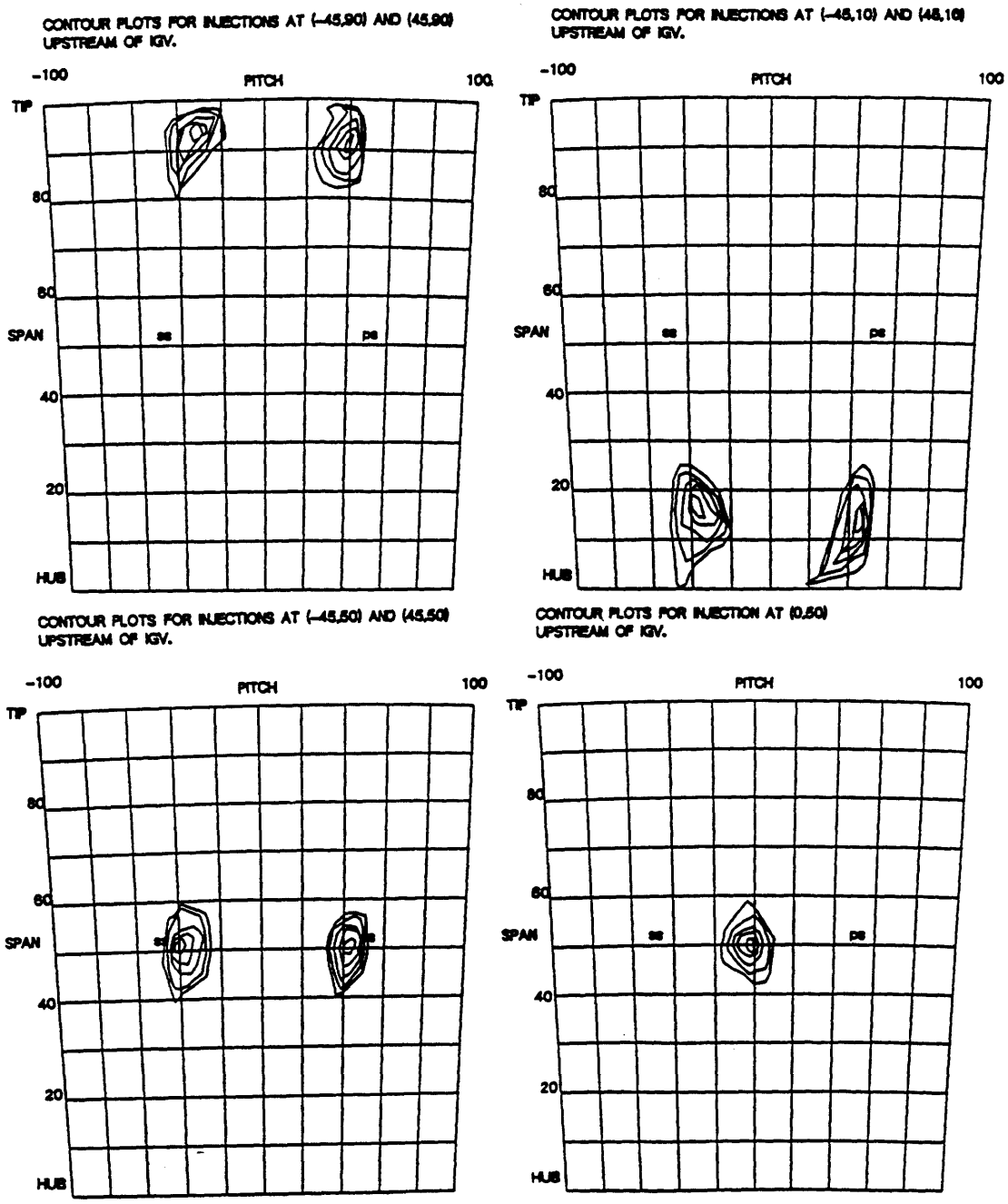

Fig. 45 Contour Plots for Tracer Gas Spreading Across IGV at Increased Loading. Contour Levels : 97,80,60,40,20.

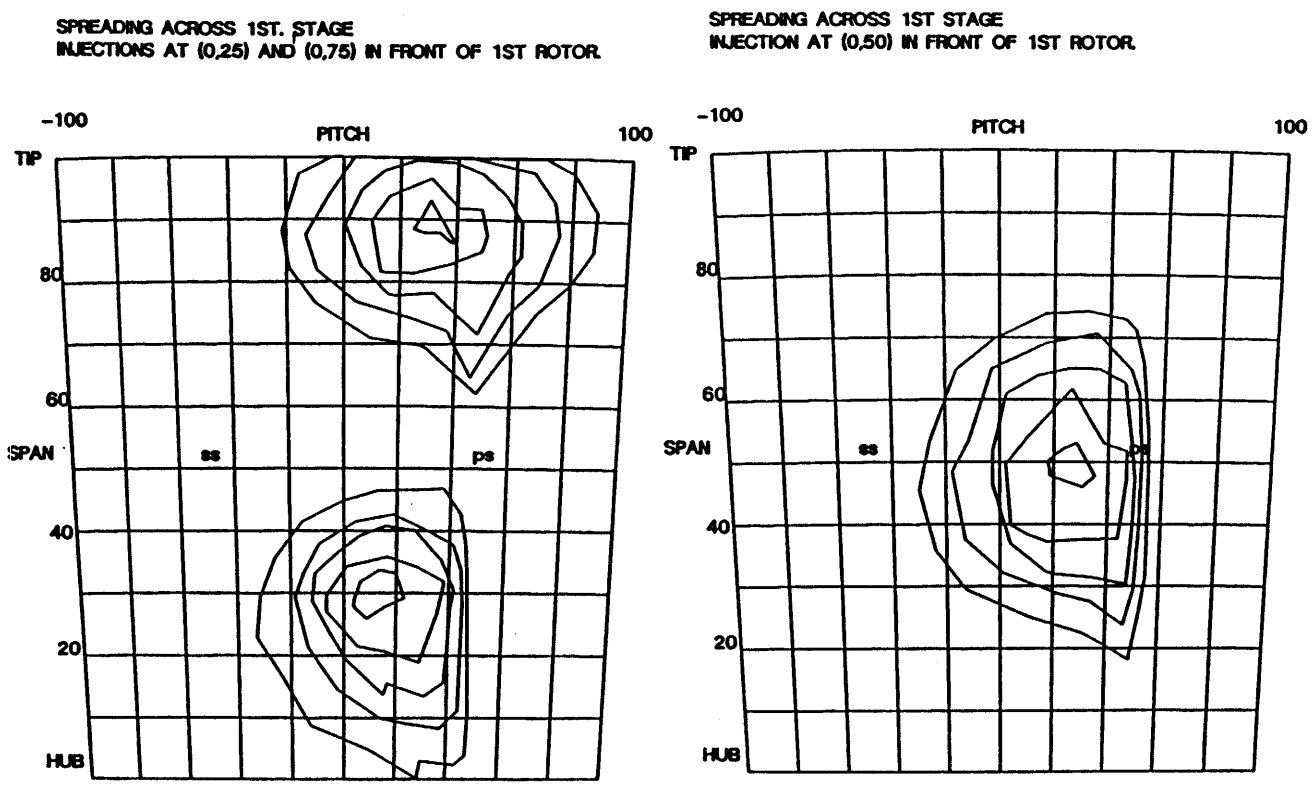

Fig. 46 Contour Plots for Tracer Gas Spreading Across 1st. stage at Design Point Loading. Contour Levels : 97,85,70,55,40.

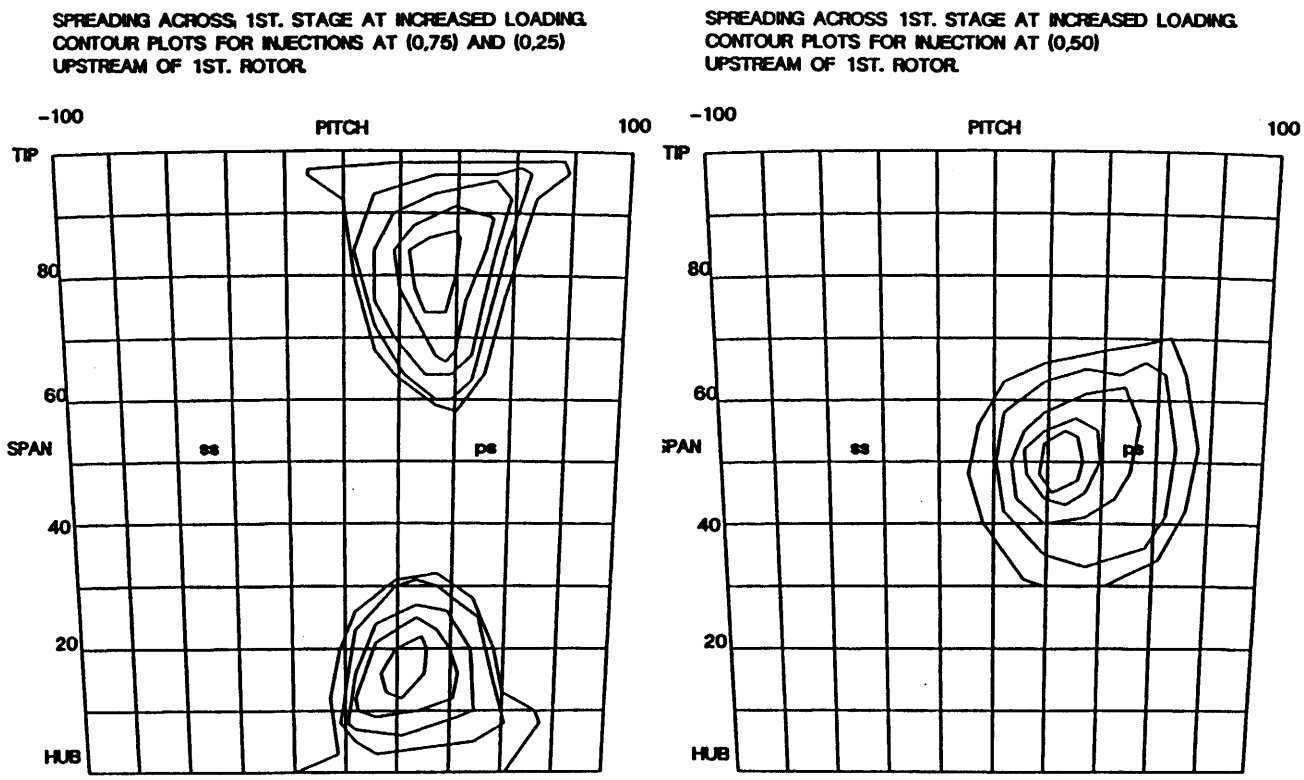

Fig. 47 Contour Plots for Tracer Gas Spreading Across 1st. Stage at Increased Loading. Contour Levels : 97,85,75,70,65.

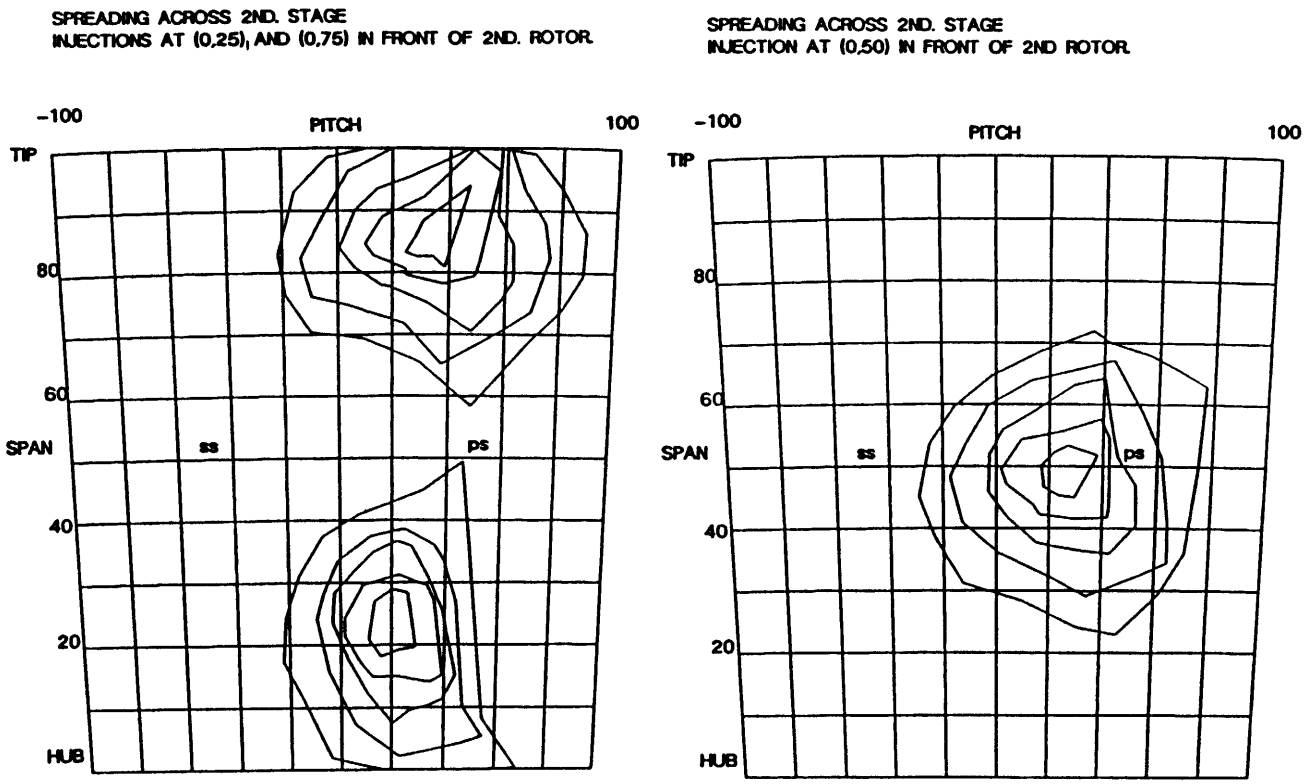

Fig. 48 *Contour Plots for Tracer Gas Spreading Across 2nd. stage at Design Point Loading. Contour Levels : 97,85,70,55,40.*

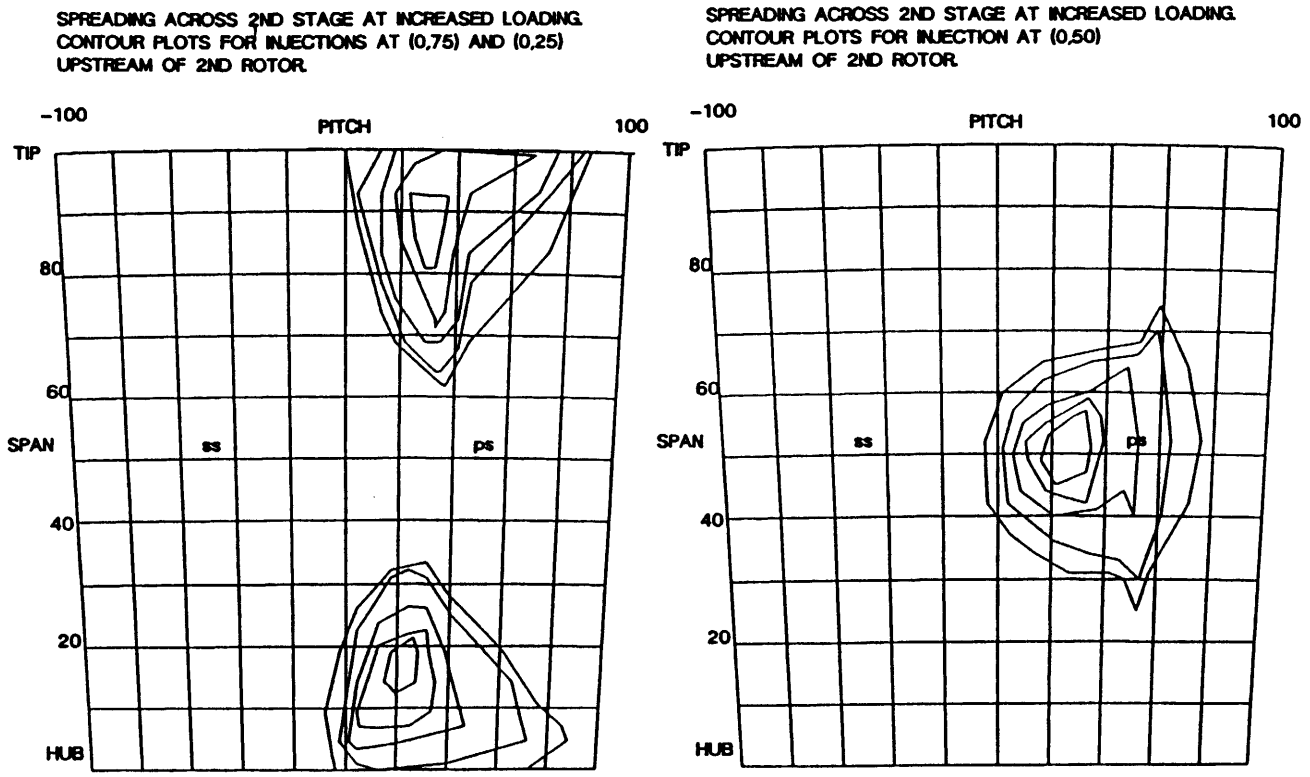

Fig. 49 *Contour Plots for Tracer Gas Spreading Across 2nd. Stage at Increased Loading. Contour Levels : 97,85,75,70,65.*

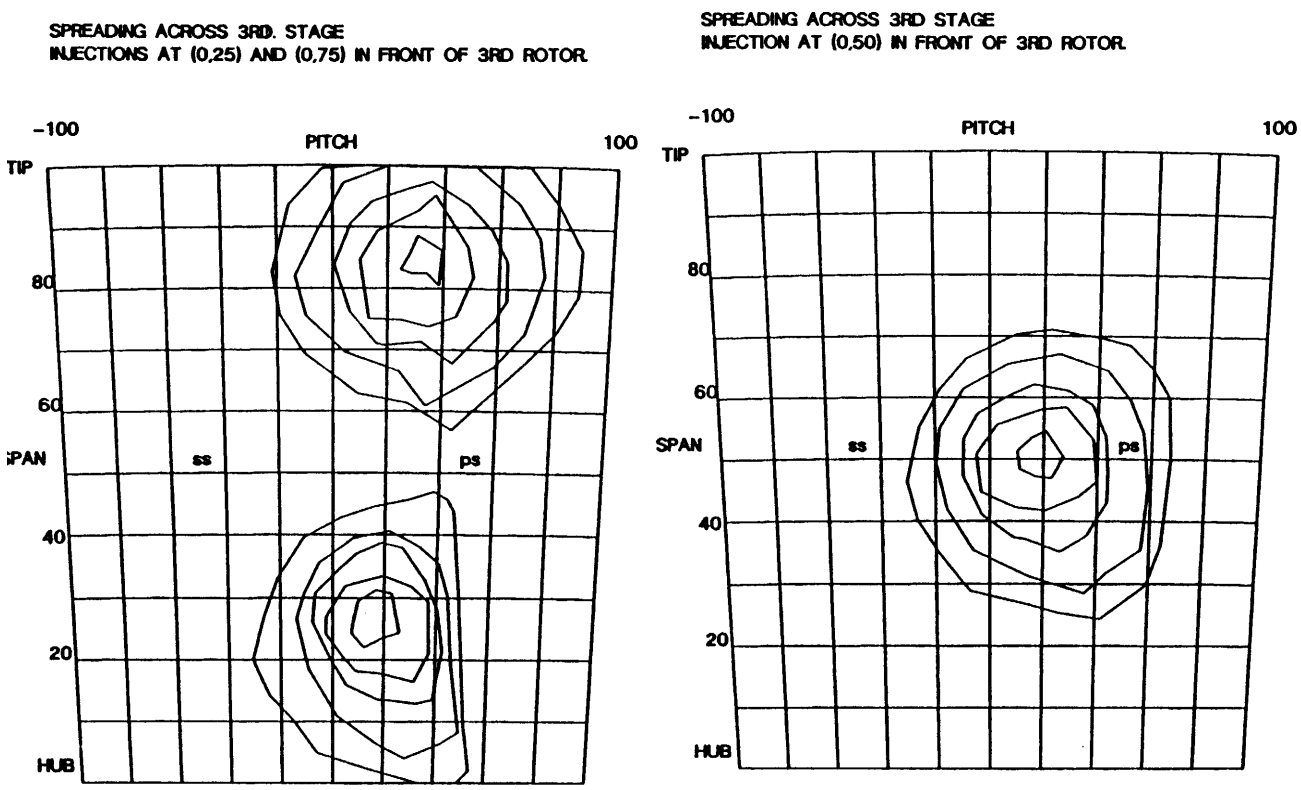

Fig. 50 Contour Plots for Tracer Gas Spreading Across 3rd. stage at Design Point Loading. Contour Levels : 97,85,70,55,40.

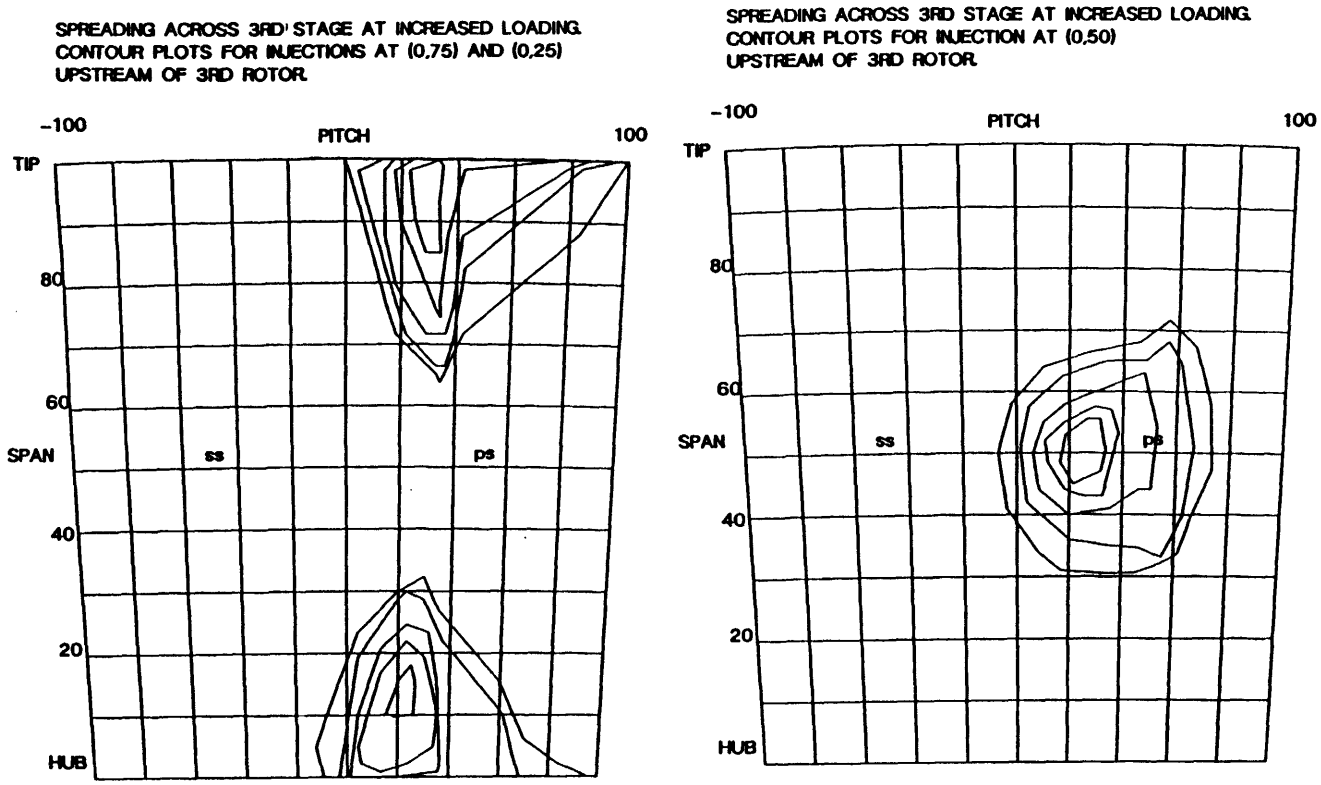

Fig. 51 *Contour Plots for Tracer Gas Spreading Across 3rd. Stage at Increased Loading. Contour Levels : 97,85,75,70,65.*

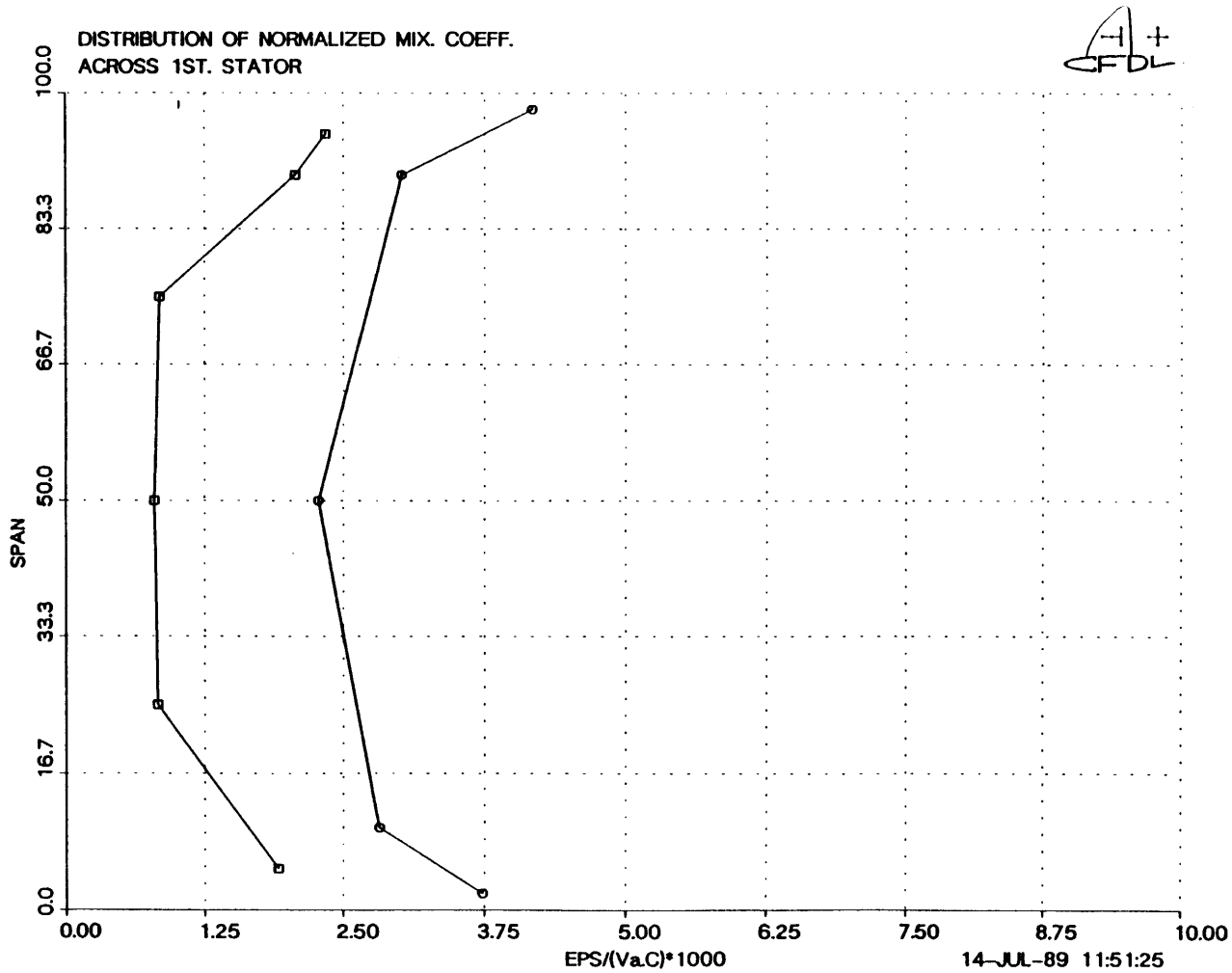

Fig. 52 *Radial Distribution of Mixing Coefficient for 1st. Stator.*

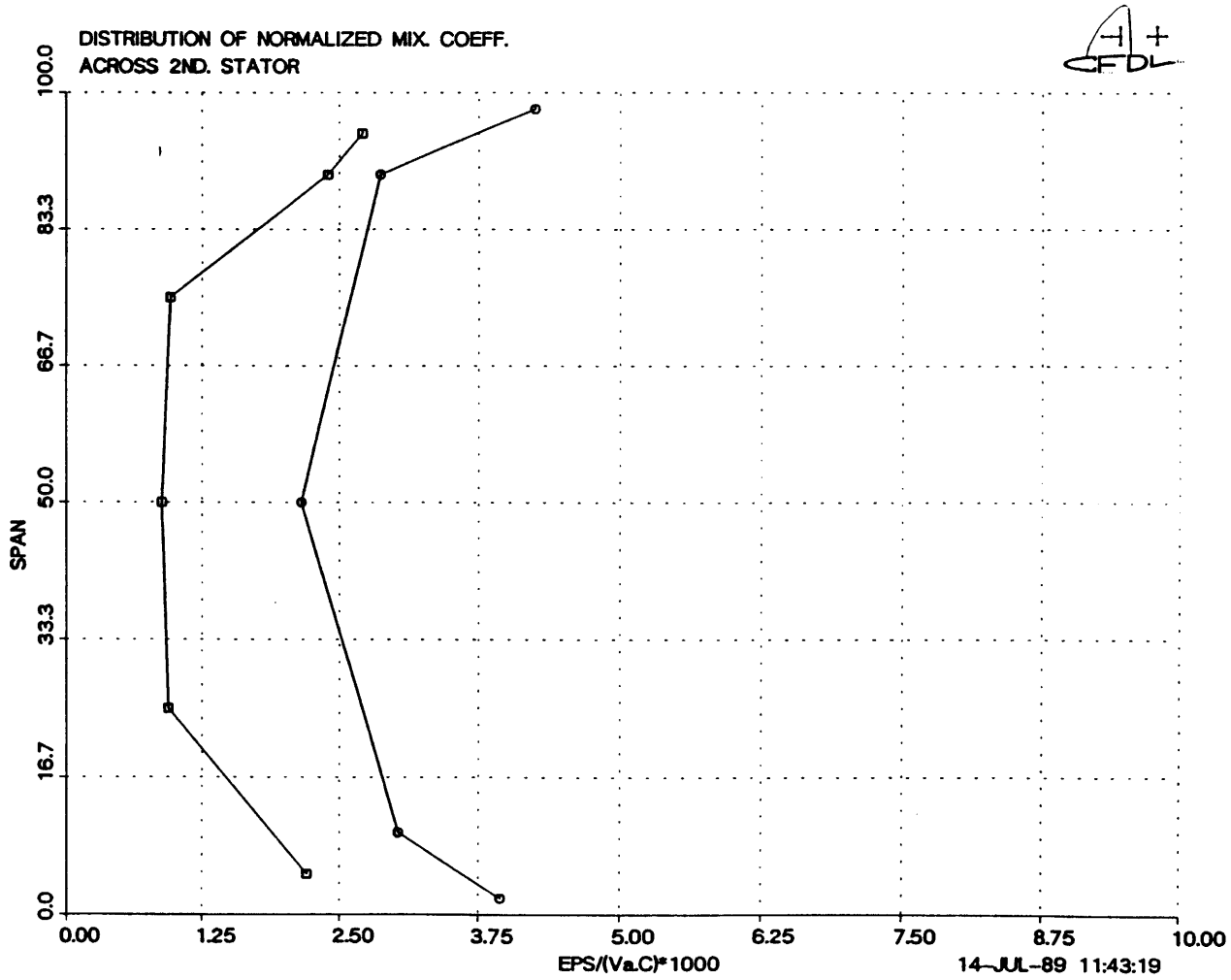

Fig. 53 Radial Distribution of Mixing Coefficient for 2nd. Stator.

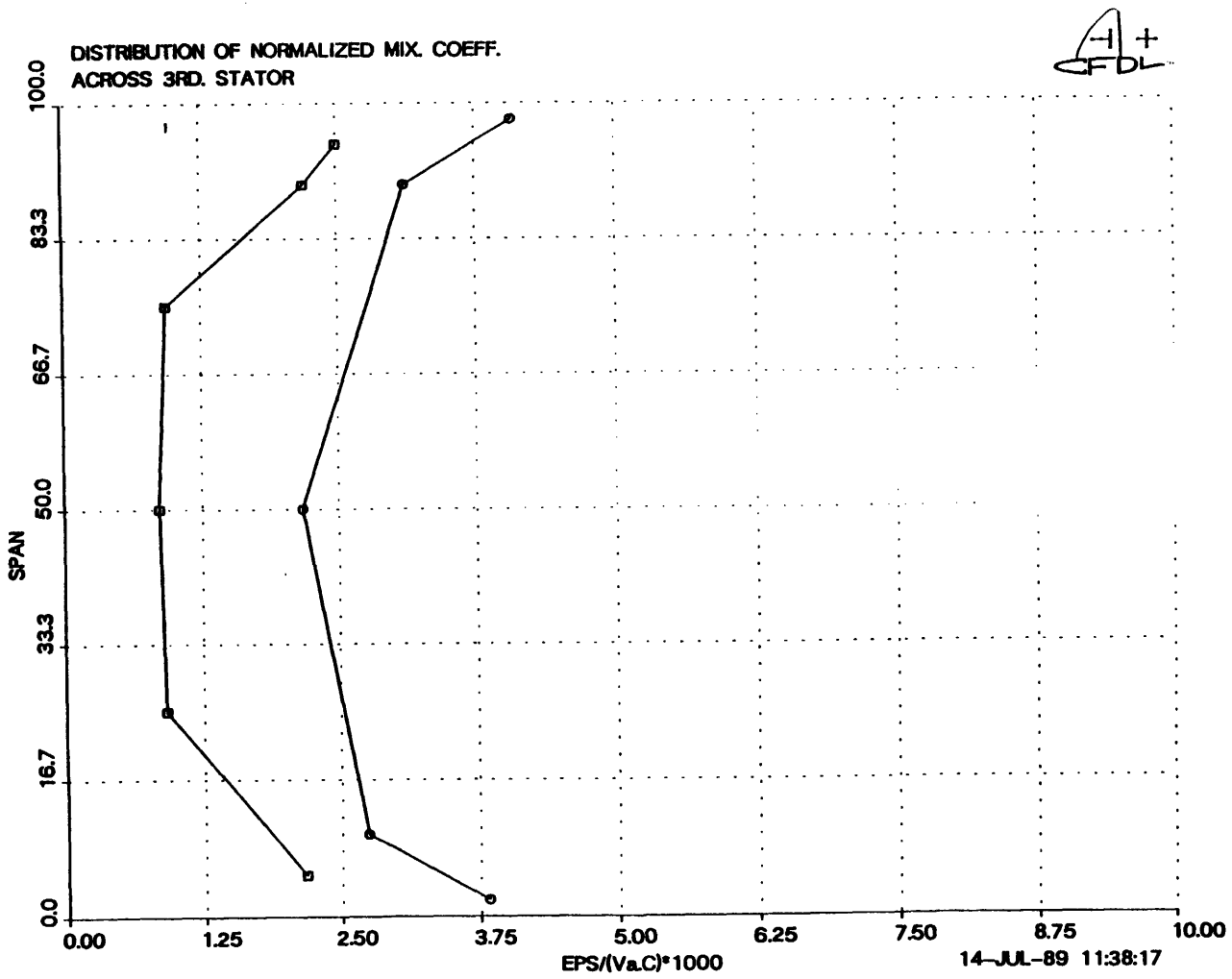

Fig. 54 *Radial Distribution of Mixing Coefficient for 3rd. Stator.*

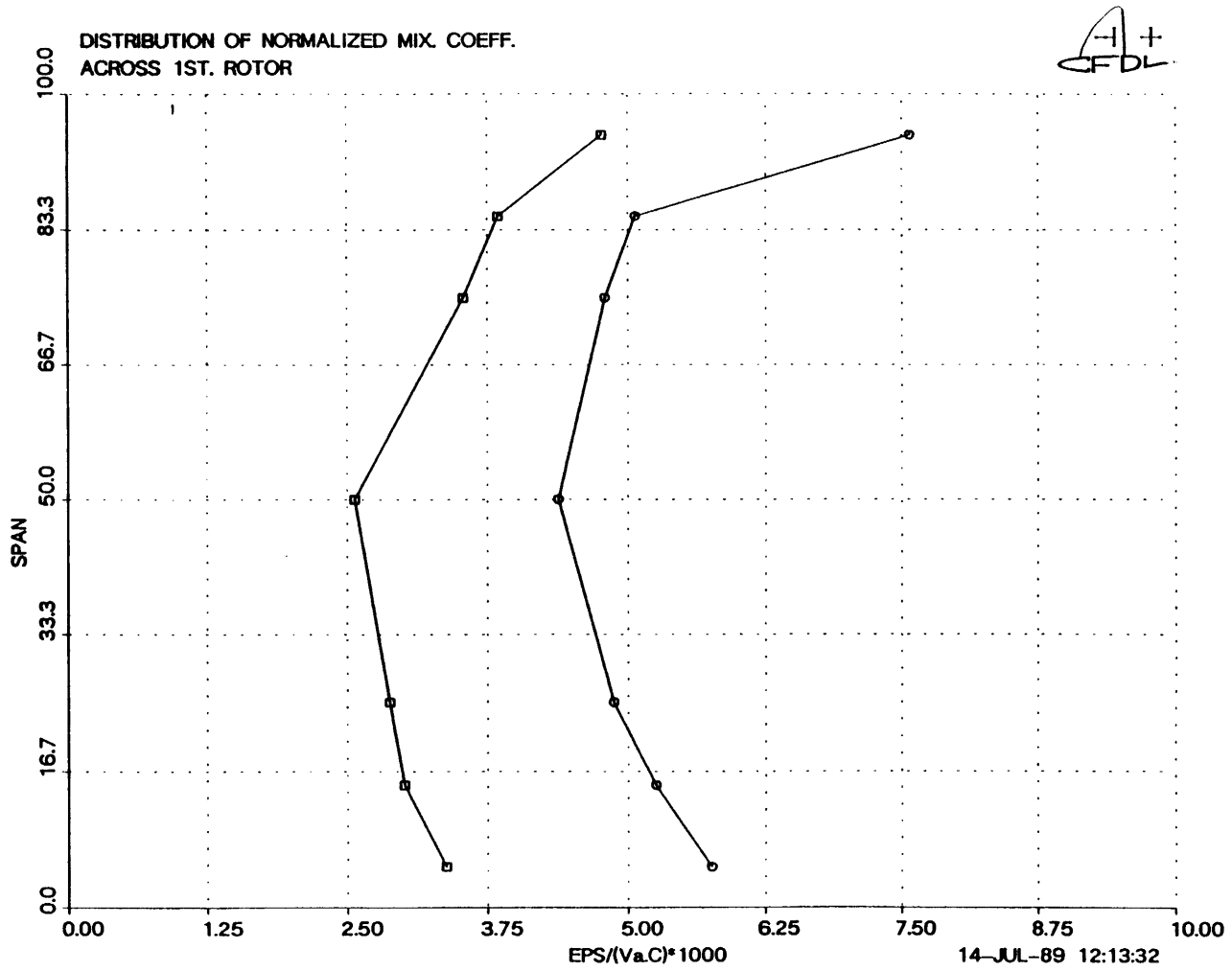

Fig. 55 *Radial Distribution of Mixing Coefficient for 1st. Rotor.*

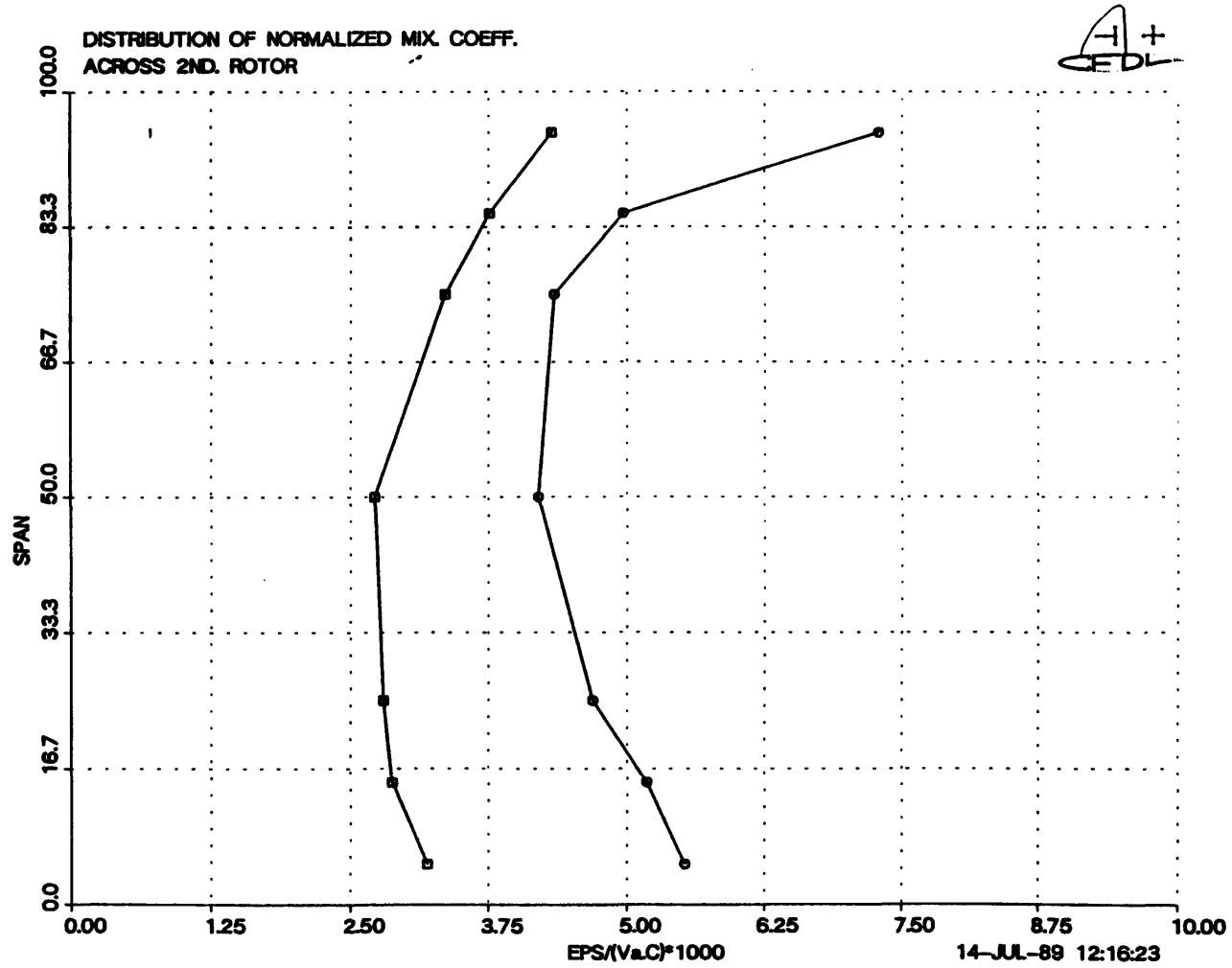

Fig. 56 Radial Distribution of Mixing Coefficient for 2nd. Rotor.

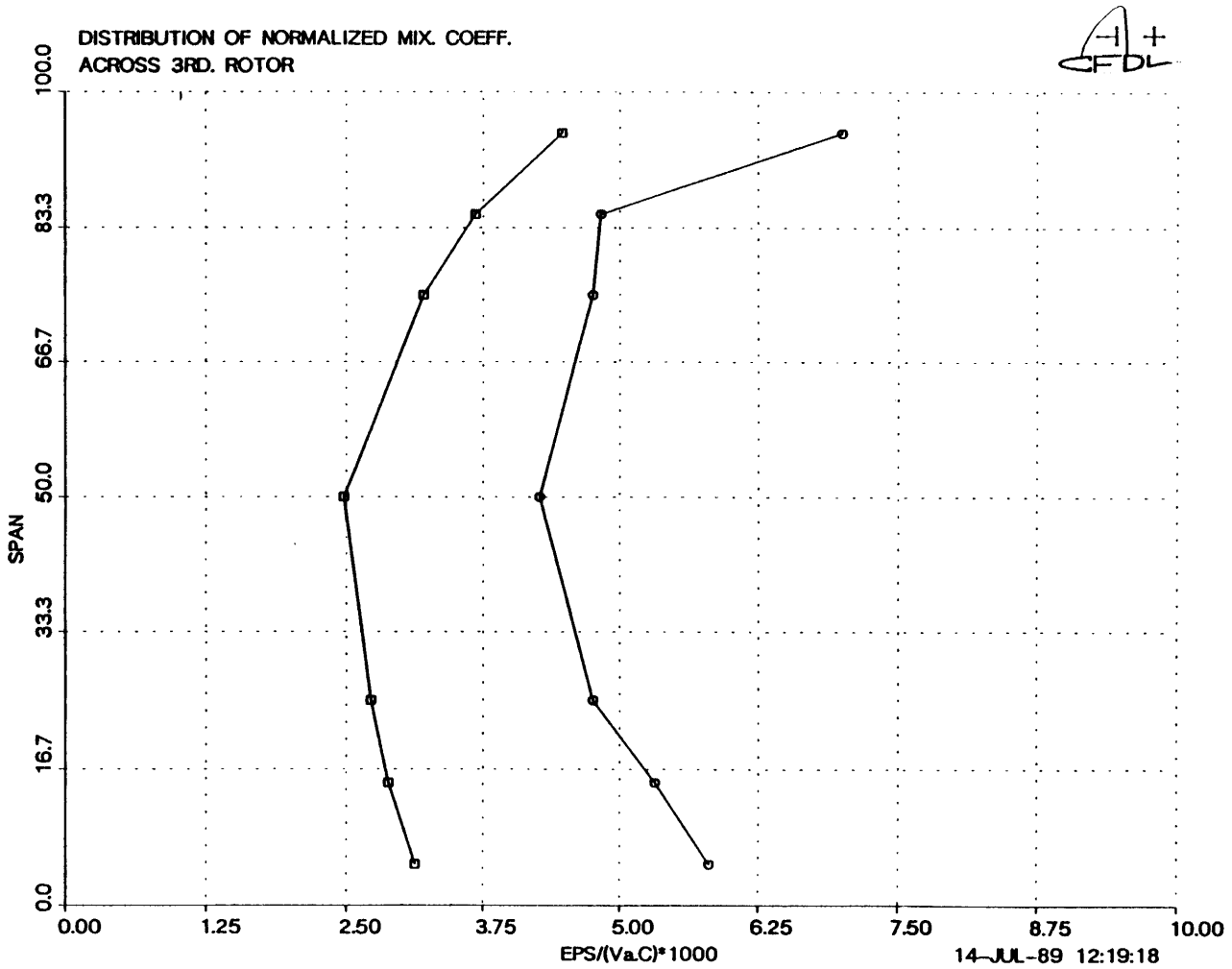

Fig. 57 *Radial Distribution of Mixing Coefficient for 3rd. Rotor.*

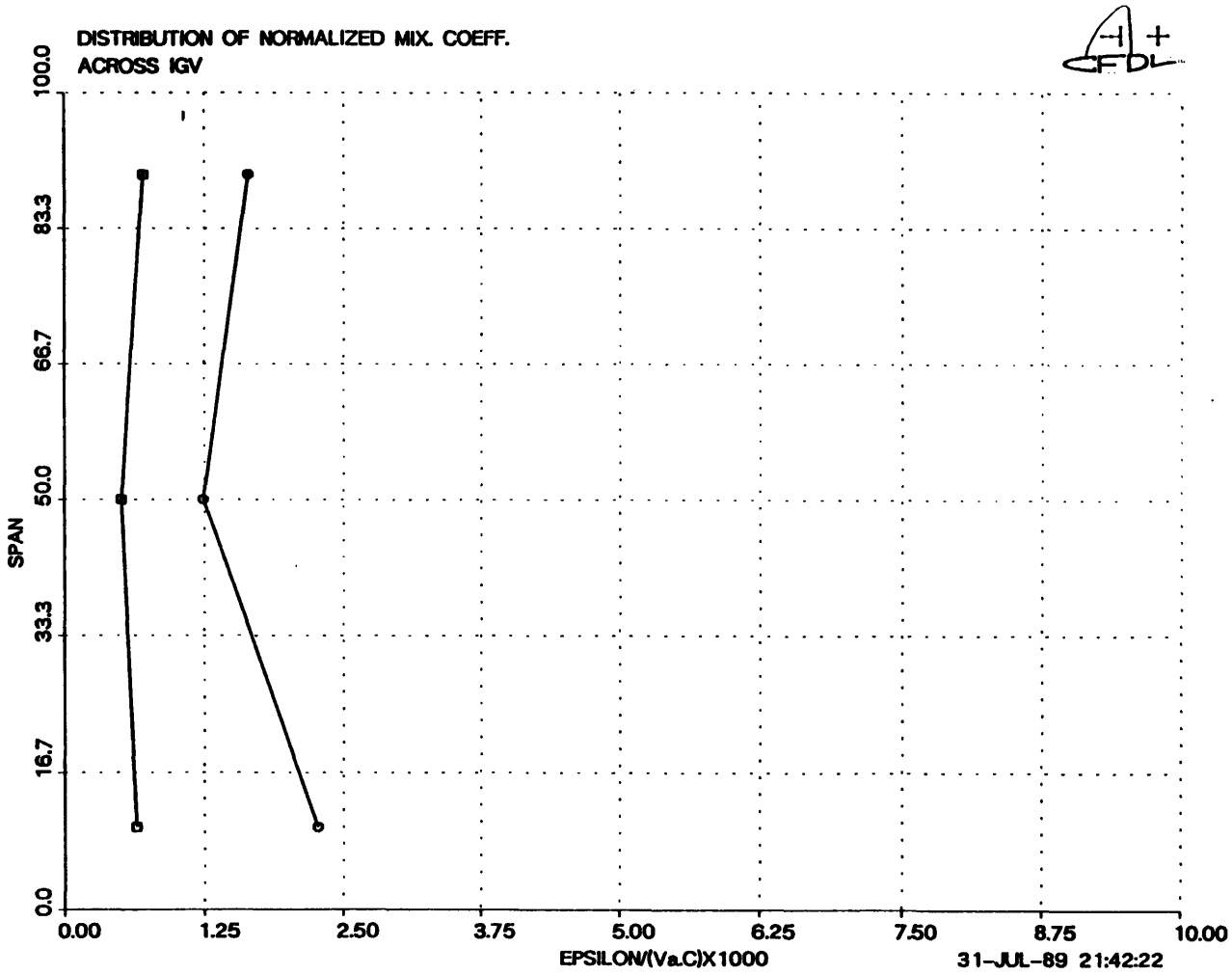

Fig. 58 *Radial Distribution of Mixing Coefficient for IGV.*

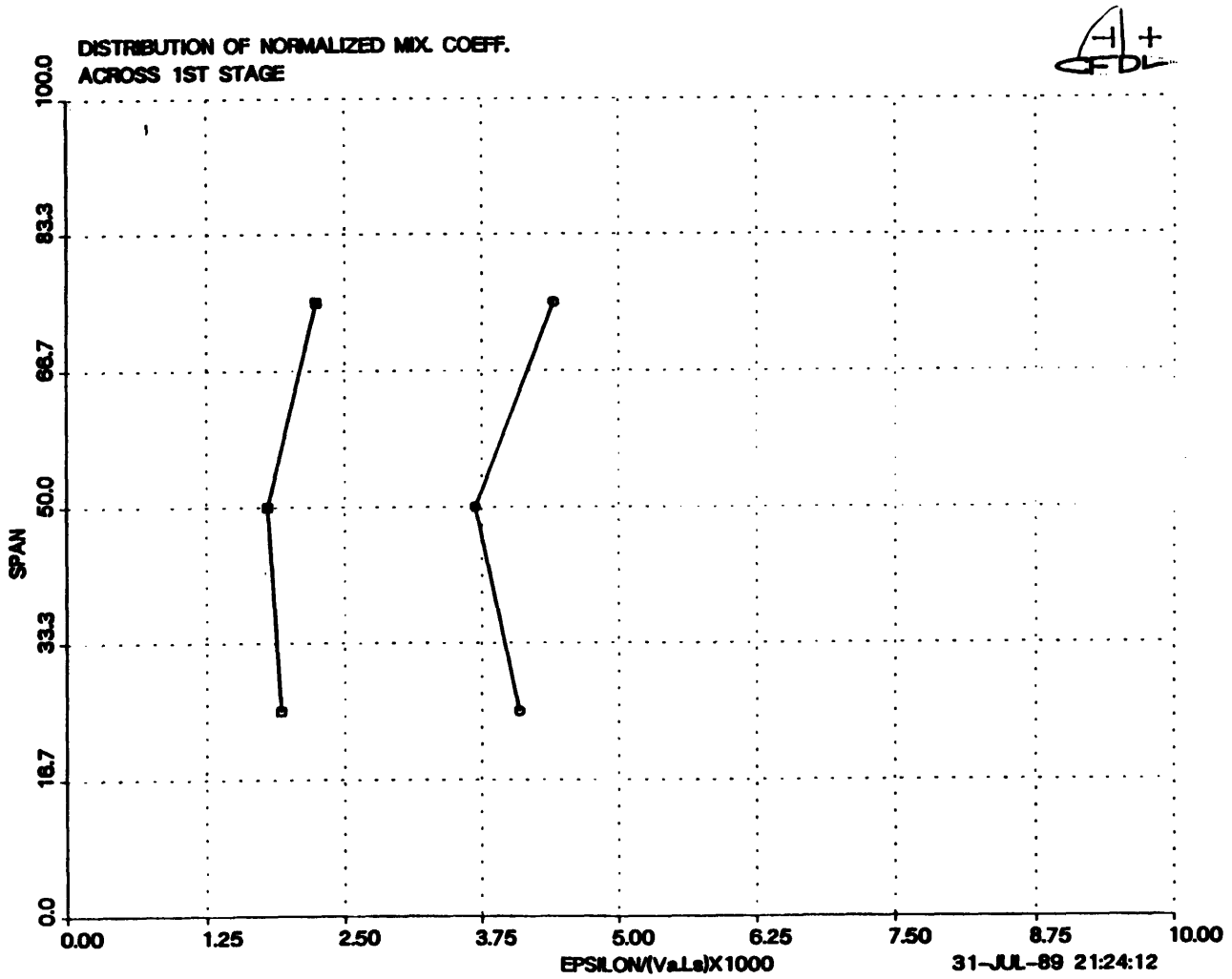

Fig. 59 Radial Distribution of Mixing Coefficient for 1st. Stage.

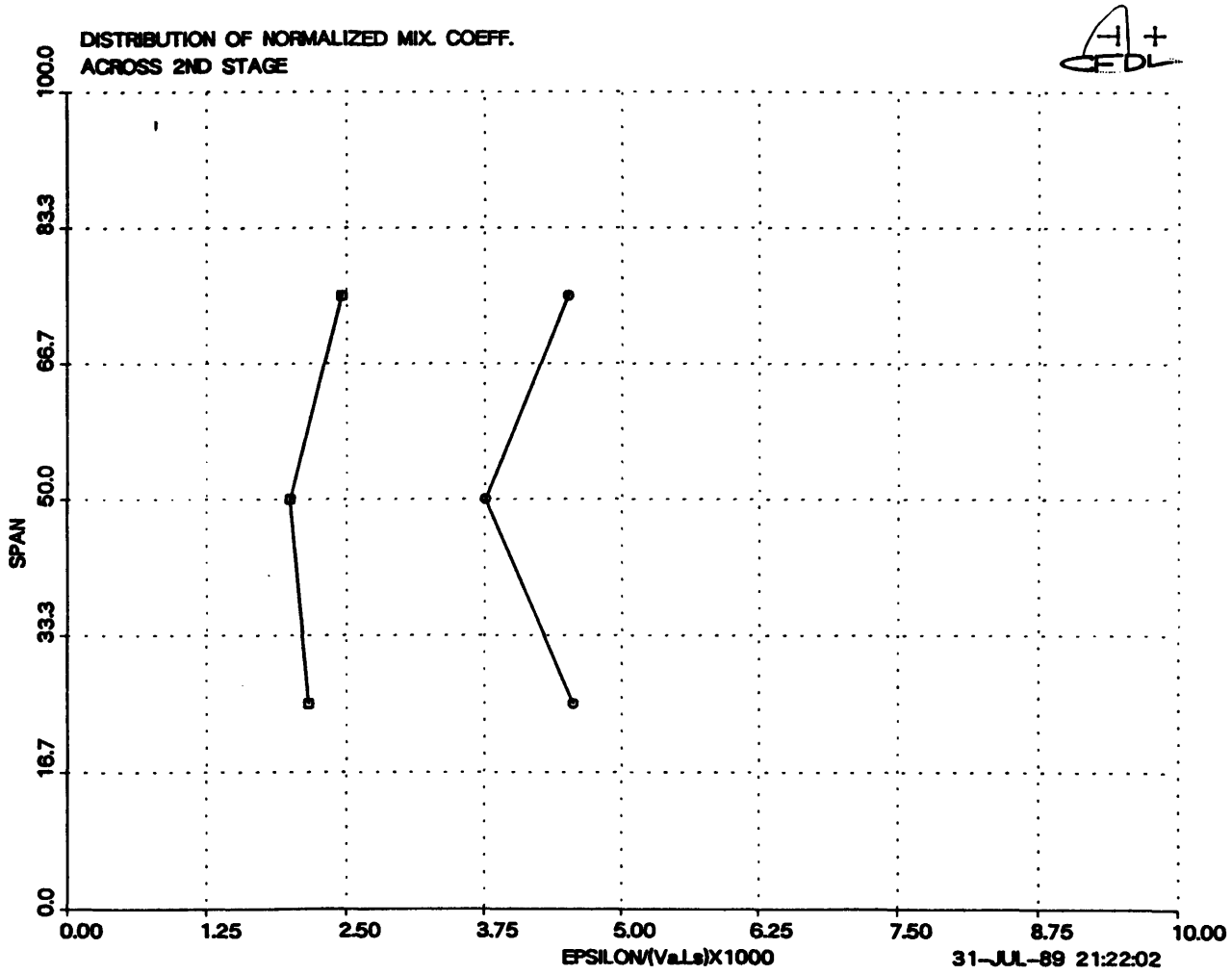

Fig. 60 *Radial Distribution of Mixing Coefficient for 2nd. Stage.*

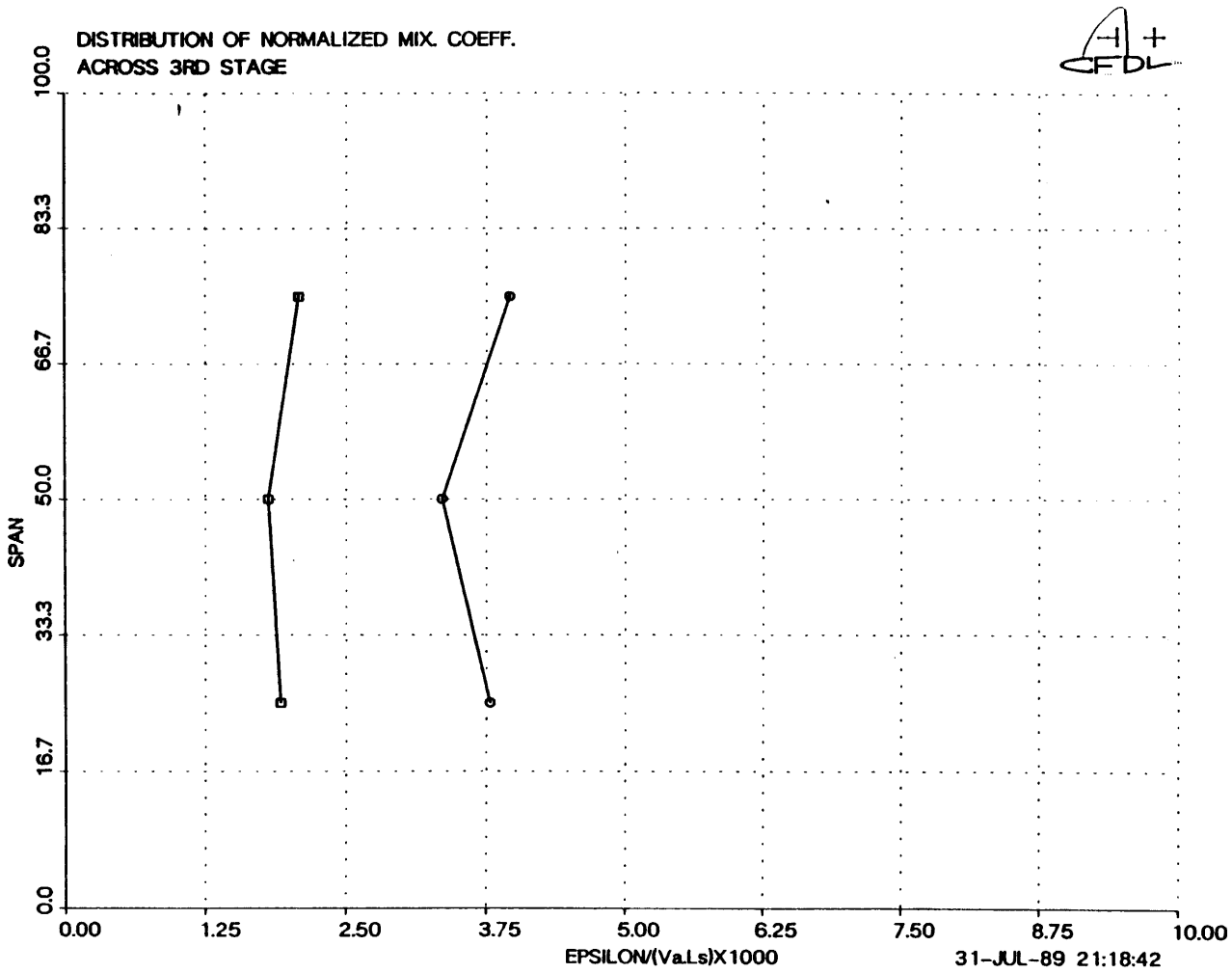

Flg. 61 *Radlal Distribution of Mixing Coefficient for 3rd. Stage.*

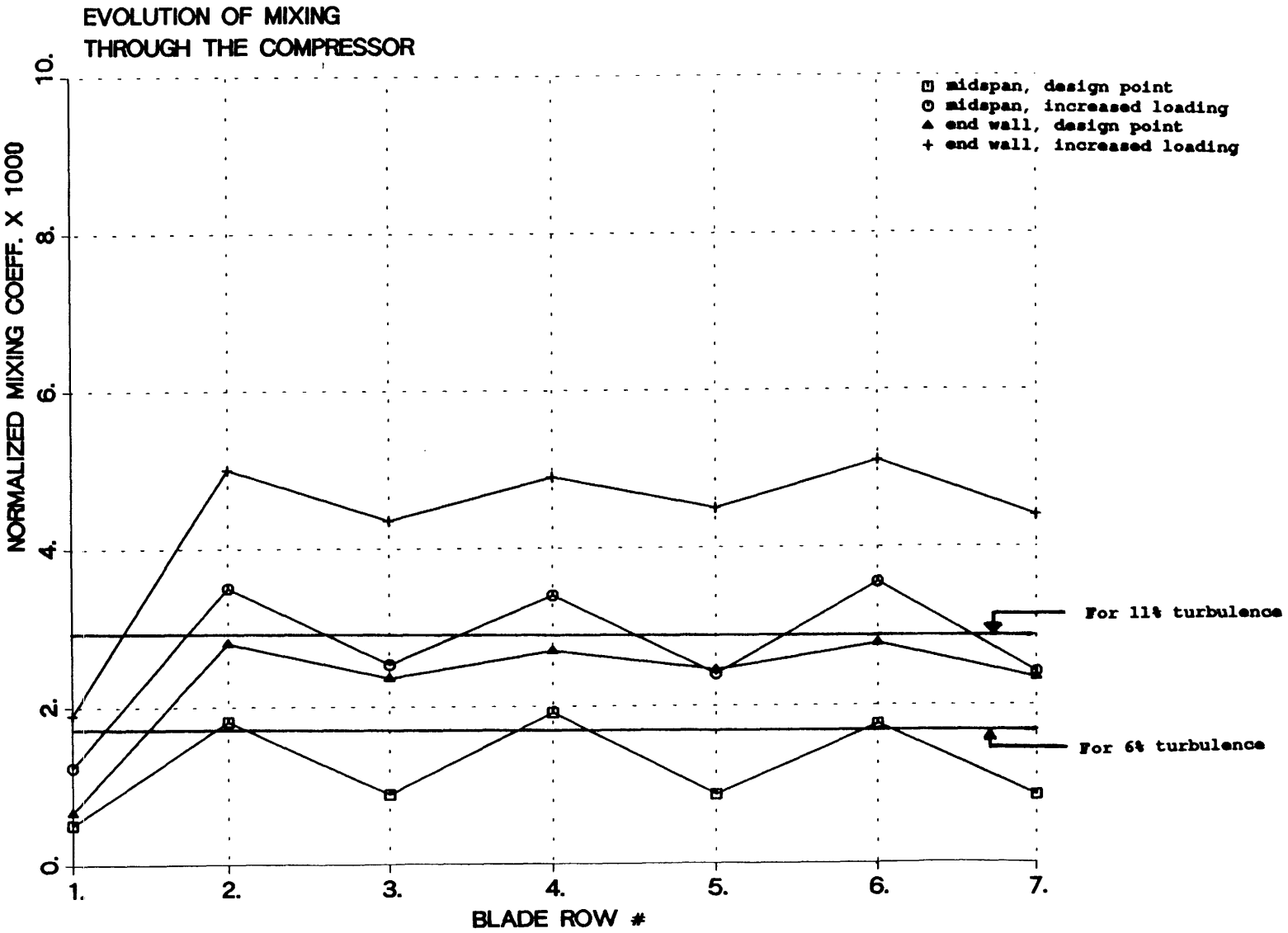
EVOLUTION OF MIXING
THROUGH THE COMPRESSOR
midspan, design point
midspan, increased loading
end wall, design point
end wall, increased loading
NORMALIZED MIXING COEFF. X 1000
0.
2.
4.
6.
8.
10.
1.
2.
3.
4.
5.
6.
7.
BLADE ROW #
For 11% turbulence
For 6% turbulence

REFERENCES

1 Newton, A.G. "Shaping the Technology of Aircraft Propulsion", Aeronautical Journal, January 1984.

2 Adkins, G.G. and Smith, L.H. "Spanwise Mixing in Axial Flow Compressors", ASME 81-GT-57.

3 Gallimore, S.J. and Cumpsty, N.A. "Spanwise Mixing in Multistage Axial Flow Compressors", ASME 86-GT-20.

4 Wennerstrom, A.J. "Low Aspect Ratio Axial Flow Compressors: Why and What it Means", The Enginnering Society for Advancing Mobility, Land Sea Air and Space, SAE/SP-86/683.

5 D.C. Wisler, et. al. "Secondary Flow Turbulent Diffusion and Mixing in Axial Flow Compressors", Journal of Turbomachinery, Oct 1987.

6 Y.S. Li and N.A. Cumpsty "Mixing in Axial Flow Compressors", Unpublished Report, Whittle Lab., Cambridge University, England.

7 Kerrebrock, J.L. and Mikolajczk,A.A. "Intra-stator Transport of Wakes and its Effect on Compressor Performance" ASME 70-GT-39.

8 Denton, J.D. and Usui, S. "Use of Tracer Gas Technique to Study Mixing in a Low Speed Turbine", ASME 81-GT-86.

9 Towle, W.L. and Sherwood, T.K. "Eddy Diffusion, Mass Transfer in a Portion of Turbulent Air Stream", Journal of Industrial Engineering Chemistry, 1939.

10 Hinze, J.O. "Turbulence", McGraw Hill Publ., 1959.

11 Moore, J. and Smith, B.L. "Flow in a Turbine Cascade Part 2: Measurements of Flow Trajecteries by Ethylene Detection", ASME 83-GT-69

12 Abramovitz, G.N., "The Theory of Turbulent Jets", MIT Press, Cambridge, Mass., 1963.

13 E.M. Laws and J.L. Livesey, "Flow Through Screens" Ann. Rev. Fluid Mech., 1978, 10:247-66.

14 Horlock, J.H. "Recent Developments in Secondary Flows", Secondary Flows in Turbomachines, AGARD CP 214, 1977.

15 B. Cantwell and D. Coles "An Experimental Study of Entrainment and Transport in the Turbulent Near Wake of a Circular Cylinder", J. of Fluid Mech. 1983, Vol. 136.

16 L.J.S. Bradbury " Measurements with a Pulsed-wire and Hot-wire Anemometer in the Highly Turbulent Wake of a Normal Flat Plate", J. of Fluid Mech. 1976, Vol. 77.

17 Townsend, A.A., "Turbulence", Cambridge Univ. Press, 1961.

18 Antonia, R.A. and Bilger, R.W. "Heated Round Jet in a Coflowing Stream" AIAA, J 14, 1976.

19 Christianson, M.B. "An Experimental Investigation of a Three-stage Axial-flow Compressor with Cantilevered Stators Using Low Aspect Ratio - Redisigned Endwork Blading in All Stages" United Aircraft Research Laboratory Report #R232752-1, 1975.

10 Gamache, R.N., Ph.D. Thesis, MIT, "Axial Compressor Reversed Flow Performance", 1985.

21 Lavrich, P.L., Ph.D. Thesis,MIT,"Time Resolved Measurements of Rotating Stall in Axial Flow Compresssor", 1988.

22 Bradshaw, P. "An Introduction to Turbulence and its Measurements", Permagon Press, Oxford, England, 1971.

23 Feynman et. al., "The Feynman Lecturs on Physics", Addison Publishing Company, 1964.